

Leibniz Institute of Virology (LIV)

and

Centre for Structural System Biology (CSSB)

HCMV uses phase separation of UL112-113 proteins at viral genomes to facilitate viral replication

Dissertation Submitted to the Department of Chemistry
Faculty of Mathematics, Informatics, and Natural Sciences
University of Hamburg

In fulfillment of the requirements for the degree of
Doctor of Natural Sciences (Dr. rer. nat.)

By
Enrico Caragliano
(born in Messina, Italy)

Prof. Dr. Wolfram Brune (First Reviewer)

Prof. Dr. Thomas Dobner (Second Reviewer)

Date of oral defense: 16.06.23

This study was conducted between February 2018 and March 2023 at the Leibniz Institute for Virology (LIV) and the Centre for Structure System Biology (CSSB) under the supervision of Prof. Dr. Wolfram Brune and Prof. Dr. Jens Bernard Bosse.

Publications, presentations, and awards

The study presented in this thesis was published in:

Human cytomegalovirus forms phase-separated compartments at viral genomes to facilitate viral replication.

*E. Caragliano ,S. Bonazza,G. Frascaroli,J. Tang, T.K. Soh, K. Gruenewald, J. B. Bosse and W. Brune ,
Cell reports, March 2022*

Herpesvirus Replication Compartments: Dynamic Biomolecular Condensates?

E. Caragliano , W. Brune J. B. Bosse. Viruses, May 2022

Additional publications:

Herpesviruses induce aggregation and selective autophagy of host signalling proteins NEMO and RIPK1 as an immune-evasion mechanism.

E. Muscolino, R. Schmitz, S. Loroeh, E. Caragliano, C. Schneider, M. Rizzato, Y.H Kim, E. Krause, V. Juranic Lisnić, A. Sickmann, R. Reimer, E. Ostermann and W. Brune. Nature Microbiology, December 2019.

A Unique Role of the Human Cytomegalovirus Small Capsid Protein in Capsid Assembly.

E.M. Borst, S. Harmening, S. Sanders, E. Caragliano, K. Wagner, T. Lenac Roviš, S Jonjić, J.B. Bosse, M. Messerle. mBio, October 2022

The data were orally presented:

LCI Symposium 2023 – Compartments of Infection, Hamburg, Germany

Congenital CMV meeting 2022, Online

GfV meeting 2021, Online

GfV - Cell Biology of viral infection meeting 2021, Schöntal, Germany

Leibniz Institute for Virology (LIV), Scientific Retreat 2019, Hamburg, Germany

Leibniz Institute for Virology (LIV), Overarching Day 2018, Hamburg, Germany

Poster presentations:

GfV meeting 2023, Ulm, Germany

EMBO workshop liquid-liquid phase separation, 2022, Heidelberg, Germany

1st joint international symposium of FOR2830 and FOR5200, 2022, Cavtat, Croatia

GfV meeting 2021, Online

Awards:

PhD award, Leibniz Institute for Virology (LIV), 2023

Best poster award, Congenital CMV meeting 2022

Best poster award, Leibniz Institute for Virology (LIV), scientific retreat 2018

Mobility grant 2018, Leibniz Institute for Virology (LIV)

Table of Contents

1 Abstract	15
2 Zusammenfassung.....	16
3 Introduction	19
3.1 Herpesviridae	19
3.2 Human Cytomegalovirus	20
3.2.1 Pathogenesis and congenital infection.....	20
3.2.2 Human Cytomegalovirus (HCMV): Treatment.....	22
3.2.3 Human cytomegalovirus: Virion structure	22
3.2.4 Human cytomegalovirus: the replication cycle	23
3.2.5 HCMV replication compartments (RC)	26
3.2.6 The HCMV UL112-113 proteins	27
3.3 Liquid-Liquid phase separation and membrane-less compartments	29
3.3.1 Mechanism of liquid-liquid phase separation	31
3.3.2 Phase separation drivers in biological systems	32
3.3.3 Condensate maturation.....	34
4 Aim of the study.....	37
5 Results	39
5.1 Pre-replication compartments are fluid biomolecular condensates formed by LLPS	39
5.2 UL112-113 forms fluid biomolecular condensates without the contribution of other viral proteins	46
5.3 Clustering of UL112-113 disordered regions by the ordered N-terminus is sufficient for LLPS	49
5.4 Exogenous DNA lowers the UL112-113 concentration threshold for liquid-liquid phase separation.....	52

5.5 UL112-113 phase separation can be locally induced below the global threshold for phase separation.....	56
5.6 Incoming viral genome localization to PRCs is essential for their replication	57
5.7 UL112-113 LLPS is essential for the recruitment of the viral polymerase accessory unit UL44	63
6 Discussion.....	69
6.1 The role of UL112-113 proteins LLPS in HCMV replication.....	69
6.3 Association of UL112-113 with viral genomes.....	72
6.4 The role of protein disorder in RC formation.....	74
6.5 The role of LLPS in the lifecycle of other herpesviruses	75
6.6 RC maturation	77
7 Materials	80
7.1 Bacteria.....	80
7.2 Cells and viruses	80
7.3 Chemicals.....	81
7.4 Antibodies.....	82
7.5 Recombinant DNA	83
7.6 Gibson cloning primers.....	85
7.7 BAC mutagenesis primers	89
7.8 Antibiotics.....	89
7.9 Kits	90
7.10 Buffers	91
7.10.1 Buffers for DNA purification and agarose gel electrophoresis.....	91
7.10.2 Buffers for SDS polyacrylamide gel electrophoresis (SDS-PAGE), Western Blot, and Immunofluorescence.....	91

7.10.3 Buffers for protein purification.....	93
7.11 Devices and equipment.....	93
7.12 Software	95
8 Methods	97
8.1 Molecular biology methods	97
8.1.1 Preparation of electrocompetent bacteria	97
8.1.2 Transformation of bacteria.....	97
8.1.3 Isolation of DNA from bacteria: Plasmid mini Prep.....	97
8.1.4 Isolation of DNA from bacteria: BAC mini Prep.....	98
8.1.5 Isolation of DNA from bacteria: BAC/plasmid midi Prep	98
8.1.6 Long-term storage of bacteria	98
8.1.7 DNA sequencing.....	98
8.1.8 Polymerase chain reaction (PCR).....	98
8.1.9 Restriction digestion of DNA	99
8.1.10 Agarose gel electrophoresis and purification of DNA fragments from gel	99
8.1.11 Gibson assembly and restriction enzyme cloning	99
8.1.12 <i>En passant mutagenesis</i>	99
8.2 Cell biology and virology methods	100
8.2.1 Cell culture	100
8.2.1 Freezing and thawing of cells	101
8.2.3 Plasmid transfection	101
8.2.4 Transfection of BAC DNA.....	101
8.2.5 Lentivirus production.....	102
8.2.6 Lentivirus transduction for production of corelet-expressing cells	102
8.2.7 HCMV virus stock production and concentration	102

8.2.8 Production of EdU-labeled stocks	103
8.2.9 HCMV titration using TCID ⁵⁰ /ml.....	103
8.2.10 Viral infections	103
8.2.11 Hexanediol and propylene glycol treatments	103
8.3 Biochemistry methods	104
8.3.1 SDS polyacrylamide gel electrophoresis (SDS-Page) and western-blot	104
8.3.2 Blue coomassie staining.....	104
8.3.3 UL112-113 proteins purification.....	104
8.4 Microscopy methods	105
8.4.1 Light microscopy modalities	105
8.4.2 Immunofluorescence	106
8.4.3 EdU label of the incoming viral genome.....	106
8.4.4 Labeling of the replicating genome by EdU and BrdU	106
8.4.5 In vitro phase separation assay	107
8.4.6 Live-cell imaging	107
8.4.7 Fluorescence Recovery After Photobleaching (FRAP)	107
8.4.8 Corelet system local and global photoactivation	108
8.4.9 Serial-block-face scanning electron microscopy (SBF-SEM).....	109
8.4.10 CLEM and SBF-SEM staining	109
8.5 Microscopy Analysis	110
8.5.1 Fluorescence intensity profiles.....	110
8.5.2 EdU surface area measurements for quantification of viral genome replication and colocalization	110
9 References.....	111
10 Appendix	124

10.1 Curriculum Vitae.....	124
10.2 Toxicity of chemicals	125
10.3 Acknowledgments.....	129
10.4 Statement of Authorship.....	130

1 Abstract

Human cytomegalovirus (HCMV) is the leading cause of congenital infections worldwide and causes severe disease in immunocompromised patients. Upon injection of HCMV genomes into the host cell nucleus, cellular and viral factors necessary for the replication of the viral genome accumulate in membrane-less compartments called viral replication compartments (RCs). How RCs form at viral DNA and control their composition is poorly understood. Liquid-liquid phase separation (LLPS) has recently emerged as a mechanism for explaining the formation of cellular membrane-less compartments. Using live-cell imaging, fluorescence recovery after photobleaching (FRAP), and chemical inhibitors, we found that the essential UL112-113 proteins undergo liquid-liquid phase separation (LLPS) and form membrane-less compartments in both transfected as well as infected cells. We observed biophysical differences between the pre-replication (PRC) and the replication compartments (RC), suggesting a phase transition induced after the initiation of the DNA replication. UL112-113 LLPS was independent of other viral factors as purified proteins could phase separate and form droplets *in vitro*. Indeed, using a photo-inducible oligomerization domain, we showed that clustering the intrinsically disordered regions (IDRs) of UL112-113 was sufficient to induce phase separation. Using cells stably expressing UL112-113, we found that exogenous DNA reduced the local concentration threshold for UL112-113 droplet formation, suggesting that DNA can serve as a scaffold for UL112-113 clustering. We used click-chemistry and nucleoside analogs to visualize the viral genome and distinguish between the incoming and the replicating one. Interestingly, most of the incoming viral genomes localized with UL112-113 compartments in infected cells, and this association was essential for viral DNA replication. We further show that the viral polymerase accessory unit UL44 is recruited into UL112-113 droplets through its C-terminal IDR. Consequently, perturbation of UL112-113 LLPS abrogated UL44 recruitment and blocked the formation of mature replication compartments. In summary, our data suggest that HCMV uses genome-triggered local LLPS to cluster UL112-113 proteins at viral genomes, thereby generating phase-separated compartments that facilitate viral DNA replication by recruiting essential factors.

2 Zusammenfassung

Das humane Cytomegalovirus (HCMV) ist weltweit die Hauptursache für kongenitale Infektionen und verursacht schwere Erkrankungen bei immungeschwächten Patienten. Nach der Injektion von HCMV-Genomen in den Zellkern der Wirtszelle sammeln sich zelluläre und virale Faktoren, die für die Replikation des viralen Genoms erforderlich sind, in membranlosen Kompartimenten an, die als virale Replikationskompartimente (RCs) bezeichnet werden. Wie sich die RKs an der viralen DNA bilden und ihre Zusammensetzung kontrollieren, ist kaum bekannt. In jüngster Zeit hat sich die Flüssig-Flüssig-Phasentrennung (LLPS) als ein Mechanismus für die Bildung von membranlosen Zellkompartimenten herauskristallisiert. Mit Hilfe von Live-Cell-Imaging, Fluoreszenzerholung nach Photobleichung und chemischen Inhibitoren konnten wir feststellen, dass die essentiellen viralen UL112-113-Proteine eine Flüssig-Flüssig-Phasentrennung (LLPS) durchlaufen und membranlose Kompartimente sowohl in transfizierten als auch in infizierten Zellen bilden. Wir beobachteten biophysikalische Unterschiede zwischen den Kompartimenten vor der DNA-Replikation (PRCs) und der Replikation (RCs), was auf eine Veränderung der biophysikalischen Eigenschaften nach dem Beginn der DNA-Replikation hindeutet. UL112-113 LLPS war unabhängig von anderen viralen Faktoren, da gereinigte Proteine *in vitro* eine Phasentrennung vornehmen und Tröpfchen bilden konnten. Durch die Verwendung einer photoinduzierbaren Oligomerisierungsdomäne konnten wir zeigen, dass die Konzentrierung der intrinsisch ungeordneten Regionen (IDRs) von UL112-113 ausreicht, um eine Phasentrennung zu bewirken. Bei der Verwendung von Zellen, die UL112-113 stabil exprimieren, konnten wir feststellen, dass exogene DNA die lokale Konzentrationsschwelle für die Bildung von UL112-113-Tropfen senkt, was darauf hindeutet, dass DNA als Gerüst für die UL112-113-Clusterbildung dienen kann. Wir verwendeten Click-Chemie und Nukleosidanaloga, um das virale Genom sichtbar zu machen und zwischen den frisch injizierten und den replizierenden Genomen zu unterscheiden. Interessanterweise lokalisierten die meisten eingehenden viralen Genome mit UL112-113-Kompartimenten und diese Assoziation war für die virale DNA-Replikation essentiell. Wir konnten außerdem zeigen, dass die virale Polymerase-Einheit UL44 über ihre C-terminale IDR in UL112-113-Tröpfchen rekrutiert wird. Folglich führte eine Störung von UL112-113 LLPS zu einer Aufhebung der UL44-Rekrutierung und blockierte die Genomreplikation. Zusammenfassend legen unsere Daten nahe, dass HCMV Genom-angestrichelte lokale LLPS nutzt, um UL112-113-Proteine an viralen Genomen zu clustern und dadurch phasengetrennte Kompartimente

zu erzeugen, die die virale DNA-Replikation durch die Rekrutierung wesentlicher Faktoren erleichtern.

3 Introduction

3.1 Herpesviridae

Herpesviruses are a family of dsDNA viruses that are widespread and can infect different species, including vertebrate and invertebrate animals. A common ancestor for the family can be estimated to have emerged in the Devonian Period, around 400 million years ago ¹, indicating that these viruses co-existed for millions of years with their hosts. Many of these viruses can also infect humans, causing different pathologies. There are 9 known human herpesviruses divided into three subfamilies based on biological criteria and the typical architecture of infectious particles: *Alphaherpesvirinae*, *Betaherpesvirinae*, and *Gammaherpesvirinae* ². They all share a long double-stranded DNA genome ranging from 120 to 240 kb and the expression of many proteins. They are associated with a variety of diseases and life-long infections. In particular, one of the most peculiar characteristics of herpesviruses is the ability to establish latent infections in different kinds of cells, depending on the subfamily. The latent nature of herpesvirus infections leads to recurrent reactivation events, which can be physically and emotionally distressing for those affected. Herpesviruses are highly adapted to their hosts, and severe symptoms of infection are usually limited to very young or immunosuppressed individuals. Among the *Alphaherpesvirinae*, we find three human pathogens: varicella-zoster virus (VZV) and herpes simplex virus (HSV) 1 and 2, which share common genetic traits such as the ability to establish latency in neurons. HSV-1 and 2 are the etiologic agent of *herpes labialis* and *genitalis*. They cause various pathologies ranging from asymptomatic infection to self-limiting skin ulcers to severe encephalitis. Both viruses replicate during primary infection in epithelial cells or fibroblasts, ascend the axon through a retrograde mechanism, and establish a latent infection in the nervous system cells. Here they persist for the host's life and re-infect the epithelial cells after reactivation after traveling along the axon in an anterograde direction ^{3,4}. VZV is the etiologic agent of two diseases: chickenpox during primary infection and shingles during reactivation. Chickenpox coincides with the primary infection, while shingles are the pathology resulting from the reactivation of the virus after a period, often very long, of latency. Although HSV can reactivate frequently, VZV usually only reactivates once in an individual's lifetime. Among the betaherpesviruses, three viruses are known: human cytomegalovirus (HCMV), human herpesvirus 6 (HHV-6), and 7 (HHV-7). HCMV often causes asymptomatic infections in humans, establishing latent infections in monocytes but can cause severe diseases in newborns or immunocompromised patients. HHV-6 is the etiologic agent of

roseola infantum in children and other febrile illnesses. There are two distinct species of HHV-6, A and B, with HHV-6B being the more prevalent and the cause of most human infections. Nearly 100% of the global human population is infected by HHV-6 A or B or by both variants. While the genome is maintained as an episome during latency in most herpesviruses HHV-6 can integrate its genome at telomeres in different cell types, including germinal ones ⁵. Similarly to HHV-6, primary infections of HHV-7 occur during childhood and include manifestations such as roseola infantum and other febrile-associated diseases. Reactivation events can occasionally lead to the insurgence of encephalitis, with potentially lethal outcomes ⁶. Epstein Barr virus (EBV) and Kaposi's sarcoma associated virus (KSHV) are two viruses belonging to the gamma herpesvirus subfamily and can both undergo lymphocyte latency. Usually, they cause asymptomatic infections, but they have also been highlighted as risk factors for developing several diseases. For instance, EBV is the causal agent of Burkitt's lymphoma, and EBV infection was recently described as one of the major factors correlating with the development of multiple sclerosis ⁷. KSHV is the causal factor of Kaposi's sarcoma (KS). However, it is also associated with lymphoproliferative diseases in immunocompromised patients like primary effusion lymphoma (PEL) or the KSHV-associated multicentric Castleman disease (MCD) ⁸. Factors like immunosuppression or coinfections can drastically increase the chance of developing diseases. In particular, immunosuppression by Human immunodeficiency virus (HIV) in the stadium of acute immune deficiency syndrome (AIDS) dramatically increases the risk of developing a KSHV-related malignancy in infected individuals ⁹. Despite the prevalence and impact of herpesviruses, current treatments for these infections are limited and often not consistently effective. This highlights the urgent need to develop more effective therapies for herpesvirus infections. Studying herpesviruses and exploring new therapeutic strategies is paramount, improving the lives of those affected by these viruses and reducing the economic burden of herpesvirus-associated diseases.

3.2 Human Cytomegalovirus

3.2.1 Pathogenesis and congenital infection

Among the herpesviruses, HCMV is one of the most spread among humans and is the prototype of the betaherpesviruses. It was first isolated from blood cells in 1950 and was named by the characteristic enlargement of the infected cells, *cytomegaly*. HCMV has a very high seroprevalence worldwide of 60% to 90% depending on socio-economic status ¹⁰. Like other herpesviruses, it causes life-long latency after primary infection and can reactivate. HCMV infection is primarily

asymptomatic in healthy patients, while it can lead to severe infections in immunocompromised patients such as transplant recipients. Reactivation of the virus in these patients is associated with high titer viremia in the blood and dissemination of the virus in various organs. HCMV can spread horizontally via body fluids, like blood and urine, and vertically through intrauterine transmission from the mother to the fetus ^{11,12}. The symptomatic congenital disease occurs most often after primary maternal infection in pregnancy. The vertical transmission of HCMV has been estimated to occur in around 1% of seropositive mothers due to infection with a different strain or reactivation.

In comparison, this value increases to 40/50% of the primarily infected mother, making it the most common congenital infection in the developed world ^{13,14}. About 8-10% of the infected newborns develop neurological abnormalities, regardless of the severity of the disease at birth ^{15,16}. The most common of those are hearing loss and microcephaly. In the United States, 25% of hearing loss cases in children were estimated to be caused by HCMV infection ¹⁷. As the consequences of HCMV infection can be severe and permanent, developing antivirals and treatment is vital.

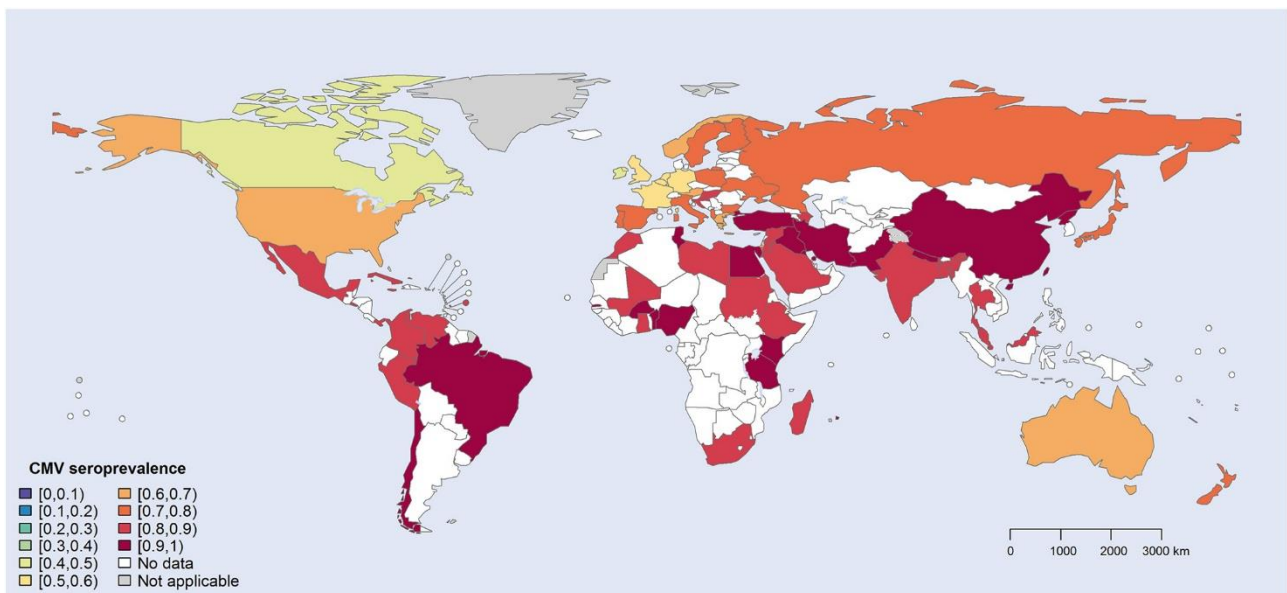


Figure 1: Graphic showing HCMV seroprevalence worldwide adapted from Uhair M, Smit GSA, Wallis G, et al. Estimation of the worldwide seroprevalence of cytomegalo-virus: A systematic review and meta-analysis. *Rev Med Virol.* 2019;29:e2034. <https://doi.org/10.1002/rmv.2034>.

3.2.2 Human Cytomegalovirus (HCMV): Treatment

Given the severe outcome of HCMV infection in newborns and transplant patients and the subsequent public health burden, developing an HCMV vaccine is of high priority. Several vaccine candidates have been evaluated and are currently in clinical trials, but none have been approved (reviewed in ¹⁸). However, several drugs have been approved for treatment against HCMV. Ganciclovir (GCV), for example, was one of the first therapeutics developed against HCMV diseases. GCV is an acyclic nucleoside analog of deoxyguanosine, phosphorylated initially by the viral protein kinase pUL97 in infected cells ¹⁹. After additional phosphorylation by the cellular kinases, it is incorporated into the viral genome, acting as a chain terminator. Valganciclovir, a valine esterification of ganciclovir, has similar efficacy in preventing viremia in transplant patient ²⁰. Ganciclovir and valganciclovir effectively prevent hearing and neurodevelopmental malformations ²¹. Mutations in the viral kinase pUL97, which prevents GCV phosphorylation, can form resistant strains ²². Foscarnet is a structural analog to pyrophosphate (PPi), and since it does not require activation by pUL97, it also inhibits strains coding for pUL97 mutants. Both Foscarnet and Ganciclovir are limited by significant side effects and the selection of viral mutations conferring antiviral drug resistance ²³. Recently, Letermovir has also been approved. This compound targets pUL56, a component of the viral terminase complex, interfering with the packaging of viral DNA into the capsids ²⁴ but is only approved for prophylactic use in patients with allogeneic HSCT, and mutations in UL56 can lead to resistant strain formation. All authorized antiviral agents only target replicating viruses and cannot affect the latent virus reservoir. As HCMV is never cleared from the host, virus replication can reoccur after suspending drug treatment. Therefore, drugs targeting the latent reservoir are highly desirable ²⁵. To this end, basic research aimed at the replicative cycle of HCMV is essential to define new therapeutic strategies.

3.2.3 Human cytomegalovirus: Virion structure

HCMV virions range from 200 to 300 nm in diameter, making it one of the largest human viruses. The virions comprise an icosahedral nucleocapsid, a proteinaceous matrix, a tegument (Fig. 2, A-B), and an envelope. Each capsid contains a portal complex, which allows the viral DNA to be packaged and ejected. The tegument between the capsid and envelope contains proteins and RNA of cellular and viral origin, which are released into the host cell upon fusion and primes the cell in the initial phase of infection ^{26,27}. The envelope is a lipid membrane of cellular origin containing different viral

glycoproteins, which mediate the entry of the virions into the cell by fusion with host membranes. HCMV has the largest genome amongst the human herpesviruses, with a length of around 235 kbp, with small strain-dependent variations²⁸. It is predicted to express about 751 translated open reading frames, encoding hundreds of proteins identified in proteomic studies, and around 26 MicroRNAs (miRNAs)^{29–32}. The genome of HCMV is divided into a unique long (UL) and unique short (US) region, each flanked by a pair of the terminal (TRL/TRS) and internal (IRS and IRL) inverted repeat³³.

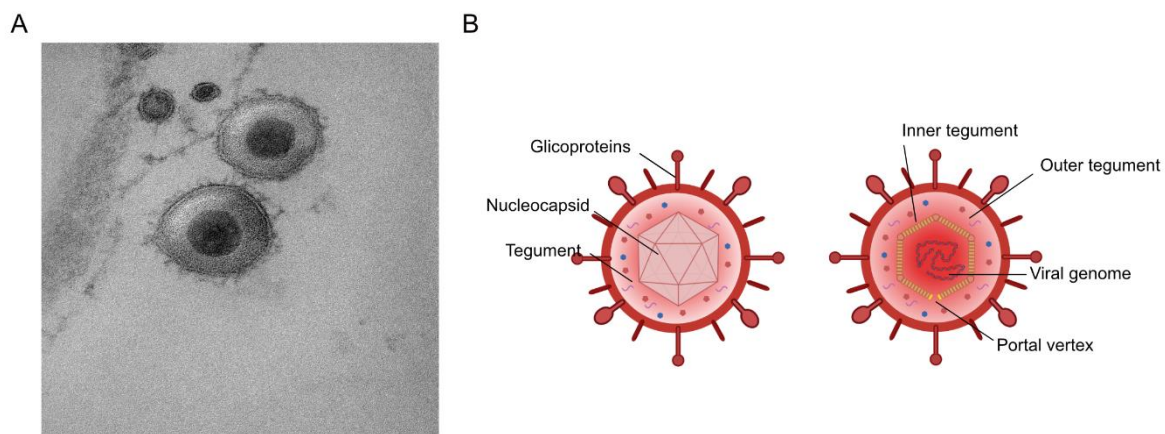


Figure 2: HCMV virion structure. A) Transmission electron micrograph of HCMV particles (by Felix Flomm). B) Schematic of an HCMV particle. The HCMV mature virion comprises an outer membrane called the envelope in which viral glycoproteins are embedded. An amorphous layer of proteins called the tegument is positioned between the envelope and the capsid. The icosahedral nucleocapsid surrounds the linear genome (created with Biorender.com).

3.2.4 Human cytomegalovirus: the replication cycle

Entry of HCMV virions is mediated by a range of glycoprotein complexes on the envelope that mediate initial engagement, attachment, and fusion by interacting with cellular receptors. At least two glycoprotein complexes mediate different spread modes and cell type tropism. The gH/gL/gO trimeric complex allows the cell-free spread of virions. In contrast, the presence of the pentameric gH/gL/UL128/UL130/UL131A complex allows the cell-associated spread in endothelial, epithelial, or myeloid cells^{34,35}. After fusing with cellular membranes, the capsid is released into the cytoplasm, where large parts of the tegument proteins dissociate from the capsids and contribute to the modulation of the host immune response (Fig. 3, A)²⁶. Inner tegument proteins, such as pp150, remain strictly associated with the capsid, while outer tegument proteins, such as pp71 or pp65,

move to different cellular localizations ²⁶. The capsid travels via active transport mediated by the cellular cytoskeleton to the nuclear pore complex, where the genome is expelled from the capsid through the vertex (Fig. 3 B) ³⁶. The genome then circularizes and is targeted by PML- Nuclear bodies (PML-NB), which contributes to their chromatinization as early as 30 minutes after infection ³⁷.

Modulating PML-NB antiviral proteins like Daxx and sp100 by tegument proteins and the dispersal of PML-NB itself allows early viral gene expression. Proteomics analysis showed the existence of 4-5 protein kinetic classes for HCMV expression ³¹. Classically, HCMV gene expression is divided into three kinetic classes similar to other herpesviruses: immediate early (IE) genes, early (E), and late genes (L). IE genes modulate antiviral pathways and allow the expression of E genes. E genes modulate cell metabolism and produce the viral DNA polymerase complex. L genes include the expression of virions components, such as capsid proteins, teguments, and glycoproteins. The RNA polymerase II-dependent expression of IE genes at the major immediate early promoter (MIEP) and the expression of the IE1 and 2 proteins are essential for the modulation of the innate immune system and act as transactivators of DE genes. The genome replicates in a virus-induced compartment called the viral replication compartment (RC), where many viral and cellular proteins localize ³⁸⁻⁴⁰. One of the earliest E genes, UL112-113, marks the formation of pre-replication foci at 5-6 hpi ^{40,41}. The viral polymerase UL54 and the polymerase accessory protein UL44 mediate the DNA replication at the origin of viral replication (OriLyt) through a rolling circle by producing long, concatemeric DNA. L genes encode proteins necessary for virions assembly, maturation, and egress. There are two classes of late genes: Gamma 1, which is expressed with a late kinetic but also at low levels at earlier time points, and Gamma 2, or true late genes, whose expression depends on viral DNA replication ⁴². After the start of DNA replication and expression of L genes, procapsids are assembled in the nucleus at the periphery of the viral replication compartment ⁴³.

The concatemeric DNA is cut by the terminase complex and injected in the procapsids by interacting with the vertex portal protein UL104 (Fig. 3, C) ⁴⁴. Two viral proteins, UL50 and UL53, form the nuclear egress complex (NEC) and mediate the passage of capsids to the cytoplasm by an envelopment-de-envelopment step through the nuclear membranes ⁴⁵. The DNA-filled capsids then migrate to the viral assembly compartment (AC). The AC is a donut-shaped structure built from cytoplasmic membranes and structured into domains ^{46,47,48}. Secondary envelopment, the cumulative morphogenesis step in which tegumented capsids bud into host-derived membranes, is

mediated in the AC. Enveloped capsids are then transported to the plasma membrane in exocytic vesicles, where they fuse, and release enveloped virus particles (Fig. 3, D)⁴⁹. Several non-infectious-like particles are also produced, such as non-infectious enveloped particles (NIEP), which lack the viral DNA inside the capsids, or dense bodies (DB) lacking a capsid⁵⁰.

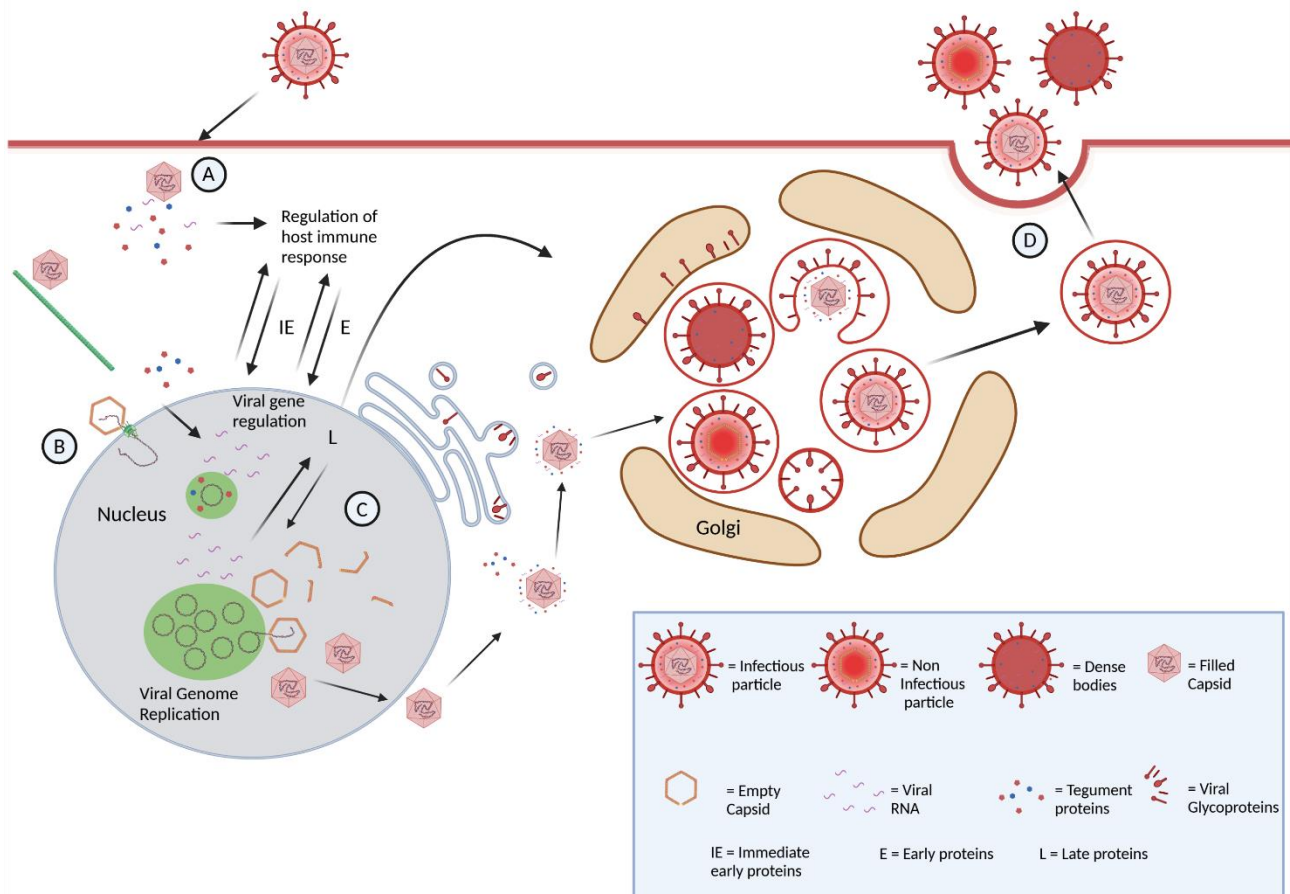


Figure 3: HCMV life-cycle: The virion interacts with cellular receptors for entry, and the viral membrane fuses with the cellular membranes. The capsid and the tegument are released into cell (A). The capsid is then transported to the nuclear pore complex on microtubules, where the linear viral genome is injected inside the nuclei (B). The linear genome then circularizes, and immediate-early and delayed early genes are transcribed. Viral replication occurs in viral replication compartments (RC) (C). Afterward, the newly synthesized genomes are packaged into capsids. Capsids leave the nucleus by an envelopment-de-envelopment step at the nuclear membranes. Final tegumentation and envelopment at cellular membranes are mediated in the assembly compartment (AC). Enveloped particles are then released by the fusion of exocytic vesicles with the plasma membrane (D). Created with Biorender.com.

3.2.5 HCMV replication compartments (RC)

The HCMV genome replication and transcription occur in specialized nuclear microenvironments called viral "replication compartments" (RCs). The RC is a membrane-less compartment that maintains a similar architecture and function in the whole *Herpesviridae* family. After the genome is injected into the host nucleus, PML-nuclear bodies (PML-NB) localize close to incoming viral genomes, where the early RC arises^{51,52}. PML components like sp100 or Daxx localize at the viral genome to suppress transcription and replication⁵³. Here the viral genome is chromatinized, as Daxx promotes histone deposition of H3 histones on it⁵⁴. The tegument protein pp71 then induces the degradation of Daxx, and IE1 expression leads to PML-NB dispersal by inhibiting the de novo SUMOylation of PML proteins⁵⁵. The degradation of repressive factors allows the localization of RNA polymerase II at the early RC and the transcription of viral genes⁵⁶. 11 proteins are essential for HCMV genome replication. These include the six core replication proteins conserved in herpesviruses (viral polymerase and its processivity factor, UL54, and UL44, tripartite helicase-primase complex (UL70, UL102, and UL105), and the single-stranded binding protein UL57⁵⁷. The two polymerase subunits, UL57 and UL44, co-localize at the RC as early as 12 hpi and are often used for identifying the RC⁴⁰. The UL44 polymerase accessory factor localizes at the periphery of the RC, where viral DNA synthesis occurs, with the newly produced DNA migrating to the center of compartment⁵⁸. The UL57 ssDNA binding protein is localizing with UL44 and the viral DNA at the periphery of the replication compartment^{40,58}, and it is thought to have a role in DNA repair. In addition to the 6 core proteins, HCMV needs another five accessory proteins to replicate its genome (RS1, UL36-38, UL84, immediate early 2 (IE2), and UL112-113^{60,59,60}. Of the five accessory proteins, only UL84, IE2, and UL112-113 are present in the RC. IE2 is expressed immediately upon infection and represents the major transactivator for viral gene expression⁶¹. IE2 promoter activity is regulated by UL84, which is only essential in some of the HCMV strains⁶². IE2 and UL84 can interact and repress each other's activity⁶³. The IE1 and IE2 proteins are localizing early with the viral genomes, essential for initiating transcription^{51,64}. The UL112-113 proteins are localizing to the RC at around 6 hpi, and it was proposed that UL112-113 proteins could orchestrate the assembly of the HCMV replication machinery⁴⁰. Nevertheless, their initial role in the RC formation is not well understood.

3.2.6 The HCMV UL112-113 proteins

The UL112-113 gene is divided into four exons and two introns. Its expression gives rise to 4 different isoforms by alternative splicing, p34, p43, p50, and p84, which share the same N-terminus encoded by exon 1 and have a C-terminus of variable length (Fig.4) ^{65,66}. The amino acid sequence of the N-terminus of UL112-113 is highly conserved among the *betaherpesviridae* family and is crucial for mediating the self-interaction of the 4 isoforms ^{67,68}. Moreover, UL112-113 proteins are cleaved by calpain-1 and 2, forming additional isoforms. p34 can be cleaved into p20, p26, p28, while p43, p50, and p84 can be cleaved into p38 and p34c ⁶⁹. By splice site mutagenesis, it was shown that the virus could grow to high titers in the absence of p34 and p50, while it was highly impaired in the absence of p84, and replication was not detected without p43 expression ⁶⁸.

UL112-113 proteins can bind to single-stranded (ssDNA) and double-stranded DNA (dsDNA) and localize with viral DNA before and during viral replication in infected cells ^{65,66}. How UL112-113 binds DNA is not known. The UL112-113 isoforms have transcriptional transactivator activity, mediated by two domains in the p84, p50, and p43 isoforms not present in p34 ⁷⁰. UL112-113 can also induce the lytic replication cycle of the Kaposi sarcoma virus, suggesting that its transactivator activity may not be limited to HCMV ⁷¹. Recently, a genome-wide CRISPR screen revealed that a lack of UL112-113 results in an abortive transcriptome trajectory comparable to the ones associated with latency ⁷². When expressed individually, the UL112-113 proteins localize in foci reminiscent of the early-stage RC formed adjacent to PML-nuclear bodies (PML-NBs) ⁵². The smallest isoform, p34, lacks nuclear localization signal (NLS) and localizes mainly in the cytoplasm when expressed alone ⁶⁷. The expression of the other three isoforms can restore the nuclear localization of the p34 in these structures ⁶⁷. UL112-113 proteins can form a complex in infected cells with IE2, UL84, and UL44 and directly interacts with UL44 ⁷³. Expression of UL112-113 proteins can induce the re-localization of UL44 and other viral core proteins inside foci formed by the UL112-113 ^{52,68}. This feature may implicate a structural role for the UL112-113 proteins in shaping the RC architecture by creating a space for localizing the replication machinery proteins.

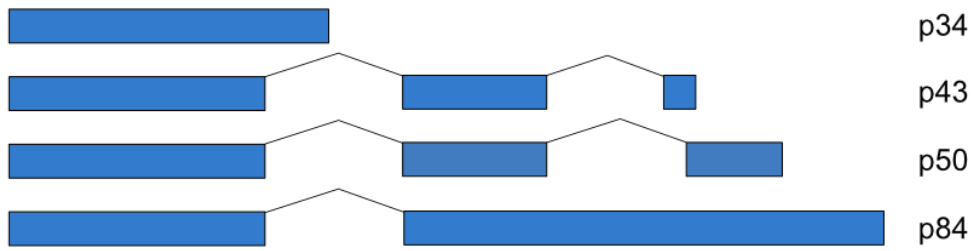


Figure 4: UL112-113 gene structure. 4 exons (shown in blue) and 2 introns form the UL112-113 gene. Alternative splicing results in four isoforms: p34,p43,p50, and p84, sharing the same N-termini and having a C-terminus of variable length. Scheme adapted from ⁷⁴.

3.3 Liquid-Liquid phase separation and membrane-less compartments

Cellular life depends on compartmentalization, and membrane-enclosed compartments have been studied extensively. Recently, membrane-less compartments and their genesis have come into focus, even though Edmund Beecher already hypothesized in 1899 that cytoplasm is a liquid emulsion. When studying starfish eggs, he defined their protoplasm as a meshwork in which the space is filled by drops of "liquids occupying spherical spaces" ⁷⁵. One hundred years later, in 1995, Walter and Brooks proposed that micro compartmentalization, which refers to the spatial organization of cellular matter, might arise due to phase separation mediated by macromolecular crowding in the cytoplasm ⁷⁶. In 2009 Brangwynne et al. then described liquid properties of P-granules exhibiting surface tension, high molecule mobility in the compartment, and, most importantly, concentration-dependent demixing and compartment formation ⁷⁷. These three characteristics defined the P granules as an assembly with liquid properties (Fig. 5, B). They proposed a model in which the formation of P granules is regulated by the phase separation of proteins from a soluble to a condensed phase, controlled by their solubility ⁷⁸. This process is called Liquid-liquid phase separation (LLPS), consisting of creating two distinct phases, one denser and one more dilute, which occurs when a group of molecules overcomes the thermal barrier for nucleation and separates from the solvent. Many other cellular compartments have been described to form different forms of phase separation, now known as biomolecular condensates ⁷⁹.

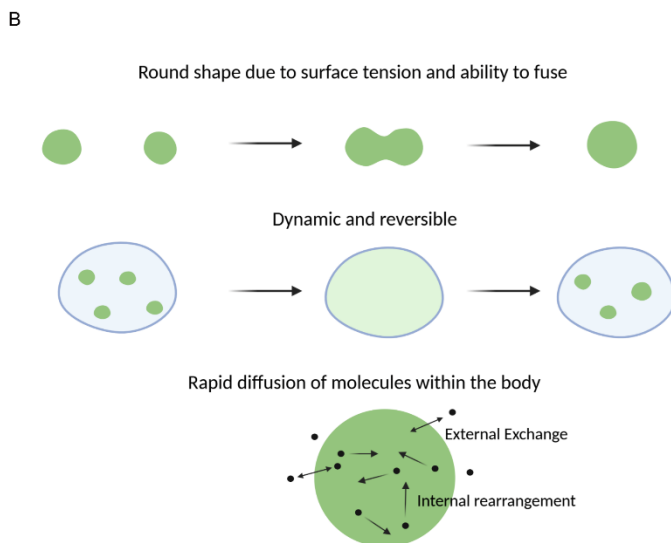
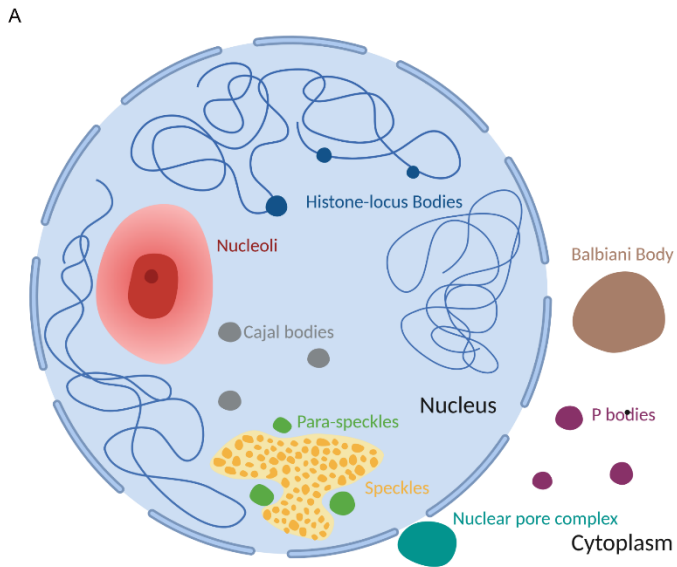


Figure 5: Membraneless organelles A) Graphic depicting different cellular membrane-less compartments in the nuclei and cytoplasm Adapted from ⁷⁹. B) Properties of compartments formed by LLPS. Circularity due to surface tension, Rapid reversibility of formation, and High diffusivity within the body. Images Created with Biorender.com.

3.3.1 Mechanism of liquid-liquid phase separation

LLPS has been a known mechanism in soft matter physics since it was established that polymers could form condensates governed by inter and intramolecular interaction. Brangwynne et al. proposed that biological LLPS may follow similar rules to polymer LLPS ⁷⁸. Phase diagrams can describe the phase behavior of a mixture of two components in a solution and their concentration-dependent separation into two phases as a function of their environment (such as pH, temperature, and pressure). In a simple binary mixture of a macromolecule in a solvent, the mixture is in the one-phase regime as the protein concentration is below the concentration saturation (C_{sat}). If the concentration of the molecule increases above the C_{sat} , the interaction between the solvent and the macromolecule becomes unfavorable, giving rise to a two-phase solution, with one component enriched in one phase and less present in the other and *vice versa*. The two phases are formed by spinodal decomposition (Fig.6, red line), a process that does not involve nucleation and occurs when there is no thermodynamic barrier to phase separation. In the binodal range at lower protein concentration, phase separation is limited by a thermodynamic barrier, which must be overcome through nucleation at specific sites and subsequent droplet growth (Fig.6, blue line) ⁸⁰. In biological systems, condensates are formed by a mixture of several components. In such complex systems, individual component concentrations rarely reach the concentration required for spinodal decomposition.

For this reason, spinodal decomposition is typically only observed in cases of very high overexpression of a specific component ^{81,82}. Therefore, LLPS in biological systems occurs mainly in the binodal regime via nucleation. In a non-living system, the nucleation rate is defined by the classical nucleation theory, which describes the kinetics of forming new phases by overcoming the energy barrier imposed by surface tension after reaching supersaturation ⁸³. In these systems, the location of the nucleation event can be regulated by surface heterogeneity ⁸⁴. Nucleation in biological systems may follow similar rules to nucleation in non-living systems, influenced by the supersaturation of a component and the significant heterogeneity of the cellular composition ⁸². In particular, the presence of slower-moving proteins or nucleic acids can provide a scaffold for the induction of protein nucleation even below the spinodal concentration threshold for LLPS ^{81,82}.

participate in attractive interactions by creating reversible physical interactions with the same molecule or with others through protein-protein and protein-nucleic acid interactions.

Usually, stickers are short sequences of around 10 amino acids. Their deletion drastically decreases the capability of the molecules to undergo phase separation, with their valency and stoichiometry being the essential characteristics ⁸⁹. The spacers increase the solvation volume and the inter-domain distance, modulating the strength of the bounds formed by the stickers and contributing to keeping the liquid characteristic of the condensates ⁹⁰. Systems featuring stickers and spacers comprise intrinsically disordered or hybrid proteins with one or multiple disordered domains and folded domains. These proteins often possess repetitive units given by the enrichment in some specific residues, conferring them multivalency and flexibility, necessary for establishing multiple but weak interactions. Proteins enriched in condensates typically incorporate intrinsically disordered proteins (IDPs) and intrinsically disordered protein regions (IDPRs).

The number of multivalent interactions between aromatic residues, like tyrosine, and positively charged residues, like arginine, can strongly influence the C_{sat} of a protein ⁹¹. Disordered domains can mediate interactions that include ionic bonds, hydrogen bonds, and interactions mediated by solvents. Another critical requirement for proteins involved in biological LLPS is the presence of domains that promote heterotypic interactions. These include domains that promote stable dimers or multimers and nucleic acid binding domains. The formation of heterotypic interactions can be vital for the localization-dependent induction of condensates. Below the saturation concentration (C_{sat}), no condensates should form, but local concentration can be increased locally by the presence of immobilized enzymes or nucleic acids ⁹². For example, interaction with nucleic acids, such as open chromatin, may provide a scaffold, locally decreasing the concentration threshold for LLPS ⁹³. The resulting condensates have different functions, such as controlling the chromatin structures or recruiting factors at the telomers ^{93,94}. The presence of RGG/RG domains in low complexity disordered regions can also mediate the formation of electrostatic interaction with RNA, increasing the valency of the molecule ⁹⁵. Overall, proteins undergoing LLPS in biological systems usually have three common characteristics: the presence of intrinsically disordered regions (IDRs), modular domains, and nucleic acids binding domains. These characteristics give these proteins the capability to phase-separate, but the mechanism underlying the formation of complex and functional compartments is much less understood.

3.3.3 Condensate maturation

Liquid condensates have been described to mature ^{96–98}. The maturation of protein condensates refers to a process in which the properties of condensates change over time and become less liquid. The slowing down of compartment dynamics induced by this transition has been considered one of the causes of several neurodegenerative diseases. An example is the liquid-to-solid transition of the RNA-binding protein FUS in amyotrophic lateral sclerosis (ALS) patients. Typically, FUS partitions into liquid compartments such as DNA damage sites and stress granules, but the presence of a mutation increases the tendency to form aggregate ⁹⁶. There are several potential avenues for this transition. Gelation is one example where the formation of additional crosslinks results in the transition from a viscoelastic fluid into a more solid structure. In contrast, liquid-to-glass transitions happen much slower until the components are rigidly arranged but lack long-range order.

Another way liquids can become solid is by forming fibers or crystals. Tau liquid droplets, for example, represent the first step for aberrant fiber deposition in the brain ⁹⁹. While the liquid-to-solid transition can be associated with several diseases, it has been proposed that biomolecular condensates are complex fluids that change biophysical properties over time. Passive and active rheology experiments have shown that the material properties of in vitro condensates are time-dependent ¹⁰⁰. Over time, analyzed condensates decrease their surface and diffusivity while the relaxation time increases linearly, behaving similarly to Maxwell fluids. In these fluids, elasticity changes little with the aging process, while the viscosity increases over time. As the condensates increase in concentration and the density increases, molecular components diffuse slower by increasing interaction with surrounding molecules ¹⁰⁰. Temperature also determines the condensates' aging behavior, with high temperatures blocking the aging process ¹⁰¹. Living cells can modulate the maturation processes, as different factors can affect phase transition. The fluidity of cellular condensate and its formation and dissolution depends on ATP concentration, indicating active processes, which cannot be recapitulated in vitro, as determinants for LLPS ¹⁰². The lack of defined structures makes disordered proteins quite susceptible to post-translation modifications (PTMS), which can affect the valency or the charges of the proteins involved in LLPS (reviewed in ¹⁰³). Nucleic acids can also play a role in tuning the material properties of condensates. While DNA molecules can form condensates on their own, shorter molecules induce the formation of liquid condensates.

In comparison, longer DNA molecules are associated with more irregular or solid-like states. Experiments with increasing the DNA length molecules and the histones 1 protein showed that the fluidity of these condensates is directly dependent on the number of interactions between molecules⁹⁷. While liquid-to-solid condensate transitions are often associated with pathological or non-functional conditions, there are examples of functional membrane-less compartments showing gel or solid-like properties. The Nuclear pore complex (NPC) is a typical functional hydrogel. The FG domain of the protein Nup153 forms a "Polymer brush"¹⁰⁴, which allows the restriction of the traffic molecules at the interface between the nucleus and cytoplasm. The Balbiani body is another example. This membrane-less structure is formed in the vertebrate oocyte only during dormancy. They are characterized by an amyloid-like structure, mediated by the prion-like domain of the protein Xvelo, forming a matrix in which mitochondria and RNA are incorporated¹⁰⁵. Balbiani bodies are dissolved upon oocyte reactivation, releasing their content. The mechanism of condensate aging is not yet well understood, but many compartments show similar properties, like slow-down dynamics and higher density (Fig. 7). Overall, the aging of liquid compartments is an important topic and might play a role in several human diseases¹⁰⁶.

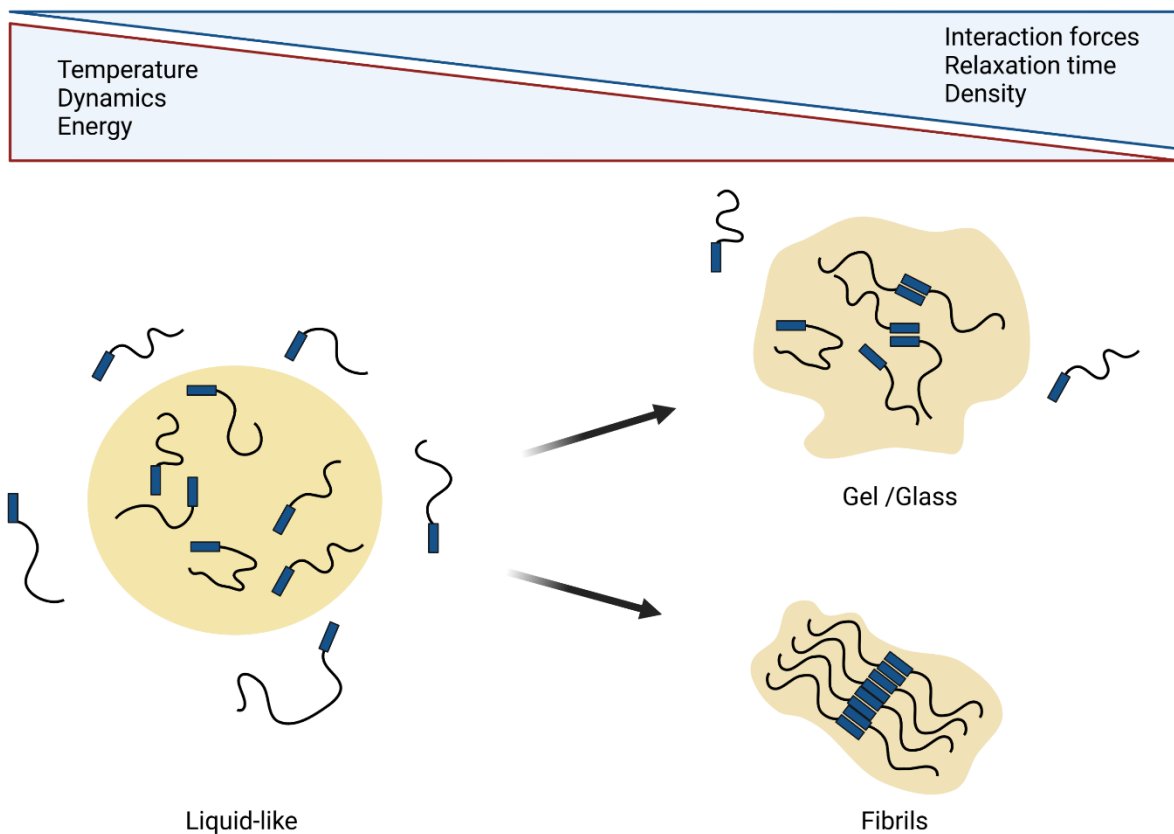


Figure 7: Potential mechanisms of condensate aging. Liquid condensates show high molecular dynamics. Transition into gel/glass or fibrillar states by increasing ordered interactions results in diminished dynamics. Image made with Biorender.com.

4 Aim of the study

HCMV forms a specialized membrane-less replication compartment where it replicates its large genome. It is still poorly understood how this process is regulated and which proteins are involved in its formation. Liquid-liquid phase separation (LLPS) has recently emerged as a framework for forming several cellular membrane-less compartments and the spatial-temporal regulation of biochemical function. We hypothesized that HCMV forms RCS by LLPS. We aimed to understand the HCMV replication compartment's formation dynamics and essential scaffold proteins that could play a significant role in its formation.

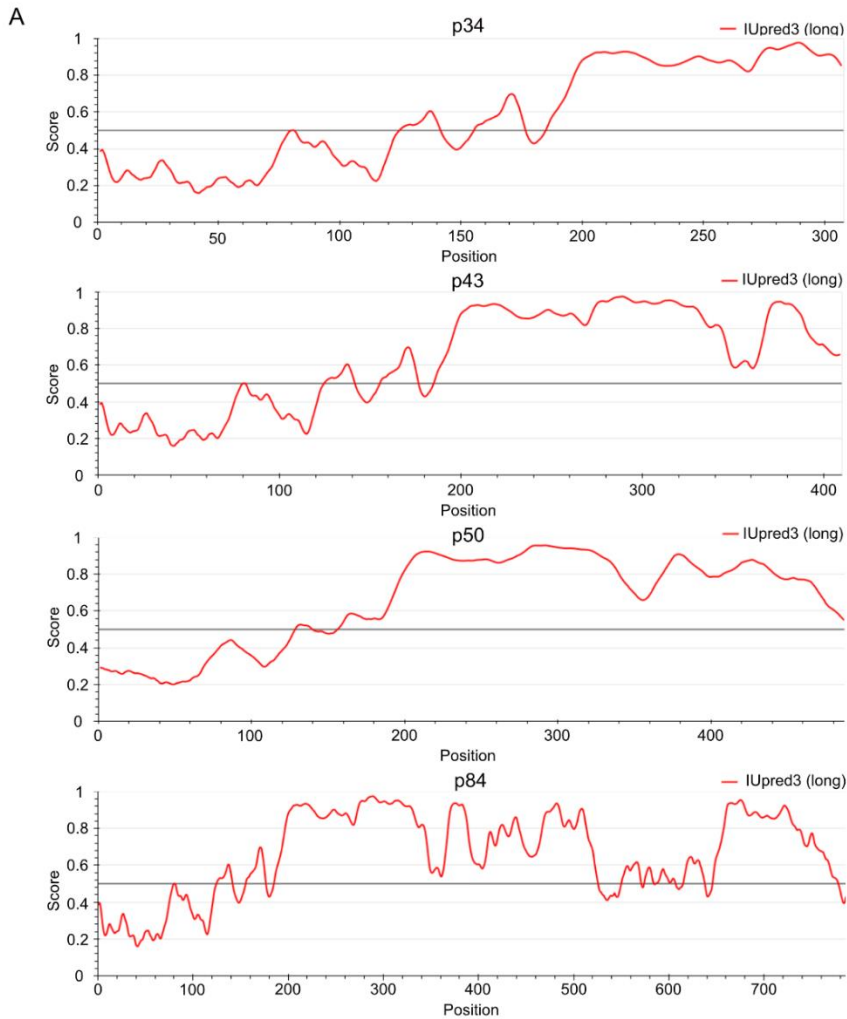
Furthermore, we wanted to assess if RC formation can occur *de novo* or if it needs the presence of pre-existing structures or seeds. Finally, we wanted to understand if LLPS is an essential feature for HCMV replication and how it contributes to it. This study provided a new structural function for the UL112-113 proteins and a model for HCMV replication compartment formation by LLPS. This mechanism might be conserved in other herpes or DNA viruses and a potentially novel drug target.

5 Results

5.1 Pre-replication compartments are fluid biomolecular condensates formed by LLPS

Wanting to identify viral proteins that could play a key role in HCMV replication compartment formation, we did an *in silico* analysis of proteins essential for viral DNA replication by analyzing their content in disordered regions. The UL112-113 gene gives rise to 4 alternatively spliced transcripts (p34,p43,p50, and p84; Fig. 4) that share a common N-terminal region encoded by the exon 1 and a variable length C-terminus. We found that the common N-terminus is highly ordered, and the C-terminal regions of all 4 isoforms are enriched in glycine/serine repeats and highly disordered (Fig 8, A). We also used AlphaFold2 to generate a structural model of the largest isoform, p84¹⁰⁷. Based on this prediction, the N-terminal part of the protein forms a beta-barrel core, while the rest of the protein is highly disordered (Fig. 8, B).

Moreover, UL112-113 proteins are already known to have high valency by being capable of dimerizing through their N-terminus, binding to DNA, and interacting with the processivity factor UL44. When UL112-113 proteins are expressed outside the viral context, they can form intranuclear foci reminiscent of early viral RC⁶⁸. Together, this information highlighted UL112-113 proteins as possible scaffolds for forming the RC by LLPS. Several biophysical properties usually characterize liquid biomolecular condensates: sphericity by surface tension, high internal and external molecular mobility, as well as the capacity to form and dissolve in a short time (Fig. 5, B)^{78,79}. Wanting to analyze the RC biophysical properties by live fluorescence microscopy, we used *en passant* mutagenesis to modify the HCMV TB40 BAC4¹⁰⁸. A fluorescent mNeogreen tag was fused with a 6x GGS linker to the shared N-terminus of the gene to tag all 4 isoforms. Virus growth was only slightly affected at the later time points (Fig. 9, A).



B

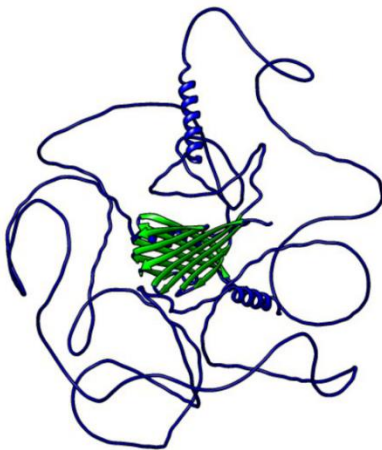


Figure 8: The C-terminus of UL112-113 isoforms is highly disordered (A) Disorder plots of the UL112-113 isoforms. UL112-113 protein isoforms were analyzed by IUPred3¹⁰⁹ to predict disordered regions. The degree of disorder is scored on a scale from 0 to 1, with 1 indicating the highest level of disorder. Extended disordered regions are found in all four isoforms. The shared N-terminus is highly ordered. B) AlphaFold2 prediction of the largest UL112-113 isoform p84. The ordered N-terminus is highlighted in green.

As the growth defect of the virus was minimal, we decided to use the recombinant virus as a model for studying the RC by microscopy assays. By infecting fibroblasts with the newly generated fluorescent virus, we could visualize the formation of RCs by fluorescent live-cell imaging. We could detect a fluorescence signal as early as 5 hpi, followed by the appearance of fluorescent foci resembling the pre-replication compartments (PRCs), which slightly enlarged, keeping the same shape till 24 hpi (Fig. 9, B). Optical sections of these early structures mainly had areas of 1-2 μm^2 (Fig. 9, C), quite dynamic as we regularly observed them moving in the nucleus. Their aspect ratio was close to 1, indicating a primarily spherical shape (Fig. 10, D). Analysis by fast live-cell imaging revealed that PRCs readily coalesced (Fig. 9, E-F). These results indicate that PRCs exhibit surface tension similar to other described biomolecular condensates^{78,79,110}.

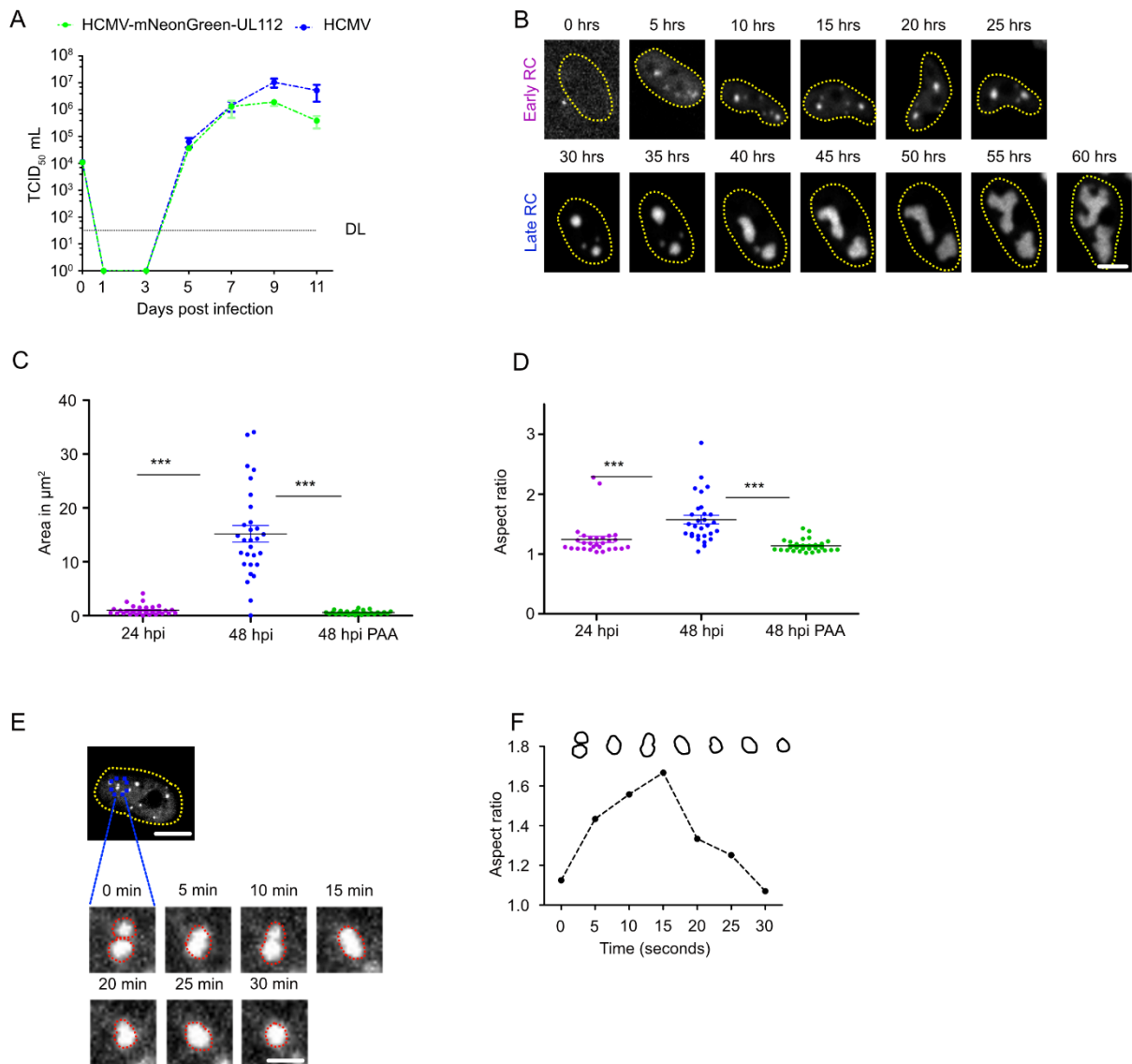


Figure 9: UL112-113 forms liquid condensates: (A) Growth kinetics of Wt and HCMV-mNeongreen-UL112 viruses in MRC-5 cells. Cells were infected at an MOI of 0.1, and the supernatant virus was titrated by TCID50. (B) The transition of pre-replication compartments to mature replication compartments. Time-lapse imaging of MRC-5 cells infected with HCMV-mNeongreen-UL112 at an MOI of 10, analyzed by spinning disk microscopy. Pictures show a z-maximum projection of 10 z-stacks—a frame every 20 minutes was recorded. Yellow dotted lines nuclear boundaries. The scale bar is 10 microns. (C-D) Quantifying size (C) and aspect ratio (D) of PRC and RC in MRC-5 cells infected with HCMV-mNeongreen-UL112. Infected cells were imaged at 24 hpi, 48 hpi, or 48 hp in the presence of phosphonoacetic acid (PAA). ImageJ analyzed images. An aspect ratio close to 1 indicates roundness. Higher values indicate an irregular structure. (E) Time-lapse of an MRC-5 cell infected with HCMV-mNeonGreen-UL112 at an MOI of 1. At 24 hpi, UL112-113 droplets undergoing fusion were imaged by spinning disk microscopy. One frame was recorded every 5 minutes. The images show a z-maximum projection of 15 stacks each. The scale bar is 10 microns and 2 microns in the insets. (F) The aspect ratio of fusing foci from (E) was analyzed for every frame by ImageJ.

Starting from 24 hpi, PRCs appeared less dynamic and began to expand, losing sphericity (Fig 9, B). At 48 hpi, the mature RC grew 15-fold while transforming into a pleiomorphic irregular structure, as indicated by the higher aspect ratio compared to PRC (Fig 9, C-D). We could not detect any fusion events of RCs as these structures appeared immobilized or moved much slower than PRCs. These data suggested that the PRC's shape is governed by surface tension, while in mature RCs, intramolecular bond strength might be higher than surface tension allowing the formation of an irregular shape. Next, we asked if weak interactions govern PRC and RCs formation. 1,6 Hexanediol (1,6-HD) is often used to characterize biomolecular condensates, as it impedes the weak interactions between the disordered domains¹¹¹. We treated infected cells at 24 hpi and 48 hpi for 90 minutes and imaged them by live spinning disk microscopy. 2% vol/vol 1,6-HD led to a rapid dissolution of PRCs, with a subsequential fluorescence intensity loss in the foci and the dispersal of UL112-113 proteins (Fig. 10, A). By contrast, it only partially affected mature RCs, which appeared dimmer immediately after adding the compound, indicating that only a fraction of molecules in the RC are sensitive to the treatment (Fig 10, A). 90 minutes after the 1,6-HD addition, we replaced the conditioned media with fresh media without the drug. Notably, the treatment appeared reversible, as we observed the reappearance of spherical foci at 24 hpi and increased fluorescence intensity in the RCs at 48 hpi right after removing the inhibitor (Fig. 10, B). Then, we wanted to know if data obtained with 1,6-HD could be repeated with another less toxic compound, as 1,6-HD was reported to affect membrane stability and cell viability¹¹¹. We took advantage of propylene glycol (PG), as it was recently used to affect rotaviruses compartments in the cytoplasm, and it is well tolerated by cells when used below 5% vol/vol^{112,113}. Like the previous experiment with 1,6-HD, we observed a fast dissolution of PRCs upon adding 5% PG; meanwhile, RCs were unaffected by it (Fig. 10, C). These data suggest weak interactions as a major player in the formation of the PRC; meanwhile, it argues for the formation of more stable bonds in the RC, which are not affected by LLPS inhibitors. As high mobile fractions and high diffusivity usually characterize biomolecular condensates, we wanted to analyze the recovery rates of PRC and RC by Fluorescence Recovery After Photobleaching (FRAP). We observed a fast and almost total recovery of fluorescence intensity in PRCs (Fig. 10, D-E). The high exchange of molecules within the PRC, indicated by nearly 100% of mobile fraction and fast half-time recovery of around 20 seconds (Fig. 10, G-H), revealed high molecular trafficking, comparable with many liquid biomolecular condensates. By contrast, photobleaching of RCs resulted in a slower and incomplete recovery (Fig. 10, D-E), as the percentage of mobile UL112-113

decreased by 15-20% and the half-time recovery slightly increased (Fig. 10, G-H). As UL112-113 was shown to bind DNA in infected cells and all data indicated a shift in biophysical properties right after the onset of viral DNA replication, we asked if inhibition of DNA replication would affect UL112-113 mobility. When we treated infected cells with phosphonoacetic acid (PAA), PRCs did not transform into RCs but remained small and spherical (Fig. 10, C-D). Photobleaching at 48 hpi resulted in a faster fluorescence intensity recovery than the RC (Fig. 10, D-E). We calculated a highly mobile fraction and half-time recovery of around 15 seconds (Fig. 10, G-H), indicating that the absence of newly synthesized DNA or DNA replication was responsible for the immobilization of UL112-113 in the RC. Overall, PRCs appeared to possess all the characteristics of a fluid biomolecular condensate, as the shape was governed by surface tension, they were sensitive to inhibitors of weak interactions, and 112-113 molecules showed high diffusivity. By contrast, the onset of viral DNA replication appeared to induce a further phase transition, leading to a more complex, less fluid structure (Fig. 7).

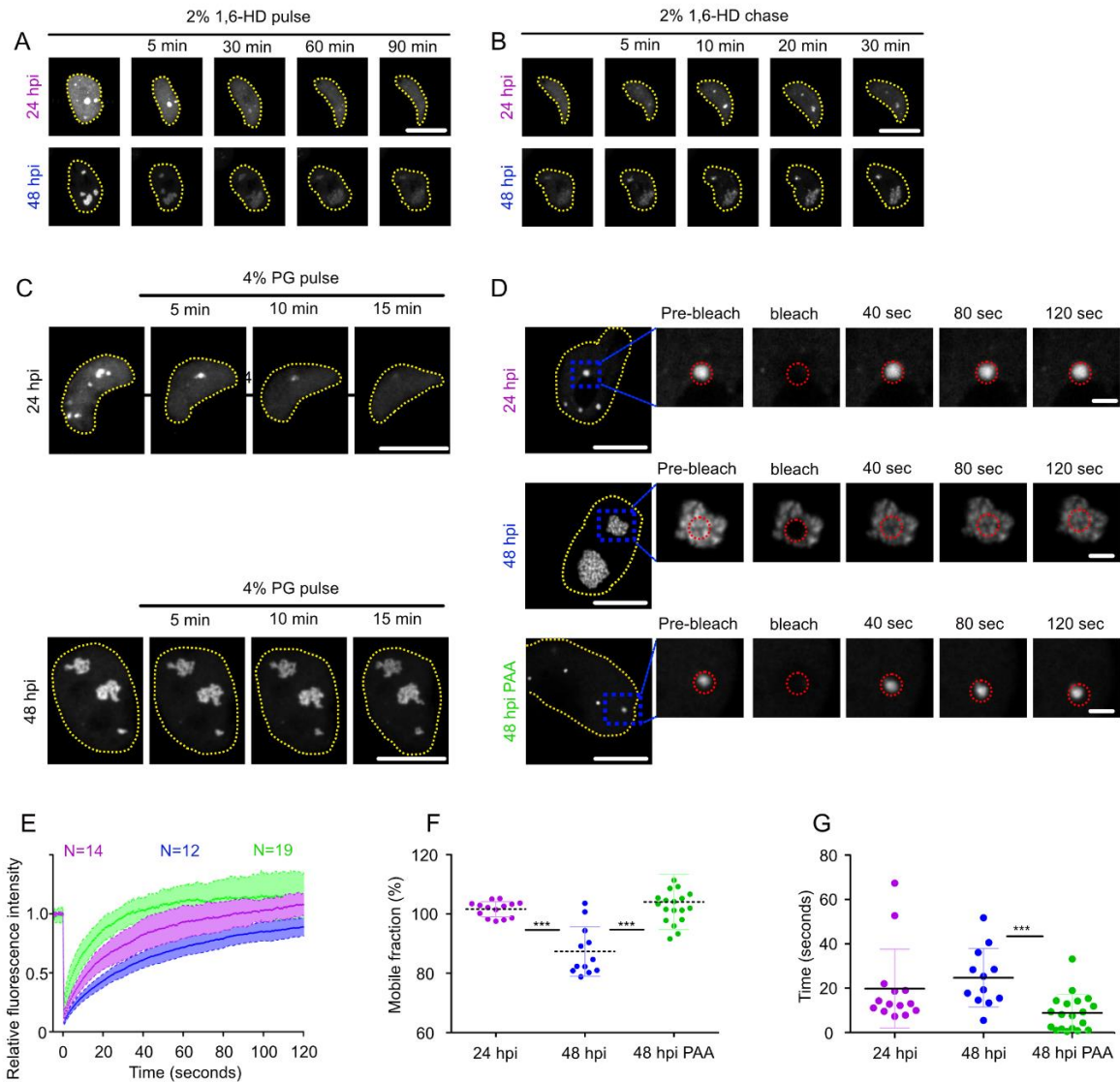


Figure 10: The onset of viral DNA replication induces immobilization of UL112-113 proteins and RC phase transition (A-B) Chemical inhibition of LLPS in infected cells by 1,6 Hexanediol (1,6-HD). MRC-5 cells were infected with HCMV-mNeonGreen-UL112 at an MOI of 1 for either 24 h or 48 h and treated with 2% 1,6-HD for 90 minutes (A, pulse) and imaged by live-cell spinning disk microscopy for 90 minutes. Afterward, 1,6-HD containing medium was replaced by a traditional medium, and cells were imaged for another 30 minutes (B, chase). Pictures show a z-maximum intensity projection of 9 slices. (C) Chemical inhibition of infected cells by Propaneglycol (PG). MRC-5 cells were infected with HCMV-mNeonGreen-UL112 at an MOI of 1 for either 24 h or 48 h and treated with 4% 1,6-HD (pulse). Cells were imaged by live-cell spinning disk microscopy for 15 minutes. Pictures show a maximum intensity from 9 z- stacks. (D) Fluorescence recovery after photobleaching (FRAP) kinetic of MRC-5 infected cells. Cells were infected with HCMV-mNeonGreen-UL112 at an MOI of 1 for 24 or 48 hpi or treated with 250 $\mu\text{g}/\mu\text{l}$ phosphonoacetic acid (PAA) for 48 h and analyzed by FRAP. Ten frames were recorded to obtain the initial average fluorescence intensity, then a 1 μm spot was bleached, and fluorescence recovery was recorded for two frames per second for 120 seconds. (E) FRAP curves show the average recovery rates of N cells from each condition. (F) Mobile fraction and (G) half-time recovery extrapolated from (E). Data are shown as mean \pm SD. Yellow dotted lines indicate nuclear boundaries. The scale bar is 10 microns and 2 microns in the insets.

We used Correlative Light and Electron Microscopy (CLEM) to generate a first approximation of RC ultrastructure. We seeded MRC-5 cells in gridded thin-film growth supports and infected them at an MOI of 0.1. At 72hpi, we acquired confocal 3D stacks of infected nuclei (Fig. 11, A). As observed before, UL112-113 marked compartments took most of the nuclear space and formed a pleiomorphic structure. Afterward, cells were fixed and prepared for Serial Sectioning Block Face Scanning Electron Microscopy (SBFSEM) (Fig. 11, B). Correlation of the resulting 3D volumes indicated that fluorescent 112-113 signals overlapped with electron-dense areas in EM, indicating that RCs are dense nuclear structures (Fig. 11, C). As expected, we did not observe any membranes surrounding the RC, confirming its membrane-less nature.

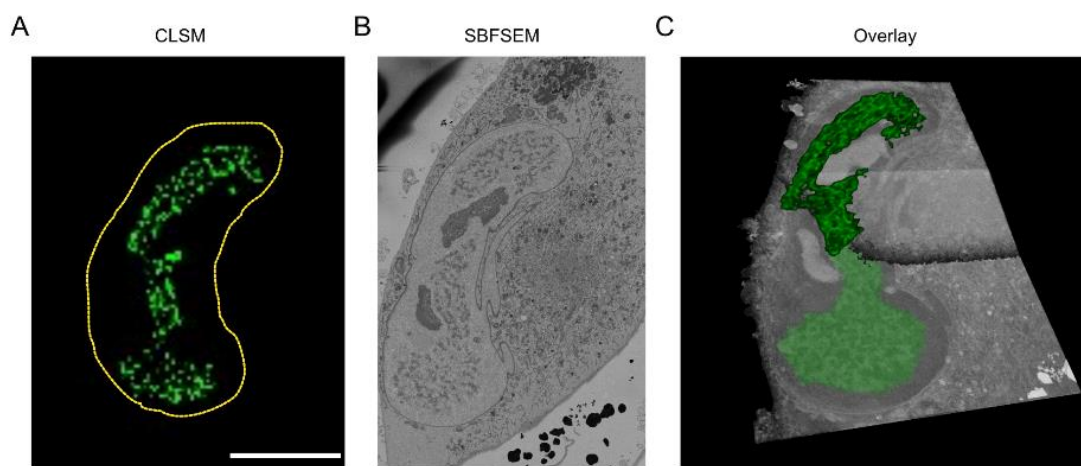


Figure 11: The RC is an electron-dense structure. A) Correlative Light and Electron Microscopy (CLEM) of HCMV-mNeonGreen-UL112 infected cells. MRC-5 cells were seeded on gridded growth supports and infected at an MOI of 0.1. Seventy-two hours post-infection, infected cells were imaged live by confocal laser scanning microscopy (CLSM), and 3D stacks were recorded. B) Subsequently, cells were prepared for volume imaging by Serial Sectioning Block Face Scanning Electron Microscopy (SBFSEM). C) Overlay of the CLSM and SBFSEM volumes of the same cell. Yellow dotted lines indicate nuclear boundaries. The scale bar is 10 microns.

5.2 UL112-113 forms fluid biomolecular condensates without the contribution of other viral proteins

UL112-113 proteins can be found in nuclear foci when expressed in transfected cells without other viral components⁶⁸. These foci have a shape reminiscent of PRCs, and the polymerase processivity factor UL44 is recruited into these foci. Therefore, we next transfected cells with UL112-113 to

characterize the properties of these foci. We could detect the expression of all four isoforms in transfected cells (Fig. 12, A). About 10-20 foci were typically found per nucleus, as previously observed^{68,114}. Threedimensional confocal imaging revealed that these foci were almost perfectly spherical (fig. 12, B). Analysis by fast live-cell imaging indicated that UL112-113 foci were highly mobile and prone to fuse. (Fig. 12, C-D). Next, we tested the susceptibility to 2% 1,6-HD. As a negative control, we used the mCherry-tagged M45. This viral protein from murine cytomegalovirus was shown to form an insoluble cytoplasmatic aggregate in infected and transfected cells¹¹⁵. When co-transfecting mNeongreen-UL112-113 and mCherry-M45 in 293A cells, we observed the formation of large M45 inclusions (magenta) in the cytoplasm and UL112-113 (green) spheres in nuclei (Fig.12, F). As expected, the addition of 2% 1,6-HD barely affected the integrity of M45 inclusions, as proteins in the inclusions interact by covalent binding of their IPAM domains¹¹⁵. By contrast, 1,6-HD inhibition completely dissolved UL112-113 droplets in less than 1 hour (Fig. 12, F). Removal of the compound reversed dissolution, indicating the specificity of the treatment. We further confirmed these results by using 4% 1,2-PG. Again, we observed rapid dissolution of UL112-113 foci, while M45 inclusions remained unaffected (Fig. 12, G). Next, we analyzed the molecular mobility of UL112-113 in transfected cells by FRAP. As controls, we used M45 cytoplasmatic aggregates and the phase-separating nucleolin and photobleached a region of 1 micron^{115,116}. Photobleaching of nucleolin indicated an extremely fast and complete recovery after photobleaching, highlighting quick exchange between nucleoli and nucleoli as previously reported¹¹⁷. M45 aggregates only recovered to about 5-10%, as previously reported (Fig. 12, F)^{115,117}. Fully bleached UL112-113 droplets recovered almost entirely within a minute (Fig. 12, F), resulting in a mobile fraction of nearly 100%, indicating a high molecular turnover comparable with other biomolecular condensates (Fig. 12, I)¹¹⁸. Overall, these experiments showed that UL112-113 proteins could form liquid biomolecular condensates without the contribution of other viral proteins.

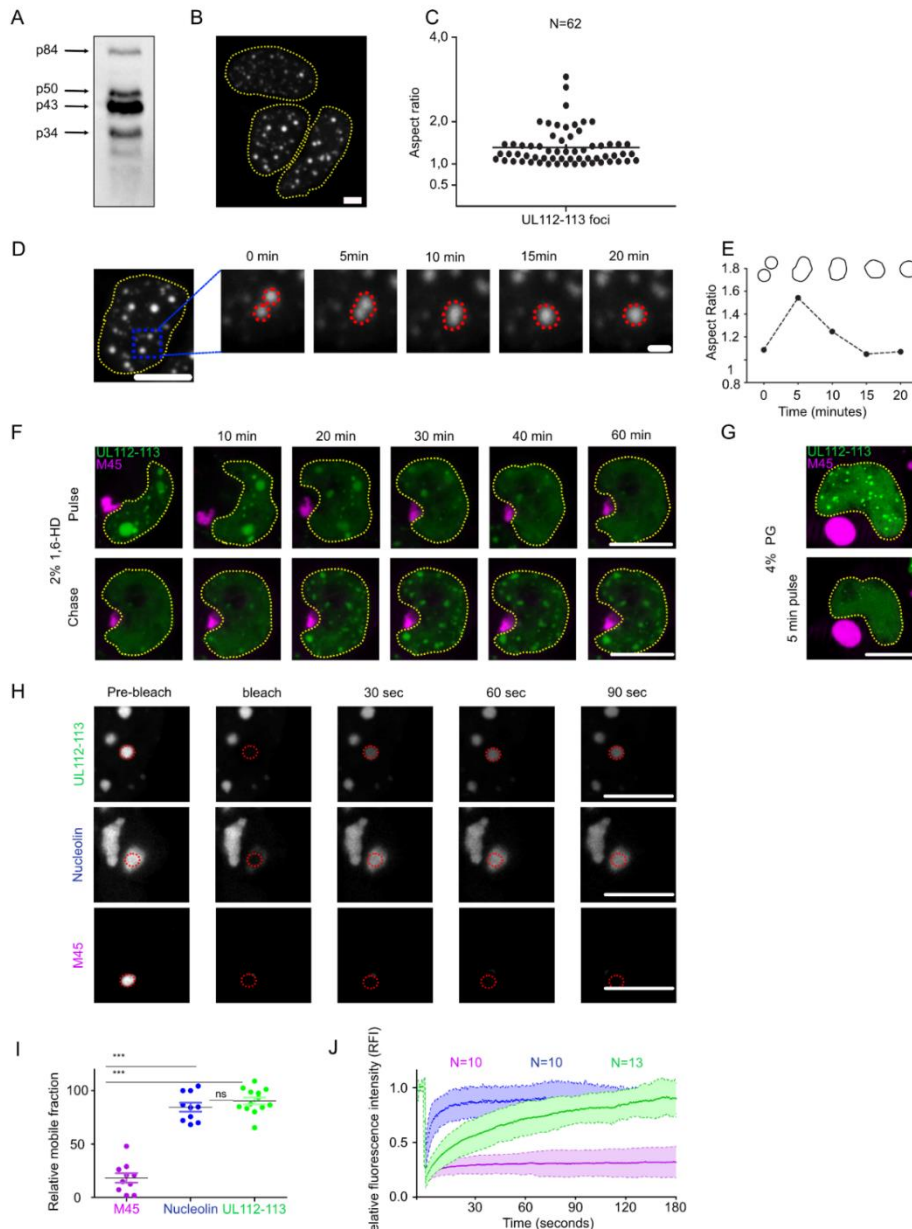


Figure 12: UL112-113 phase separation is independent of other viral factors. A) 293A cells were transfected with the plasmid encoding mNeogreen-UL112-113. All four isoforms were detected by mNeogreen antibody. B) mNeogreen-UL112 transfected cells were visualized by spinning disk microscopy at 48hpt. C) Quantification of mNeogreen-UL112 foci aspect ratio from (B). D) Live cell imaging of mNeogreen-UL112 cells to analyze foci movement and fusion. Pictures show a maximum z-projection of 11 stacks. E) Aspect ratio of foci from (D) was analyzed frame by frame with ImageJ. F-G) 293A cells were co-transfected with mNeogreen-UL112 or mCherry-M45 for 48 hours, pulsed with 2% Hexanediol 1,6(1,6 HD) (in F) or Propanglycol (PG) (in G) and analyzed by live-cell spinning disk microscopy (Pulse). To assay the reversibility of the treatment, 1,6 HD was replaced with a normal medium (Chase). H) Fluorescent recovery after photobleaching (FRAP) experiment of 293A cells transfected with mNeogreen-UL112, mCherry-Nucleolin, or mCherry-M45. A spot of 1 μ m diameter was bleached, and fluorescence was recorded at two frames per second for 2 minutes. I) Relative mobile fraction extracted from (H). J) Recovery curves of FRAP experiment of N cells per conditions. The yellow dotted lines indicate nuclear boundaries. The scale bar is 10 microns and 2 microns in the insets.

5.3 Clustering of UL112-113 disordered regions by the ordered N-terminus is sufficient for LLPS

As we could show that the UL112-113 proteins form liquid compartments in transfected cells without other viral proteins, we wanted to know if they could undergo LLPS *in vitro*. We used a naturally present 6x Histidine tag in UL112-113 of interest and purified protein from 293 cells expressing mNeongreen-UL112-113. The SDS page indicated some impurities, while the western blot of the lysate confirmed the presence of all 4 isoforms (Fig. 13, A). We could not eliminate nucleic acid contaminants during the preparation as we observed a 260/280 nm ratio of 1.2 even after extensive nuclease treatment. Mixing the purified protein with a low salt concentration buffer induced the formation of spherical fluorescent droplets (Fig. 13, B) reminiscent of PRCs and those observed in UL112-113 transfected cells. The number and size of droplets increased significantly with the used protein concentration. Droplet formation could be omitted by increasing salt concentrations, while droplet formation was enhanced in physiological or lower salt concentrations (Fig. 13, C-D). As salt inhibits ionic interactions, ionic interactions mediated by UL112-113 IDRs may be essential for establishing the phase. In line with previous results, 1,6 HD inhibits *in vitro* droplet formation of UL112-113 (Fig. 13, B). Purified mNeongreen did not form any droplets at any condition (Fig. 13, B). We concluded that the UL112-113 proteins could undergo LLPS *in vitro*, likely mediated by weak interactions due to their sensitivity to high salt concentrations and 1,6-HD. As we could not obtain nucleic acid-free UL112-113, we cannot exclude the importance of nucleic acids in UL112-113 LLPS.

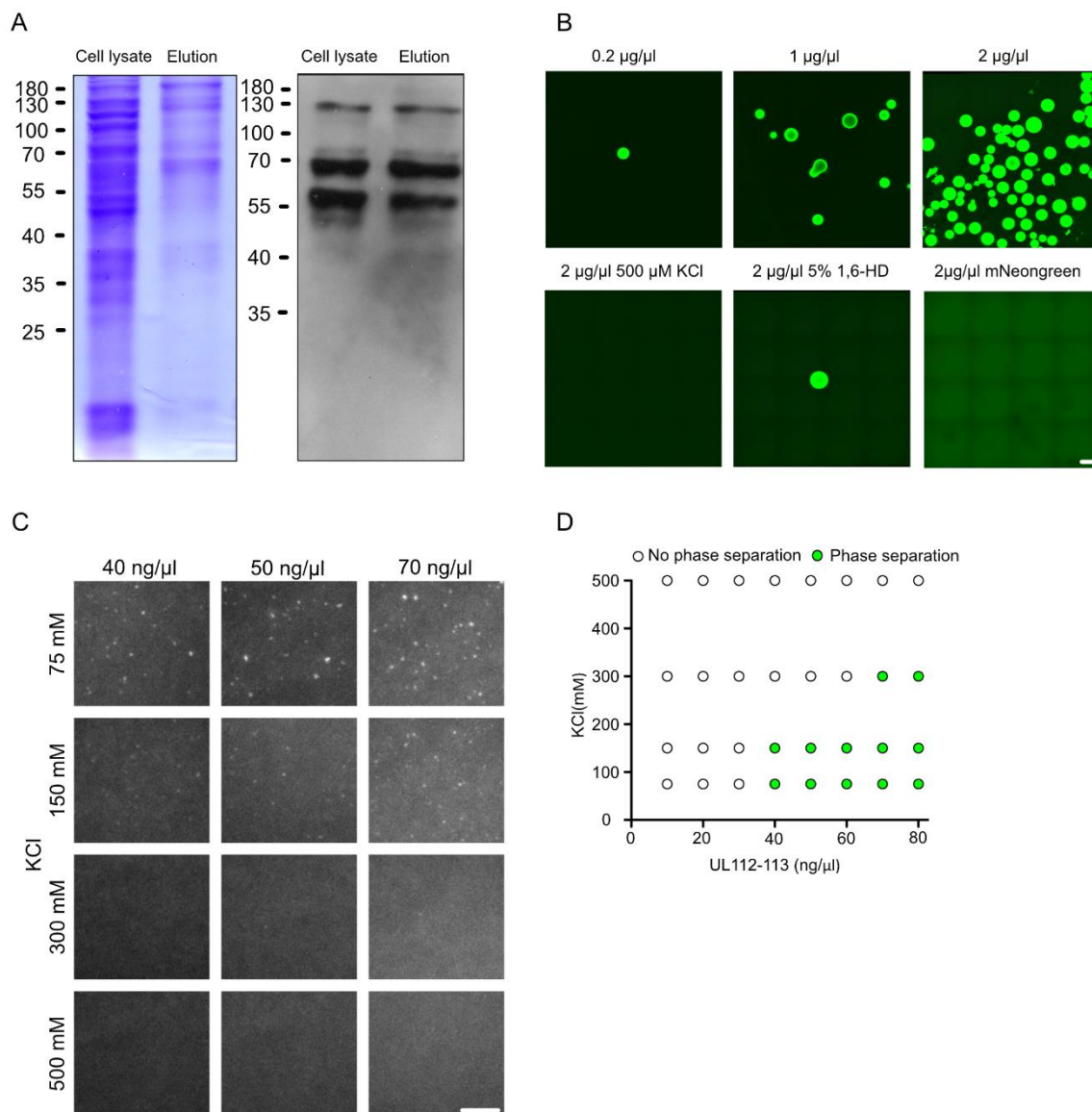


Figure 13: UL112-113 proteins can form liquid compartments in vitro: A) Blue Coomassie and western blot of 293T-Rex cells expressing mNeogreen-UL112 after and before the elution from Histidine beads. UL112-113 isoforms were detected by mNeogreen antibody. B) In vitro phase separation assay of mNeogreen UL112 purified protein. Phase separation was induced by mixing the proteins with low salt concentration (75 mM KCl). High salt concentration or 5% 1,6 HD buffers inhibited LLPS. Proteins were visualized by confocal microscopy. The scale bar is 10 μm . C) In vitro phase separation assay of mNeogreen-UL112 proteins. Proteins were mixed with increasing salt concentration (75 to 500 mM KCl), spotted in a slide, and visualized by widefield microscopy. The scale bar is 100 microns. D) Quantification of observed phase separation from (C).

We were then interested in uncovering the mechanism of UL112-113 LLPS. Classically, phase-separated compartments need weak interactions driven by disordered regions and more

specific/strong bonds mediated by ordered regions. UL112-113 proteins have an ordered N-terminus responsible for the oligomerization of the isoforms, and an intrinsically disordered C-terminus fulfills this structure (Fig. 8, A-B). To study this mechanism, we used the "corelet" system, a recent technology to study phase separation in living cells⁸¹. This system consists of a ferritin protein (FTH1) that can self-assemble into a 24-mer core, conjugated to a GFP for visualization and to a conditional oligomerization domain (iLID). A disordered domain of a protein of interest is mCherry-sspB (Fig. 14, A). When both components are expressed in the cells, they are not interacting, as iLID is inactive. When iLID on the ferritin core is activated by blue light, each of the 24 subunits of the core can bind an sspB/IDR component, and phase separation is induced. To test if UL112-113 IDRs are sufficient to drive LLPS when clustered, we cloned the IDR of the most important isoforms, p84, and p43, onto mCherry-sspB⁶⁸. We omitted the shared N-terminal part essential for oligomerizing the isoforms (Fig. 14, B)⁶⁷. We worked only with p43 and p84; as previously shown, they are the isoform most crucial for viral replication⁶⁸. As a negative control, we used a vector encoding mCherry-sspB, lacking an IDR, and the IDR of HNRPA1, a stress granule protein, as a positive control. Without blue light, both components are dispersed in the cell nuclei (fig. 14, C). Upon activation with blue light, we could immediately observe clustering and droplet formations in cells expressing p43 or p84-sspB, with a similar kinetic of cells expressing HNRPA1-sspB (Fig. 14, C). By contrast, we could not observe any clustering in cells expressing mCherry-sspB, indicating that the presence of an IDR is essential for driving LLPS with the corelet system (Fig. 14, C). These data suggest that UL112-113 proteins can form phase-separated compartments by clustering their disordered domains through the oligomerization domain. Moreover, they suggest that the disordered domain of UL112-113 allows the protein to undergo liquid-liquid phase separation *in cellulo*, independently of other viral and cellular proteins.

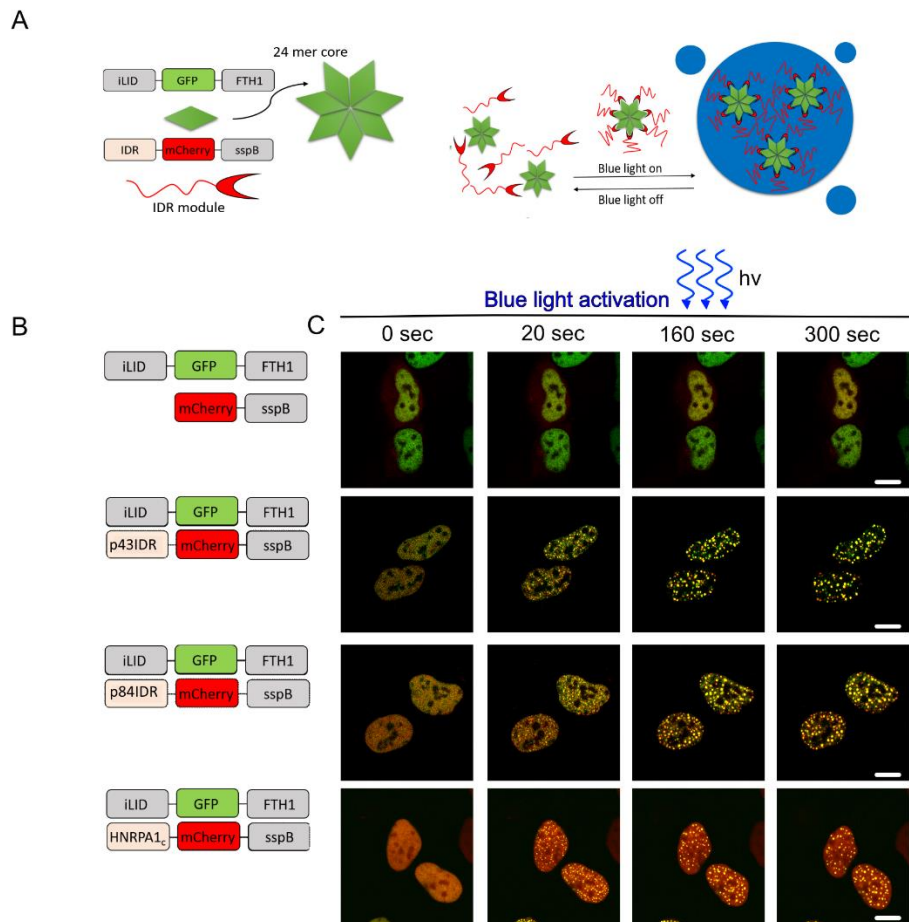


Figure 14: Clustering of UL112-113 disordered regions is sufficient for LLPS A) Scheme of the "Corelet" system adapted from Bracha et al. 2018. The ferritin core self-assembles into a 24-mer core complex, while sspB-IDR remains a monomer. The two components are not interacting, but upon blue light stimulation, the ferritin core binds the sspB-IDR module; IDRs interact with each other by weak, non-covalent interactions, eventually inducing the formation of phase-separated compartments. B) Constructs depicted were transduced in 293A cells. C) Cells transduced with constructs depicted in (B) were continuously photoactivated with blue light for 300 seconds and imaged by confocal microscopy. The scale bar is 10 microns.

5.4 Exogenous DNA lowers the UL112-113 concentration threshold for liquid-liquid phase separation

As UL112-113 proteins were reported to have DNA binding activity⁶⁶ and we observed an immobile fraction increase during viral DNA replication in infected cells (Fig. 10, F), we asked if the presence of free DNA could impact UL112-113 phase separation in cells. As both in infection and transfection,

exogenous DNA is introduced into the host nucleus, we next wanted to investigate if the UL112-113 phase separates in the absence of exogenous DNA. To do that, we produced a cell line in which mNeogreen-UL112-113 is expressed endogenously under the control of a doxycycline-inducible promoter. When cells were kept in a doxycycline-free medium, UL112-113 proteins were not expressed.

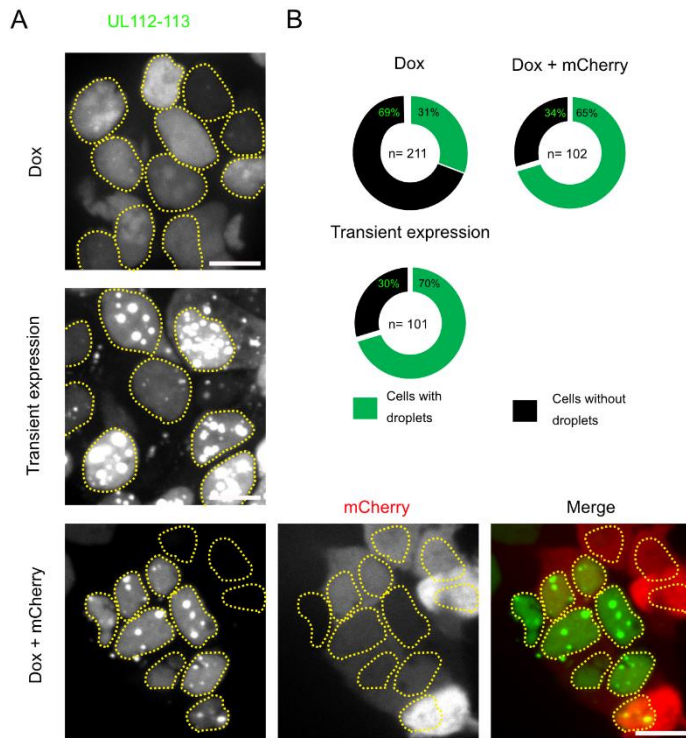


Figure 15: The presence of exogenous DNA is essential for droplet formation. A) 293 T-Rex cells were induced with 2 $\mu\text{g}/\text{ml}$ doxycycline (Dox) or transfected with a mNeogreen-UL112 plasmid (transient expression) for 24 hours. Cells were transfected or mock transfected with mCherry plasmid (Dox + mCherry) 24 hours before induction to simulate the introduction of exogenous DNA. B) Quantification of cells with or without droplets in different conditions, as shown in (A). The yellow dotted lines indicate nuclear boundaries. The scale bar is 10 microns.

The addition of 2 $\mu\text{g}/\text{ml}$ doxycycline resulted in the expression of UL112-113 proteins in 293 T-Rex cells. Surprisingly, at 24 hours post-induction, most proteins were dispersed in the nuclei in around 70% of the cells. We measured fluorescence intensity as a proxy of protein concentration in induced 293 T-Rex and infected fibroblast. We observed a 3 fold increased protein concentration in cells with droplets compared to those without them (Fig. 15, A- B). To understand whether the involvement

of episomal or exogenous DNA could play a role in droplet formation, we delivered external DNA in the nuclei by transfecting a mCherry plasmid before doxycycline induction (Fig. 15, A). We observed an increased frequency of droplets in the samples where exogenous DNA was delivered compared to the induction control (Fig. 15, B). We hypothesized that in mNeogreen-UL112-113 293 T-Rex cells, expression of UL112-113 proteins is not reaching the concentration threshold necessary for LLPS, while the presence of exogenous DNA could induce their formation at a lower concentration. Droplet formation was possible at lower protein concentrations in transfected and in a cell infected with a replication-deficient strain HSV-1 In 1374 (Fig. 16, B) ¹¹⁹. We found that droplet formation was possible at a much lower concentration in MRC-5 infected cells than 293 T-Rex-induced cells, indicating that the large concatemeric viral genome in the cells could induce more LLPS (Fig. 16, A-B). To further understand the mechanism of droplet induction by DNA, we transfected or mock-transfected 293 T-Rex cells with mCherry and induced UL112-113 expression by doxycycline.

We continuously imaged the cells in live cell imaging to further characterize the DNA dependency of LLPS. In live cell imaging, we could observe that the cells with exogenous DNA could induce the formation of droplets from 10-15 hours post-induction and at lower protein concentrations (Fig. 16, C). In cells without exogenous DNA, UL112-113 was primarily dispersed in the nuclei at later time points, and we did not observe droplet formation until 15 hours post-induction despite the high protein concentration. Wanting to quantify the concentration dependency of phase separation, we transfected or mock-transfected cells with a mCherry plasmid and induced the expression of UL112-113 protein by adding an increasing amount of doxycycline ranging from 0.25 to 4 $\mu\text{g}/\mu\text{l}$. At 24 hpi, mock-transfected cells showed mostly dispersed or metastable phenotypes, as UL112-113 formed small and unstable dots (Fig. 16, D-E). Phase separation was observed rarely and primarily in cells induced with higher concentrations of doxycycline (2-4 $\mu\text{g}/\mu\text{l}$). By contrast, we could observe more phase separation in cells with exogenous DNA in all conditions and a much higher degree. These data suggest that episomal DNA could lower the protein concentration threshold for UL112-113 LLPS.

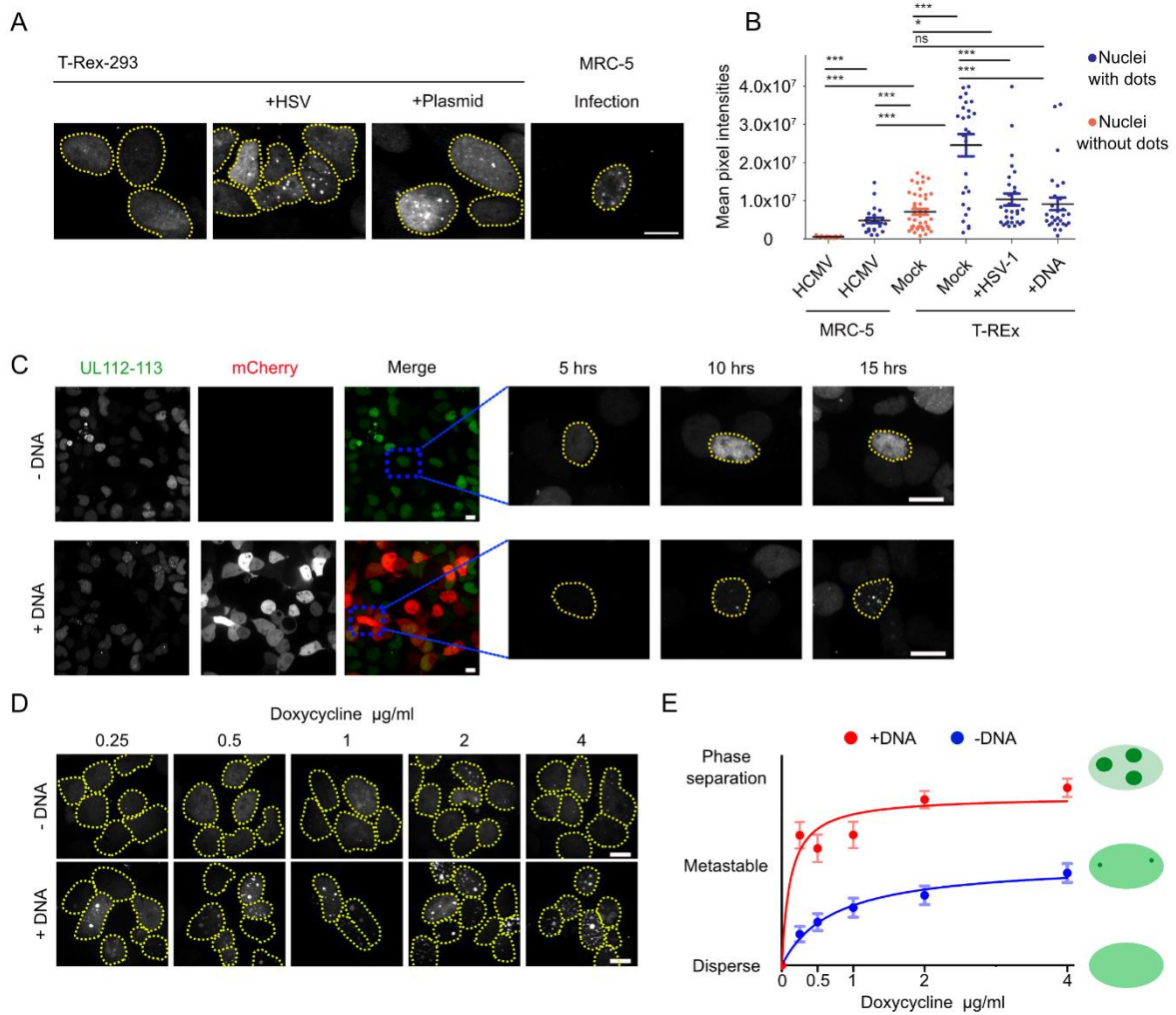


Figure 16: Exogenous DNA lowers UL112-113 concentration threshold for liquid-liquid phase separation A) 293 T-Rex cells were induced with 2 $\mu\text{g}/\mu\text{l}$ Doxycycline for 24 hours imaged by spinning disk microscope. Cells were either transfected with mCherry 24 hours before induction or infected with HSV-1 In74 1 hour after induction. MRC-5 cells were infected with the mNeogreen-UL112 virus at MOI 1 for 5 hours. B) Sum intensity of nuclei from cells in (A) was measured by ImageJ. C) Representative pictures of live cell imaging of 293 T-Rex cells transfected or mock transfected with mCherry and induced with 2 $\mu\text{g}/\mu\text{l}$ doxycycline. Cells were imaged by spinning disk microscopy every 20 minutes. Pictures show maximum z-projection. D) 293 T-Rex cells were transfected or mock transfected with mCherry, 24 hours after they were induced with different amounts of doxycycline ranging from 0.25 to 4 $\mu\text{g}/\mu\text{l}$. Cells were imaged live by confocal microscopy at 24 hours post-induction. E) Quantification of cell phenotypes from (D). Cells were divided manually into three categories: Disperse, Metastable, or Phase separation. The yellow dotted lines indicate nuclear boundaries. All Pictures show z maximum projection and a scale bar of 10 microns.

5.5 UL112-113 phase separation can be locally induced below the global threshold for phase separation

Next, we asked how exogenous DNA could lower the protein concentration threshold for UL112-113. At low concentrations, LLPS typically occurs through nucleation (Figure 6)^{82,92}. We hypothesized that exogenous DNA could decrease the concentration requirement as a scaffold for the nucleation of UL112-113. This phenomenon, called "diffusive capture," can happen when a slow diffusive scaffold starts to recruit faster-moving molecules, limiting their movement in space⁸¹. We again took advantage of the "corelet" system as proof of concept. We then used cells transduced with p84-IDR and iLiD-GFP constructs. As cells were quite heterogeneous in the expression of the constructs, we observed that some cells could undergo phase separation by photoactivation; meanwhile, in others, phase separation could not be observed even after 10 minutes of activation (Fig. 17, A). We then mapped the fluorescent intensity of the core and the IDRs as a proxy for protein concentration. We analyzed more than 100 cells and found that cells could undergo phase separation only in a specific core/IDR concentration ratio range when enough IDR could be recruited to the ferritin cores (Fig 17, B). When the core-to-IDR ratio was too high due to few IDRs or too many core molecules, phase separation could not occur. We selected cells where we did not observe phase separation (empty dots, Fig. 17, B) and photoactivated them for 5 minutes (Fig. 17, C). As expected, photoactivation did not lead to the clustering of UL112-113 IDR and droplet formation. We used a diffraction-limited activation spot to photoactivate only a few cores to simulate the function of a slow-moving scaffold such as a viral genome. In the same cells where previously LLPS was not observed, local photoactivation led rapidly to the recruitment of IDRs and the formation of droplets within seconds, indicating that activation of fewer core molecules could induce phase separation at lower protein concentrations (Fig. 17, D). In these cells, the few activated-slow moving scaffolds likely recruited all the available IDRs, which are small and fast diffusing. These data suggest that UL112-113 phase separation could be modulated by slow-moving scaffolds, such as the large HCMV DNA, indicating a potential spatial regulation of PRC formation directly at the viral genome.

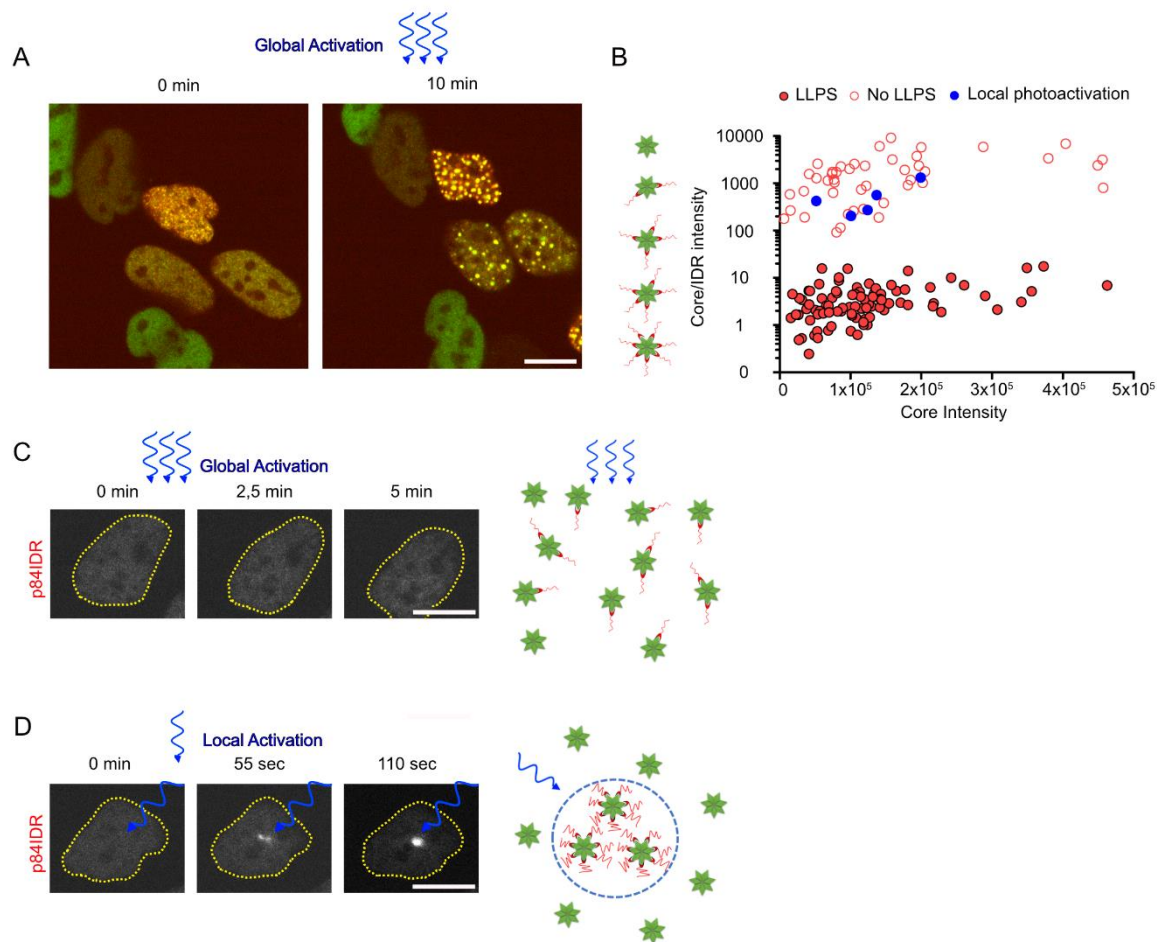


Figure 17: UL112-113 phase separation can be induced locally below the global concentration threshold A) 293A cells transduced with p84-IDR and valid-GFP constructs were photoactivated continuously by blue light for 10 minutes and imaged by confocal microscopy. Phase separation was observed in some cells while not in others. B) Quantification of protein concentration dependency of LLPS after induction from (A). The fluorescence intensity of p84-IDR and valid-GFP constructs was measured before photoactivation. Every dot represents a single cell. Full red dots represent cells in which phase separation occurred, empty dots cells in which phase separation did not occur, and blue dots represent cells in which phase separation occurred by local photoactivation. C) A single cell (as in A) was photoactivated globally for 5 minutes. D) Cell in (C) was photoactivated locally for 2 minutes after global photoactivation. Panel A-C-D shows representative pictures. The yellow dotted lines indicate nuclear boundaries. The scale bar is 10 microns.

5.6 Incoming viral genome localization to PRCs is essential for their replication

As exogenous DNA could regulate the formation of UL112-113 droplets, we wanted to know if also PRCs are formed around incoming viral genomes in infected cells. To visualize the incoming viral genome by confocal microscopy, we first established genome labeling with the modified nucleoside

analog 5-Ethynyl-2'-deoxyuridine (EdU). EdU is a thymidine analog that the viral polymerase can incorporate into the viral genome during DNA replication. EdU can be visualized via a fluorescent dye that forms a covalent bond through click-chemistry. For initial tests, we used a virus with the inner tegument protein pp150 (UL32) labeled to visualize viral capsids by light microscopy. We infected fibroblasts at an MOI of 1 with HCMV-UL32-GFP¹²⁰ and fed cells with EdU. We then harvested and purified the supernatant virus and infected fresh fibroblasts. At 2 hpi, we stained incoming genomes with Alexa fluor 555 via copper-mediated Click-chemistry.

We could observe single fluorescent particles in the cytoplasm, resembling the incoming viral genomes and pp150 dots representing capsids (Fig. 18, A). By contrast, we could not observe any EdU dots in cells infected with the unlabeled virus, indicating the specificity of the staining. In the cells infected with the virus cultivated using 2 μ M EdU, we observed that around 55% of the incoming viral genomes in the cytoplasm were co-localizing with viral capsids, indicating that the viral genome could be packaged and entered the cells efficiently. Meanwhile, the co-localization was much lower when we used 5 μ M EdU, and we also observed fewer fluorescent pp150 spots, indicating higher EdU concentrations were less suitable for genome labeling (Fig. 18, B). Therefore, we used the 2 μ M EdU concentration for further experiments and prepared an EdU-labelled virus stock using the HCMV-mNeongreen-UL112 virus.

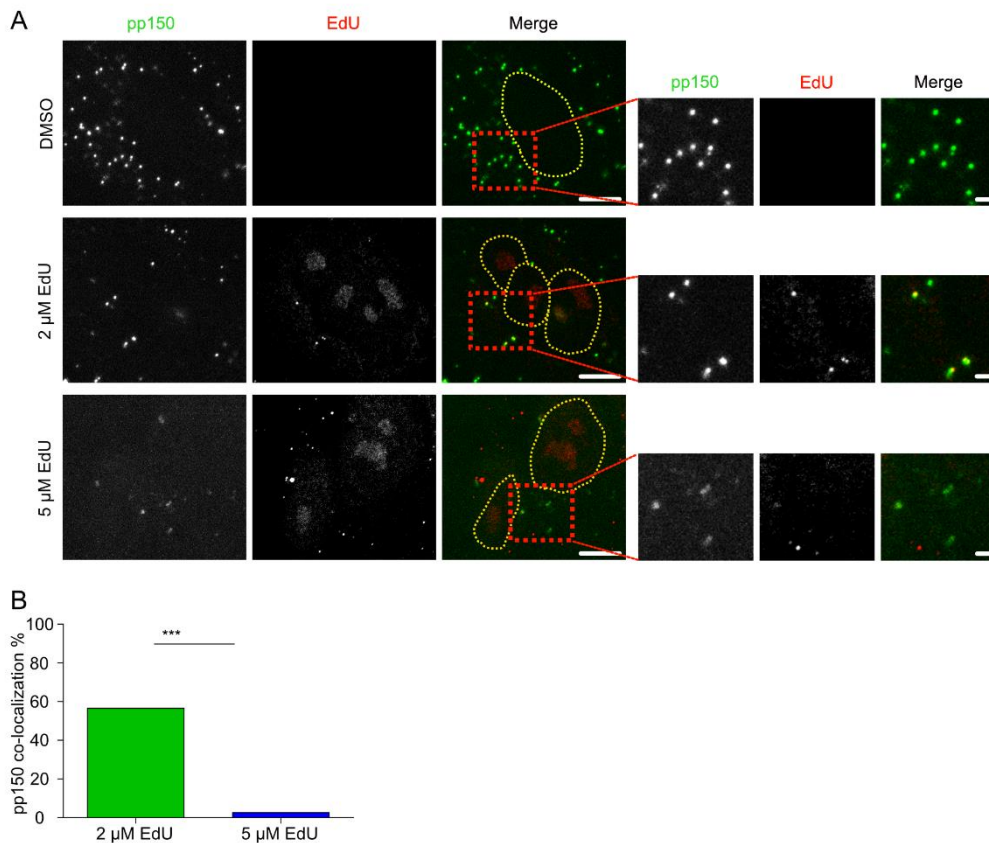


Figure 18: Validation of EdU viral genome labeling. A) pp150 labeled capsids association with EdU labeled viral genomes. HFF cells were infected at MOI 1 with HCMV-UL32-GFP virus labeled with 2 or 5 μM EdU or mock labeled using DMSO. Infected cells were fixed at 2 hours post-infection, and the viral genome was visualized by click reaction using an Alexa Fluor 555 picolyl azide. The insets show the interplay between the viral genome (EdU) and the capsids. The yellow dotted lines indicate nuclear boundaries. The scale bar is 10 microns and 2 microns in the insets.

As we wanted to investigate the relationship between the incoming viral genomes in the nuclei and the early replication compartments (PRCs), we infected fibroblast at MOI 1 with the new EdU HCMV-mNeongreen-UL112 virus and fixed the cells at 24 hpi. We observed EdU punta both in the cytoplasm and in the nuclei of infected cells, while we did not observe EdU dots in the mock-labeled virus (Fig. 19, A). Intriguingly, around 60% of the incoming nuclear genomes were co-localizing with PRCs, suggesting that UL112-113 compartments could form locally at them. Next, we tested if the presence of UL112-113 on the viral genome is a prerequisite for their transcription or replication. RNA PolIII is activated by phosphorylation and is essential for viral gene transcription. By immunofluorescence, we could observe several PolIII spots in the host nuclei, resembling the site

with active ongoing transcription. Most of the genomes associated with UL112-113 co-localize with RNA PolII spots, indicating that they are mostly transcriptionally active (Figure 19, C-D). Fewer genomes did not associate with UL112-113 and showed co-localization with PolII. These data suggest that the presence of UL112-113 genomes is not a prerequisite for transcription but a prerequisite for forming the PRC on them, as we observed almost no PRC-positive genomes without Pol II.

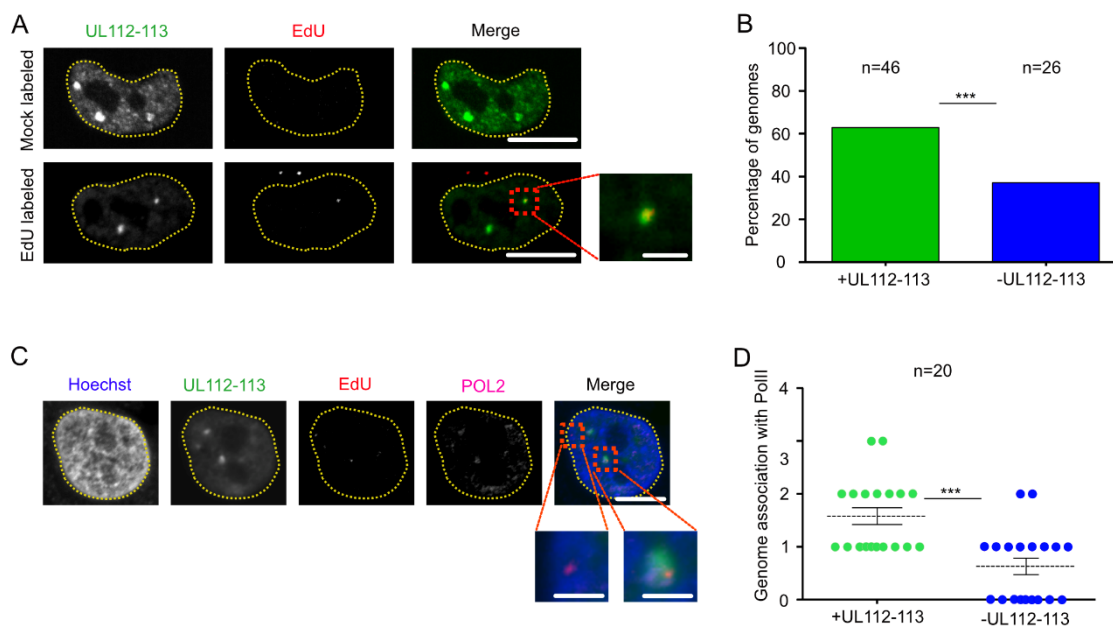


Figure 19: UL112-113 positive genomes show increased association with RNA polymerase II. A) MRC-5 cells were infected at MOI 1 with HCMV-mNeongreen-UL112 virus labeled with 2 μ m EdU or mock labeled using DMSO. Cells were fixed 24 hours post-infection, and the viral genome was visualized by click reaction using an Alexa fluor 555 picolyl azide. B) Genome association with UL112-113 foci was quantified in 72 cells. C) MRC-5 cells were infected and treated as in (A). The phosphorylated form of the RNA polymerase II was labeled by antibody and visualized by secondary anti-rabbit Alexa Fluor 647. Insets show a genome associated with UL112-113 and RNA polymerase II foci (on the right) and a non-transcribing genome (on the left). The yellow dotted lines indicate nuclear boundaries. The scale bar is 10 microns and 2 microns in the insets.

This result is in line with the fact that the viral transactivator IE2 is expressed earlier than the UL112-113 proteins and activates genome transcription before the formation of the PRC^{61,121}. Next, we wanted to know if the presence of UL112-113 droplets determines the replicative fate of viral genomes. To visualize both the incoming viral genome and the replicated one, we infected cells with

the EdU-labeled virus as before, and then at 24 hpi and we fed the cells with another nucleoside analog 5'-bromo-2'-deoxyuridine (BrdU) to be incorporated in the genome synthesized de novo (Fig. 20, A). BrdU is also a thymidine analog, which can be visualized after DNA denaturation through an antibody. At 30 hpi, we fixed infected cells and imaged them by confocal microscopy. In cells infected with the EdU mock labeled virus, we could detect newly synthesized genomes marked by BrdU, co-localizing almost perfectly with the replication compartment, but we did not detect any EdU signal (Fig. 20, B). In cells treated with phosphonoacetic acid (PAA), where viral DNA replication is blocked, we could not observe any BrdU signal in the nucleus of infected cells, and the UL112-113 marked compartments remained small, as observed previously, and EdU marked incoming viral genomes, both in the nuclei and the cytoplasm of infected cells (Fig. 20, B). We could observe both incoming and replicated viral genomes in cells infected with the EdU virus and fed with BrdU. To determine which genomes were replicating and which were not, we summed the area of BrdU signals in optical sections to obtain the total genome area. We observed that BrdU was only incorporated into the genome associated with UL112-113, resulting in an increased genome area ranging from a few μm to 20 (Fig. 20, C). On the other hand, genomes not associated with UL112-113 did not incorporate BrdU, resulting in a genome area between 0,2 and 2 μm (Fig. 20, C). We concluded that only genomes associated with UL112-113 could incorporate BrdU and replicate, indicating that the UL112-113 phase is essential for viral replication.

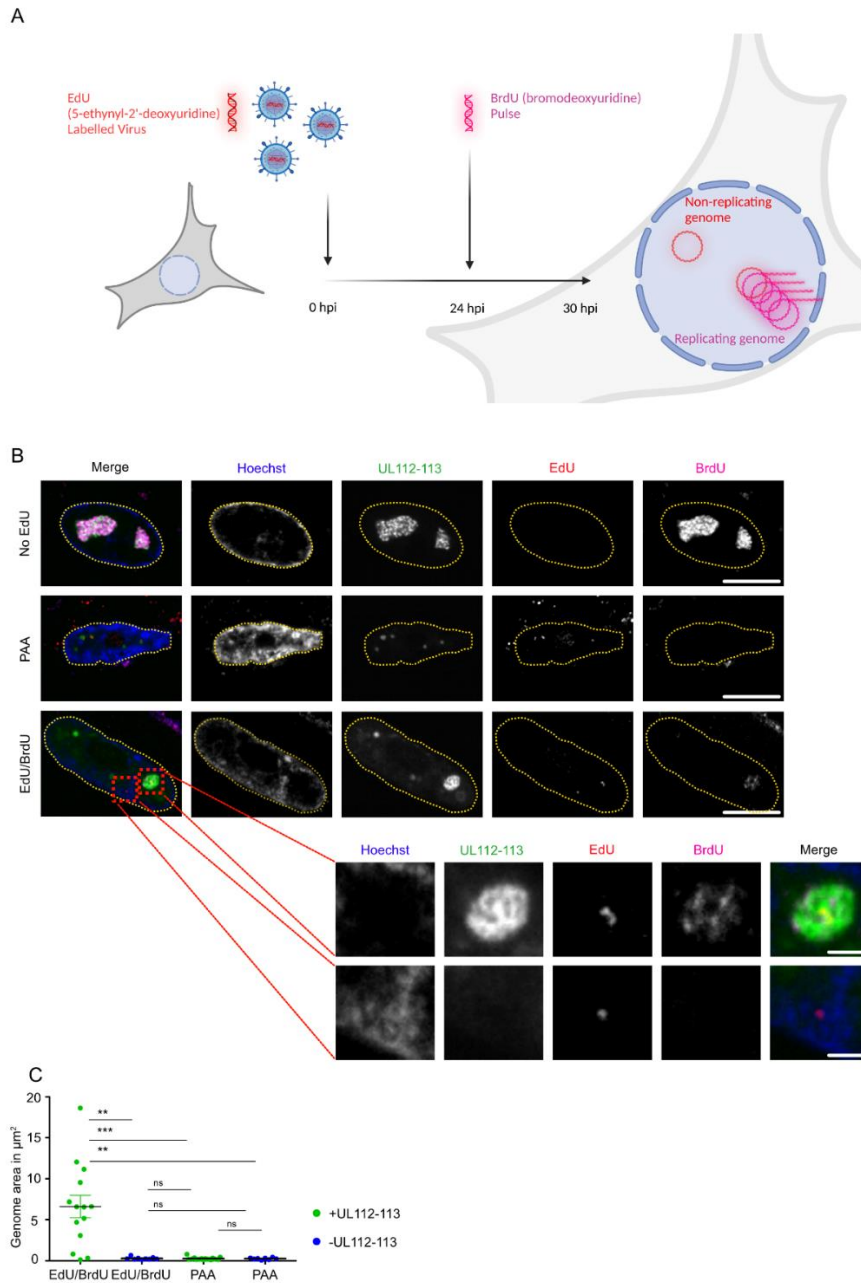


Figure 20: UL112-113 compartments facilitate incoming genome replication A) Workflow used for visualizing incoming and replicating viral genomes. B) Visualization of incoming and replicating viral genomes by confocal microscopy. MRC-5 cells were infected at MOI 1 with HCMV-mNeogreen-UL112 virus labeled with 2 μm EdU or mock labeled using DMSO. At 24 hours post-infection, cells were pulsed for 6 hours with 100 $\mu\text{g}/\mu\text{l}$ BrdU to visualize the newly replicated genome. The upper inset shows an incoming viral genome localizing to a UL112-113 compartment, which also incorporated BrdU, indicating that it is in a replicative state. The upper inset shows an incoming viral genome that is not localizing to the UL112-113 compartment and does not show any BrdU signal, indicating it is not replicating. B) Quantification of genome area of infected cells from (A). The sum of fluorescence intensity area from EdU and BrdU signals was scored as positive or negative for association with UL112-113 compartments. n= indicates the number of EdU-labelled genomes analyzed. The yellow dotted lines indicate nuclear boundaries. The scale bar is 10 microns and 2 microns in the insets. *** $p < 0.001$, ** $p < 0.01$, ns not significant.

5.7 UL112-113 LLPS is essential for the recruitment of the viral polymerase accessory unit UL44

Next, we wanted to investigate why UL112-113 compartments and liquid-liquid phase separation are essential for viral genome replication. HCMV encodes for its DNA polymerase, which is expressed as two subunits, the processivity factor UL44 and the catalytic subunit UL54. The two proteins co-localize inside replication compartments, and in particular, UL44 was shown to interact with UL112-113 in infection and transfection experiments^{67,122,123}. As phase separation plays a role in the formation of the replication compartment, we wondered if its inhibition could also affect UL44 localization and viral DNA replication. We carefully titrated 1,6-HD to find a concentration suitable for longer incubation time, as it was reported that 1,6-HD could affect cellular membrane integrity¹¹¹. We incubated the infected with different concentrations of 1,6-HD, from 1% to 10%, for 2 hours, and we analyzed cell viability by checking ATP levels. We observed that 1,6-HD significantly affected cell viability at high concentrations in mock and infected cells. We found that at 1%-2% concentration, cell viability was not affected in infected cells, while we observed decreased level of a viable cell in the mock by using 2% 1,6-HD (Fig. 21, A). It is possible that anti-apoptotic proteins expressed by HCMV could protect the infected cells by undergoing cell death¹²⁴, explaining the difference in the tolerance between infected and mock cells.

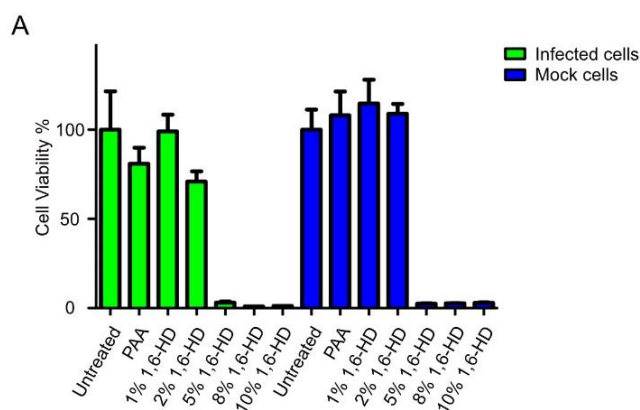


Figure 21: Low concentrations of 1,6-HD are well tolerated by MRC-5 cells (A) Cell viability after 1,6-HD treatment. Cells were infected at an MOI of 1 with the HCMV-mNeongreen-UL112 virus or mock-infected. At 24 hours post-infection, cells were treated with increasing amounts of 1,6-HD (1, 2, 5, 8, and 10%) or 250 $\mu\text{g}/\mu\text{l}$ phosphonoacetic acid (PAA) for 2 hours. Cell viability was measured using an ATP assay. Data were normalized to the viability of the untreated samples. The percentage of cell viability is a representative example of three independent biological replicates.

We treated infected cells 24 hours post-infection with 2% 1,6-HD for 2 hours, and at the same time, we fed the cells with 5 μ M EdU to detect replicated DNA. In untreated cells, UL112-113 and UL44 localized to the RC, allowing viral DNA replication as indicated by the incorporation of EdU (Fig. 22, A). As a positive control for inhibition of viral DNA replication, we treated infected cells with 250 μ g/ml PAA. In the presence of the inhibitor, the replication compartment remained small and spherical, as previously observed. UL44 still localized to the RC at the incoming viral genome, but DNA replication was stalled as PAA inhibits genome replication¹²⁵. In cells treated with 2% 1,6-HD, we observed fewer UL112-113 foci and mostly dispersed signals. As expected, replication compartment formation was impaired, and UL44 did not localize to viral genomes. Moreover, viral DNA replication was strongly inhibited or did not occur, as shown by the decreased EdU signal (Fig. 22, B-D).

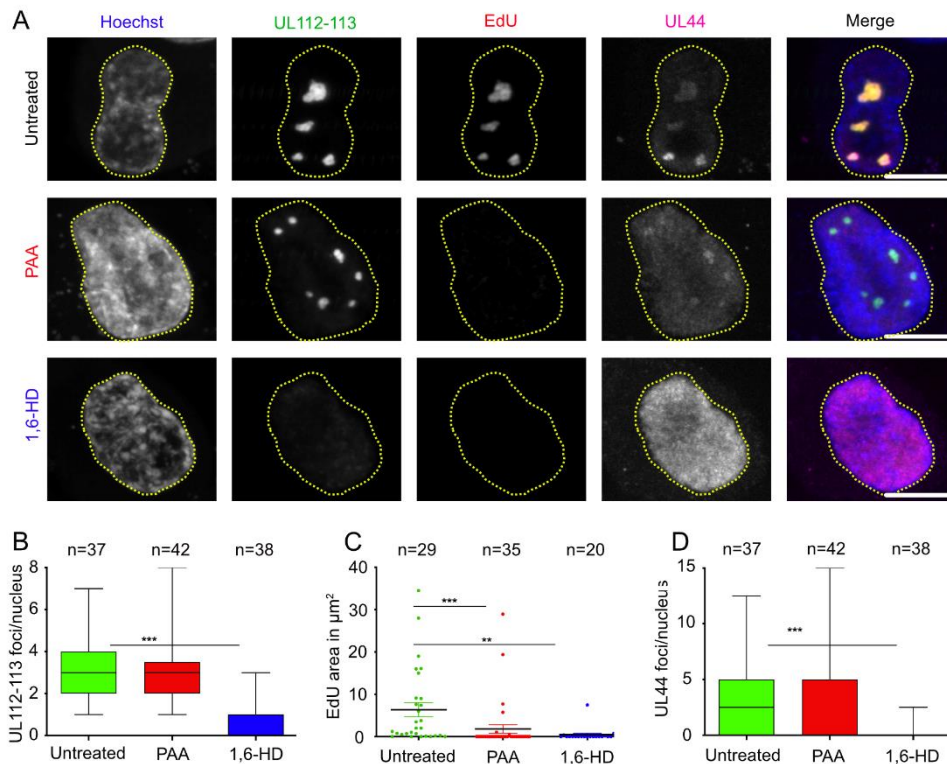


Figure 22: Inhibition of phase separation impairs UL44 localization as foci and viral DNA replication (A) MRC-5 cells were infected at an MOI of 1 with HCMV-mNeongreen-UL112 virus. At 24 hours post-infection, cells were pulsed for 2 hours with 10 μ M EdU for labeling the replicating genomes in the presence of either 2% 1,6-HD, Phosphonoacetic acid, or untreated media. Cells were then fixed at 26 hours post-infection. EdU was visualized by an AF555-Picolyl-azide, and UL44 was detected by immunofluorescence. Nuclei were counterstained with Hoescht. (B-C-D) Quantification from (A). (B) Quantification of UL112-113 foci per infected cells. The yellow dotted lines indicate nuclear boundaries. The scale bar is 10 microns.

Since our experiments indicated that inhibition of LLPS induced the mislocalization of UL44, we wanted to understand if weak interactions established by UL112-113 and UL44 proteins could mediate the protein's interaction and recruitment. To confirm that the recruitment of UL44 to PRCs was due to phase separation, we predicted the disorder content of UL44. We found that UL44 N-Terminus is highly ordered (aa 1–290), while the C-terminal part (aa 291–433) is predicted to be disordered (Fig. 23, A). An AlphaFold2 prediction confirmed this conclusion (Fig. 23, B). The N-terminus of UL44 was shown to form a dimer in the shape of a C-clamp, necessary for DNA binding function and interaction with UL54¹²⁶. The C-terminal part is dispensable for DNA interaction. However, it was shown previously to be essential for the localization of UL44 in the RC and its interaction with UL112-113^{122,127}.

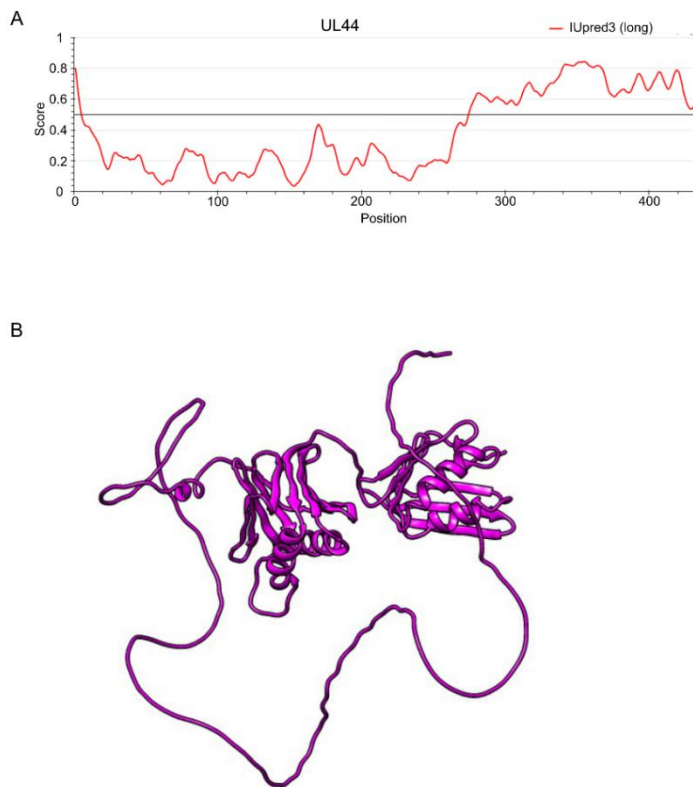


Figure 23: C-terminus of UL44 is disordered (A) Disorder plots of UL44 sequence. The UL44 sequence was analyzed by IUPred3¹⁰⁹ to predict disordered regions. The degree of disorder is scored on a scale from 0 to 1, with 1 indicating the highest level of disorder. While the N-terminus part of UL44 is highly ordered, the C-terminus, starting from the aminoacid 290, shows high disorders. (B) Prediction of UL44 tridimensional structure made with ColabFold¹⁰⁷.

As UL44 is recruited into UL112-113 positive liquid compartments, we wanted to establish if UL44 is a client of UL112-113. As disorder content is one of the major factors for recruitment into phase-separated droplets^{85,128,129}, we tested if the UL44 disordered domain is essential for the localization with UL112-113. We N-terminally tagged UL44 with mCherry and deleted either the structured N-terminus or the disordered C-terminus (Fig. 24, A). Transfected UL44 was soluble, while the co-transfection with UL112-113 induced the relocalization of UL44 into foci, as described previously⁶⁸. Interestingly, deleting the disordered C-terminal domain of UL44 impaired the co-localization of UL44 and UL112-113 foci.

In contrast, the deletion of the N-terminal domain did not affect it (Fig. 24, B), and it was shown that this domain is essential for the immunoprecipitation of UL44 and UL112-113¹²². To confirm further that the presence of a disordered domain is sufficient for the foci localization of UL44, we substituted its disordered C-terminus with the largest disordered domain from the UL112-113 isoform p43. As anticipated, adding the p43 disordered domain rescued UL44 localization to UL112-113 foci. These data indicate weak interaction between disordered domains as the leading recruitment force for UL44 inside UL112-113 droplets and in the PRCs.

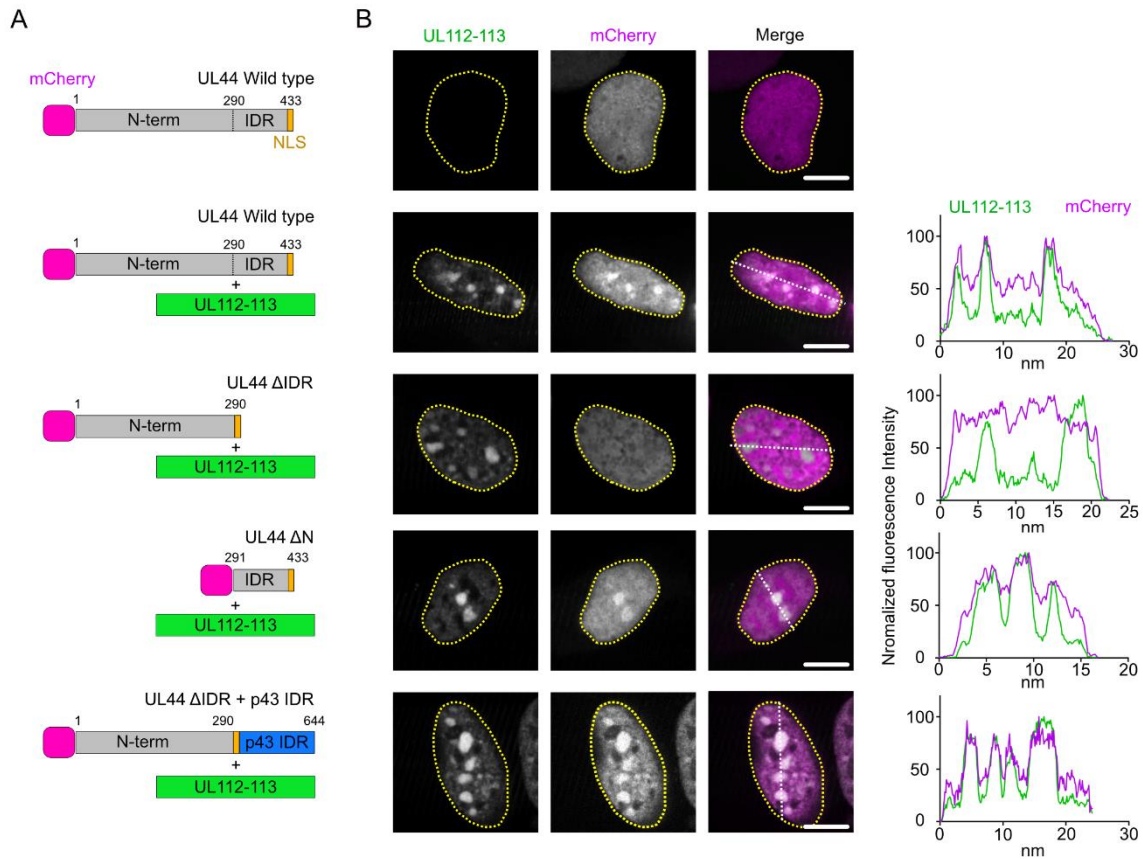


Figure 24: A disordered domain is required for the localization of UL44 in UL112-113 foci A) Schematic of mCherry-tagged UL44 constructs. UL44 is divided into an ordered N-terminal domain (from aa 1 to 290), an intrinsically disordered C-terminal domain (from aa 291 to 424), and a nuclear localization signal (from aa 424 to 433). The UL44 domains were deleted for assaying localization to UL112-113 with UL112-113 foci. B) HEK-293A cells were co-transfected with mNeonGreen-UL112-113 and mCherry-UL44 mutant as illustrated in (A) and imaged live by spinning disk microscopy at 48 hours post-transfection. The yellow dotted lines indicate nuclear boundaries. Intensity plots illustrate signal profiles along the white dotted lines. Pictures show maximum z-projection, and the scale bar is 10 microns.

6 Discussion

6.1 The role of UL112-113 proteins LLPS in HCMV replication

Upon entry into the cells, HCMV injects its genome into the host nucleus, where it is susceptible to the host response aiming to interrupt transcription and replication. HCMV encodes proteins to suppress this host response and create a pro-replicative environment known as the replication compartment. The principles of driving the formation of this membrane-less compartment were not understood. In this study, we found that UL112-113 proteins are the major players in forming PRCs by LLPS. The droplets formed by UL112-113 in infection and transfection fused and quickly regained sphericity, presumably due to surface tension. UL112-113 droplets were sensitive to inhibitors of weak interactions such as 1,6-HD or PG, indicating that their formation is reversible. FRAP analysis revealed a rapid diffusion of molecules within the droplets body and external diffusion to the nucleoplasm. Thus, UL112-113 droplets displayed properties of *bona fide* phase-separated compartments, similar to other liquid condensates^{78,118}. LLPS of UL112-113 was also independent of other viral proteins, as we observed droplet formation *in vitro*. Ionic interactions were important for forming these droplets as they were affected by high salt concentration. Using the photoactivatable “corelet” system, we found that clustering the p84 and p43 disordered domains was sufficient for LLPS. When expressed endogenously without exogenous DNA, the UL112-113 proteins underwent less likely LLPS than the transfected control, where most cells showed droplet formation. Without exogenous DNA, the UL112-113 proteins did not phase separate at concentrations where the proteins would phase separate when exogenous DNA was present. This may indicate that the LLPS of UL112-113 *in cellulo* is not regulated only by a fixed concentration threshold but is greatly affected by molecular heterogeneity, in line with other LLPS models^{82,130}. We observed that introducing exogenous DNA via transfection or infection greatly enhanced LLPS, suggesting that the DNA could provide a surface for the nucleation of UL112-113 droplets, decreasing the energy barrier for LLPS. As we showed that local activation could induce LLPS below the global concentration threshold using the “corelet” system, we hypothesized that the UL112-113 proteins could induce their clustering directly at viral genomes. Using labeled genomes, we found that most of the incoming viral genomes were localizing to UL112-113 droplets, and most were also associated with active polymerase II. However, the presence of the PRC on the genome was not a pre-requisite for genome transcription, potentially indicating that transcriptional genome activity could be important for UL112-113 LLPS.

In contrast, UL112-113 droplet formation at viral genomes was essential for genome replication, as we could see the recruitment of the polymerase accessory unit UL44 to viral genomes was dependent on UL112-113 LLPS. These results indicate a fine spatial regulation of UL112-113 LLPS, as shown for many other cellular condensates^{93,131–133}. After the start of viral genomes replication, we observed a change in the biophysical properties of the mature RC was much less dynamic, showed a decreased mobile fraction, and was much less susceptible to inhibitors of weak interactions, indicating a maturation process. Significantly, PAA, an inhibitor of viral DNA replication, inhibited the maturation process, suggesting that DNA replication caused the change in the measured RC properties. It is unclear whether these morphological changes are a requirement for DNA replication or only a consequence. Further studies are needed to understand how the RC maturation process is regulated and how it may be linked to RC function.

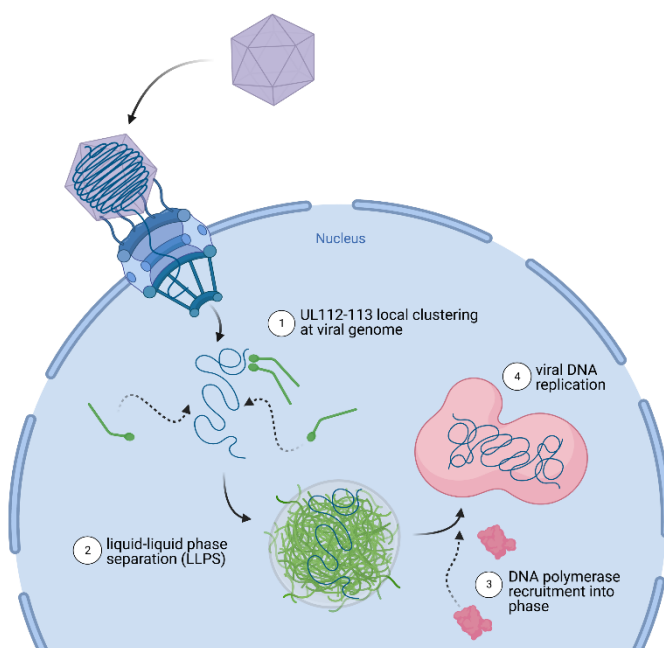


Figure 25: Graphical summary. Upon entry into the host cell, HCMV releases its genome into host nuclei. After initial transcription, UL112-113 proteins recognize the viral genome (1) and form the PRC through LLPS (2), allowing the recruitment of the viral polymerase to the genome (3). Afterward, viral DNA replication starts, and the production of newly synthesized genomes leads to the maturation of the PRC to the RC (4). Graphic made with Biorender.com by Jens Bosse from⁷⁴.

6.2 Isoforms of UL112-113 and their role in LLPS

We found that the four UL112-113 isoforms are sufficient for LLPS, as UL112-113 formed liquid droplets in transfected cells or *in vitro*. These experiments indicate that its formation is independent of other viral proteins, while we still cannot exclude the contribution of cellular proteins in the process. Notably, the biophysical properties of the droplets in transfected cells were quite similar to the PRCs in infected cells as they had similar recovery rates, high mobility, and sensitivity to LLPS inhibitors. These results indicate that the contribution of other viral factors in forming PRCs is minimal, while they are likely crucial for the transition from the PRC to the RC. Using the “corelets” system, we defined a minimal model for UL112-113 phase separation where the clustering of the disordered regions gives LLPS via an oligomerization domain. The sequence of the highly structured N-terminus of UL112-113 is highly conserved among the betaherpesviruses and is crucial for mediating the self-interaction of the 4 isoforms and overall essential for HCMV replication^{67,68}. In line, deleting the entire exon 1 impairs the efficient formation of UL112-113 foci in transfection, while deleting the C-terminal regions does not affect it⁶⁷. In our photoactivation experiment, UL112-113 phase separation was possible only upon blue light activation of the artificial oligomerization domain. This experiment may indicate the need for a modulatory domain to cluster the disordered domains. It is still unclear which UL112-113 isoforms are essential for compartment formation and how they shape their properties. Previous work by the Brune lab investigated the function of individual UL112-113 isoforms by BAC mutants⁶⁸ and found that only the p43 isoform is essential, as no viral replication is observed without its expression, while the lack of expression of p84 severely impairs viral growth compared to wild-type infection but does not entirely abolish it⁶⁸. These two isoforms are also required to recruit UL44 into the PRC. In addition, p43 plays an essential role in mediating IE2-dependent transcriptional activation of the UL54 promoter⁷⁰. By contrast, p34 and p50 are dispensable for viral replication. P34 and p50 may have redundant roles that can be rescued by the other isoforms and fulfill different functions. When expressed individually, all UL112-113 isoforms but one are all localized to the nucleus and form dot-like structures in the proximity of PML-NB. Only p34 is partially localizing to the cytoplasm due to the lack of an NLS and needs the expression of the other isoforms to be present exclusively in the nucleus¹¹⁴. As the 4 isoforms possess different lengths of disordered regions, it is tempting to speculate that condensates formed by their expression have different biophysical characteristics.

Interestingly, the deletion of the NLS in the UL112-113 gene induces the formation of punctate cytoplasmic structures ¹¹⁴. These results indicate that the LLPS of UL112-113 is not dependent on the protein's nuclear localization and therefore is not reliant on the nuclear environment. This aligns with our results, showing that the UL112-113 proteins could form liquid droplets in a cell-free environment. It was reported that the four canonical isoforms, p34, p43, p50, and p84, give rise to another 5 isoforms through calpain-catalyzed proteolysis called p20, p26, p28, p34c, and p38 ⁶⁹. These "novel" proteins were found to be associated with HCMV capsids, non-infectious particles, and dense bodies, but so far, there is no information regarding their localization in cell ¹³⁴. The p20, p26, and p28 isoforms are formed by the proteolysis of p34, while the proteolysis of p43, p50, and p84 forms p38 and p34c.

Interestingly, overexpression of p20, p26, and p28 reduced HCMV genome synthesis and overall virus production ⁶⁹. As these 3 isoforms predominantly represent the ordered N-terminus with a variable piece of the disordered region from p34, they might play a role in modulating the properties of the phase-separated compartment by acting as a dominant negative, resulting in less fluidity and stronger interactions. This mechanism might play a role in regulating viral replication and even latency or might mark an antiviral pathway. While other betaherpesviruses such as MCMV and Human herpesviruses 6 and 7, encode homologs of UL112-113, obvious sequence homologs of UL112-113 have not been identified in alpha- or gammaherpesviruses ¹³⁵⁻¹³⁷. Thus, the alpha- and gammaherpesviruses may have evolved other proteins capable of forming fluid PRCs by LLPS.

6.3 Association of UL112-113 with viral genomes

In this work, we showed the formation of UL112-113 droplets on the incoming viral genomes as essential for the recruitment of the UL44 polymerase and genome replication. Nucleic acid recognition and binding are features often found with proteins involved in forming biomolecular condensates ^{94,132,138,139}. Similarly, our data indicate that HCMV genomes serve as a polymeric scaffold for the nucleation of UL112-113 by locally inducing LLPS and lowering the concentration threshold for LLPS. However, it is still unclear how DNA binding is mediated. A previous report suggested that the UL112-113 proteins bind DNA directly using a DNA-cellulose pulldown approach ⁶⁶. Chromatin IP (ChIP) might now help determine any sequence-specificity.

Alternatively, other viral proteins may also modulate the DNA binding capacity of the UL112-113 proteins. A previous study showed that in infected cells, the UL112-113 proteins interact and co-localize with IE2 via the N-terminus⁷³. IE2 is the primary early transactivator, localizing early to the viral genome and replication compartments. The IE2 protein is disordered and forms membrane-less foci in infection. IE2 could form viral condensates before UL112-113, ensuring early protein transcription and potentially lowering the concentration threshold for the LLPS of other proteins, such as UL112-113.

Interestingly, IE2 is localizing to every viral genome, contributing to their transcription, but UL44 localizes does not, indicating that RCs arise only at specific genomes¹⁴⁰. Epigenetic modification or chromatinization could also play a role in the spatial and temporal regulation of RC formation, as histones decorate the HCMV genome upon entering the nucleus, independently of their later fate in latency or lytic replication⁵⁴. The histone deacetylase 2 (HDAC 2) is present on viral genomes where PML-NBs were displaced. Intriguingly, IE2 inhibits the deacetylation activity of the viral polymerase promoter¹⁴¹. The acetylation of viral promoters might lead to the recognition of transcriptionally active viral DNA by the UL112-113 proteins¹⁴². Preliminary predictions suggest that the N-terminus of UL112-113 has some similarities to YEATS folds, IgG-like domains which bind certain forms of chromatin acylation¹⁴³. The UL112-113 might, therefore, recognize transcriptionally active genomes through binding acetylated histones.

The RC arises at incoming viral genomes in the proximity of PML-NBs, and after its dispersal, several proteins are recruited into the RC and are essential for genome transcription. When expressed individually, the four UL112-113 isoforms localize in the proximity of PML-NB with slightly different efficacy¹¹⁴. The PML-NB could be one of the limiting factors for the replication of viral genomes, as they act as transcriptional repressors via the action of its constituent proteins such as DAXX, Sp100, and ATRX, possibly also regulating virus latency^{144,145}. Immediate early 1 (IE-1) inhibits the de-novo SUMOylation of PML, inducing PML-NB dissolution and dispersal of any components¹⁴⁶. The dispersion of PML-NB is only essential at low-multiplicity of infection, restricting the expression of many delayed early proteins such as pUL57, pUL69, pUL98, and even UL112-113¹⁴⁷.

Nevertheless, PML-NB antiviral activity is cell line dependent, and it was reported that deletion or downregulation of certain PML-NB factors could repress herpesvirus infection, arguing for an ambiguous role during herpesvirus infection^{148,149}. Many PML-NB components are essential for viral

replication and are often found in association with the RC. An HCMV mutant expressing a mutated IE1, which does not disperse PML-NBs, grows with similar kinetics to the wild type, indicating that PML-NB is not an antiviral compartment, *per se*, but it depends on the composition¹⁵⁰. Shortly after herpesvirus genomes are injected into the nucleus, PML-NBs form close to incoming genomes, so PML-NB could also signal the correct localization of the UL112-113⁵².

Finally, the growth of phase-separated condensates is governed by Ostwald ripening, where small ones shrink in the presence of large ones, which will grow. This effect is because larger droplets have a more favorable surface area-to-volume ratio and “lose” fewer molecules than small droplets. Nucleation of LLPS at genomes might be a mechanism by which the virus ensures that the initially limited amounts of UL112-113 early in infection are specifically concentrated at genomes. Recent studies in alphaherpesviruses have shown that a maximum number of 8-10 genomes can replicate per nucleus, independent of the number of input genomes¹⁵¹. Initial phase separation at select genomes and limiting droplet growth to them by Ostwald ripening might be the limiting factor for this effect. In line with this idea, a CRISPR perturbation assay screen found that targeting the UL112-113 gene expression would lead to a unique transcriptome trajectory resembling an abortive latent infection, which may indicate the formation of the UL112-113 phase as an essential step for the latent-to-lytic switch⁷². It is not surprising that UL112-113 is not expressed during latency¹⁵².

Interestingly, transient expression of the UL112-113 proteins activates lytic replication of KSHV⁷¹, indicating the formation of a liquid compartment also being beneficial for other viruses. This might imply that UL112-113 binds to a feature common in the whole *Herpesviridae* family. A previous study showed that UL112-113 proteins could bind DNA and act as a transactivator of the UL54 promoter^{66,70}. Interestingly, the complete deletion of the putative transactivator regions of p43 also affected the localization of its foci⁷⁰.

6.4 The role of protein disorder in RC formation

Previous studies have shown that the C-terminal domain of UL44 is essential for its recruitment into RCs and interaction with the p84 isoform^{73,127}. We found that this domain is highly disordered and necessary for the recruitment into UL112-113 droplets, while we did not observe any effect of deleting the N-terminus. Furthermore, when we swapped the C-terminus of UL44 with the disordered domain of the p43 UL112-113 isoform, we rescued recruitment into UL112-113 droplets

confirming the importance of a compatible disordered region for recruitment into droplets. We do not know if unrelated disordered regions would also allow recruitment into UL112-113 droplets. Several cellular proteins containing disordered regions are present in the RC, such as p53 and Nucleolin^{38,39}, and their IDRs might mediate their localization. It has been shown for *in vitro* model systems, such as FUS and p53 droplets, that the recruitment of client proteins into the condensate depends on features like the amino acidic composition and their properties, but the key factors seem to be the overall size and the disorder content of the client proteins^{128,129}. The presence of pores in the condensates can act as a size-exclusion filter for folded proteins slowing down their diffusion while not affecting the distribution of disordered proteins, which can adapt to different pore sizes due to their flexibility¹²⁹. A study using different sizes of fluorescent PEGs indicates that their diffusion on the surfaces of LAF-1 droplets is restricted to molecules ranging from 3 to 8 nm¹⁵³. Whether or not RCs have pore size and which kind of proteins are enriched is not well understood. In addition, the maturation of PRCs to RCs adds another layer of complexity. Around 33% of the eukaryotic proteins contain long disordered regions¹⁵⁴, while in the *Herpesviridae* family, the presence of intrinsically disordered regions ranges from 15-40% of the whole proteome, depending on the species¹⁵⁵. These large fractions imply the presence of a vast number of disordered proteins in infected cells, but it is unclear how many and which are recruited into PRCs and RCs. Future studies need to focus based on heterospecific phase separation.

6.5 The role of LLPS in the lifecycle of other herpesviruses

While we specifically described the role of UL112-113 in RC formation by LLPS, related viruses likely code for proteins with a similar function, such as the E1 isoforms of MCMV^{135,136}. As UL112-113 has no apparent homologs in the alpha and *Gammaherpesvirinae*, other proteins might fill a similar role. A recent study indicated that the transcriptional transactivator ICP4, an essential constituent of HSV-1 RCs, forms condensates by phase separation¹⁵⁶. Similarly to UL112-113, ICP4 can also form compartments in transfected cells and has DNA binding properties. However, ICP4 condensates are much more viscous than UL112-113 droplets. Simplexviruses have a higher percentage of disordered proteins than other herpesviruses¹⁵⁵, and it is also possible that they possess multiple proteins involved in the RC formation with redundant functions. ICP0, for example, is highly disordered, localizes in dot-like structures without other viral proteins¹⁵⁷, and is expressed with an immediate early kinetic similar to ICP4. Another study analyzed the condensate nature of HSV-1 RCS

by using the cellular RNA polymerase II (POL II) as reference molecule ¹⁵⁸. POL II is responsible for viral gene transcription in the RC and undergoes LLPS through its disordered C-terminal tail ¹⁵⁹. The authors concluded that despite HSV-1 RCs sharing many condensate features, their formation mechanism differs from classical LLPS, as the RC interface does not restrict Pol II diffusion. Unfortunately, the study did not focus on viral proteins likely to be the driver of LLPS, such as ICP4 or ICP0, as a lack of any significant change in diffusing over the RC border might be due to the high disorder content Pol II as illustrated above. Ideally, several viral proteins should be used to test if the RC boundary also limits their diffusion.

Recently, it was shown that LLPS of key viral proteins plays a role in condensate formation during latency. The latency-associated nuclear antigen (LANA) is the most abundant protein expressed during KSHV latency. LANA binds directly to the conserved TR sequences of the KSHV genome and, via the recruitment of several factors, ensures viral latency and viral chromosome maintenance ^{160,161}. LANA possesses an IDR, multimerizes, and then binds to viral DNA, which can form nuclear structures known as LANA nuclear bodies (LANA-NB). Indeed, LANA-NB is partially sensitive to agents such as 1,6 – HD, and their perturbation alters KSHV genome conformation ¹⁶². Induction of the KSHV lytic cycle induces the formation of irregular LANA ring-like structures representing the RC.

Interestingly, viral proteins associated with the lytic cycle, like K8 and ORF45, localize to the RC but not with the LANA-NB, while it is the opposite for the repressive marker DAXX ¹⁶². LANA marked RC is less sensitive to 1,6-HD and more irregular, implying a significant structural change of LANA from latency to lytic activation, also changing the relative enrichment of proteins. The results may highlight similarities to HSV-1 and HCMV RCs, where LLPS is only partially responsible for keeping the architecture.

Similarly to what we observed, the transition occurs with the onset of viral DNA replication. Unfortunately, no FRAP data are available for comparison from LANA-NBs or RCs. In Epstein–Barr virus (EBV), the transcriptional factor EBNA2 and its coactivator EBNA-LP regulate latent viral transcription and expression of numerous cellular genes. Moreover, EBNA2 interacts with DNA in an indirect manner ¹⁶³. Both proteins possess a large IDR and are responsible for creating liquid compartments at super-enhancers in transfection and in vitro ^{164,165}. EBNA2 compartments exhibit fast and almost complete recovery, a mostly spherical morphology, and sensitivity towards the

phase separation inhibitor 1,6-HD ¹⁶⁵. The EBNA2 N-terminal dimerization domains are essential for forming fluid compartments that create accessible chromatin regions and promote histone acetylation via the specific recruitment of p300 ¹⁶⁵.

Finally, many of the tegument proteins are disordered, and a recent study found that the tegument protein UL11 can undergo LLPS *in vitro* and bind to RNA ¹⁶⁶. As UL11 is essential for virus assembly, the authors proposed a model in which the outer tegument might be a biomolecular condensate that could contribute to secondary envelopment ¹⁶⁶. As herpesvirus proteomes are enriched in IDRs and functional mechanisms, they seem to be conserved, inhibiting condensate formation might be an ideal antiviral target worth exploiting.

6.6 RC maturation

Our study highlighted that the biophysical properties change from PRCs to RCs. After forming the UL112-113 liquid phase around the viral genome, the onset of the viral DNA replication likely defines the transition from PRCs to RCs. At this point, the condensates started to transform into a pleomorphic structure and grew in size 10-15-fold. Moreover, mature RCs showed a decrease in the UL112-113 mobile fraction and increased resistance to inhibitors of weak interactions. All these features indicate a drift away from the canonical elements of liquid-like compartments ⁷⁹. Inhibition of viral DNA replication prevents this transition, suggesting that the long concatemeric genomes generated during the rolling-circle replication process alter the liquid properties of RCs, possibly saturating the UL112-113 binding sites or providing a scaffold to which other proteins can bind. However, it is also possible that true late viral proteins expressed after viral DNA replication contribute to this maturation. In a recent study performed in HSV-1 infected cells, recovery after FRAP of labeled viral replicon DNA was much slower than the recovery of the DNA binding protein ICP4 ¹⁵⁶, indicating that also in HSV-1 infected cells, the concatemeric viral DNA could act as a scaffold for protein binding. Due to the newly produced DNA, the increased molecular crowding inside the compartment could force the disordered proteins to interact more strongly with surrounding molecules, creating a more rigid condensate. The changes in condensate composition might affect its pore size, altering the permeability of client proteins. As discussed previously, the biophysical properties of other herpesvirus RCs, for example, KSHV and HSV-1, are more compatible with gel-like structures rather than *bona fide* fluid condensates. This phenomenon was also observed for RCs of Adenoviruses and Rotavirus viral factories, where a more viscous state was associated with the

progression of infection ^{112,167}. It is still unknown whether RC maturation is a direct consequence of the onset of DNA replication or a pre-requisite.

Current evidence suggests that at least HCMV RCs start as liquid condensates. When condensate driver concentrations cross a certain concentration threshold, weak interactions between the molecules overcome the entropic force and droplet nucleation. Slow diffusing scaffolds such as viral DNA can nucleate this process. As the newly formed compartment is fluid, its shape is forced by surface tension into a spherical shape, maximizing the volume per surface area (Fig. 26, A-B). Further increasing the concentration of molecules with higher valency, particularly RNA or DNA, increases the interactive forces inside the condensate, which at some point overcomes surface tension and allows the condensate to assume an irregular structure (Fig. 26, C). At this stage, tighter interactions of molecules in the condensate slow down internal and external diffusion. Finally, fiber or amyloid formation might occur (Fig. 26, D), as observed in certain diseases ^{99,106}.

They were shown to be possible for some unrelated herpesvirus proteins involved in overcoming the host defense ^{115,168}. Understanding the dynamic phase transitions of herpesvirus RCs could potentially lead to novel antiviral compounds, as recently illustrated for the respiratory syncytial virus (RSV) (IB) ¹⁶⁹ and influenza virus ¹⁷⁰. In both cases, compounds were found to induce the viral replication organelle, which efficiently inhibited viral replication. As such compounds target complex protein assemblies, viral resistance development might be less of a problem.

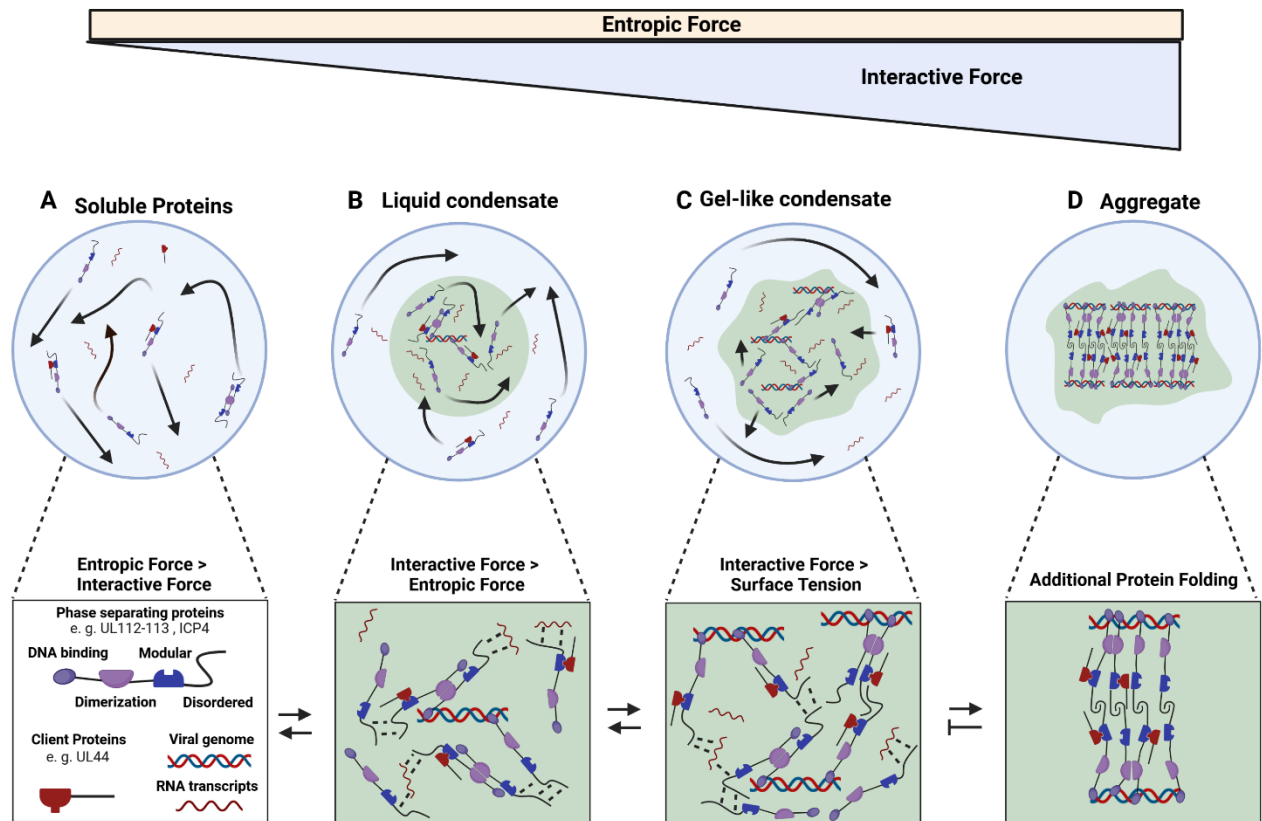


Figure 26: Model of the molecular interactions during herpesvirus replication compartment formation and maturation, adapted from ¹¹⁰. (A) At constant temperature, molecules in a solution move at a fixed rate via Brownian motion leading to a defined level of entropic force. (B) When interactive forces overcome these entropic forces, for example, by increasing the concentration of a molecule, demixing occurs. Since keeping an interface between the two phases is energetically expensive, surface tension forces the fluid compartment into a sphere, maximizing the volume per surface area. These liquid condensates are characterized by high internal molecular diffusion and selective external diffusion. (C) Increasing the concentration of components and adding in molecules with higher valency, such as long RNA or DNA molecules, induces the formation of more bonds, finally overcoming surface tension and resulting in an irregularly shaped condensate. (D) Increased bond stability can eventually force disordered regions to fold and entangle in new interactions, increasing molecular crowding and kinetically arresting the active molecules. These aggregates might not be reversible. Note that aggregate formation has not been described for herpesviruses replication compartments yet.

7 Materials

7.1 Bacteria

Name	Growth temperature	Identifier
E.coli DH10B	37 °C	Life Technologies
E.coli GS1783	30 °C	108

7.2 Cells and viruses

Name	Source	Identifier
MRC-5 human embryonic lung fibroblasts	ATCC	CCL-171
Telomerase-immortalized HFF	171	N/A
HEK-293T	ATCC	CL-11268
HEK-293A	Invitrogen	R70507
T-REx-293	Invitrogen	R71007
T-REx-293-mNeonGreen-UL112-113	This study	N/A
HCMV-NeonGreen-UL112	This study	N/A
HCMV-UL32-GFP	120	N/A
HSV-1 in1374	119	N/A

7.3 Chemicals

Name	Source	Identifier
Fibronectin bovine plasma	Millipore Sigma	F1141
Hoechst 33342	Thermo Fischer	H1399
Polyethylenimine (PEI), branched	Sigma Aldrich	408727
Doxycycline Hyclate	LKT Labs	LKT- D5897.5
Phosphonoacetic acid (PAA)	Sigma Aldrich	284270
Dulbecco's Modified Eagle's Medium (DMEM) with glucose	Sigma Aldrich	D5796
Fetal calf serum (FCS), tetracycline-free	Pan Biotech	P30-3602
Fetal calf serum (FCS)	Pan Biotech	P30-0602
1,6-Hexanediol	Sigma Aldrich	240117
HisPur Ni-NTA Resin	Thermo Fisher	88221
T4 ligase	New England Biolabs	M0202L
Propylene glycol	Sigma Aldrich	398039-25ML

Dream Taq Green DNA polymerase and buffer	Thermo Fisher Scientific	
Fast alkaline phosphatase	Thermo Fisher Scientific	EF0651
Fast Digest restriction enzymes and buffer	Thermo Fisher Scientific	
PRECISOR DNA polymerase and buffer	BioCat	1706-25-BL
5-Bromo-2'-Deoxyuridine (BrdU)	Sigma Aldrich	B5002
Pierce™ ECL Western Blotting Substrate	Thermo Fischer	32106

7.4 Antibodies

Name	Source	Identifier
Mouse anti-mNeonGreen	Chromotek	32F6
Anti-RNA polymerase II CTD repeat YSPTSPS (phospho S5) antibody	abcam	ab5131
Rat anti-BrdU	Abcam	Ab6326
Mouse anti-UL44	Virusys	10D8
Goat anti-Mouse IgG Alexa 555	Invitrogen	A32727

Goat anti-Mouse IgG Alexa 647	Invitrogen	A32728
Goat anti-Rabbit IgG Alexa 647	Invitrogen	A32733

7.5 Recombinant DNA

Name	Source	Identifier
pcDNA3.1	Thermo Fisher	V79020
pcDNA mNeongreen-UL112-113	This study	N/A
pcDNA mNeongreen	This study	N/A
pcDNA His-mNeongreen	This study	N/A
pcDNA M45-mCherry	115	N/A
pmCherry-Nucleolin	115	N/A
TB40-BAC4	172	N/A
TB40-BAC4-mNeonGreen-UL112	This study	N/A
pHR-SFFVp-NLS-iLID::EGFP::FTH1	Addgene	122147

pHR-SFFVp-HNRNPA1C::mCherry::SspB	Addgene	122668
pHR-SFFVp-mCherry::SspB	This study	N/A
pHR-SFFVp-p43ΔN::mCherry::SspB	This study	N/A
pHR-SFFVp-p84ΔN::mCherry::SspB	This study	N/A
pcDNA6/TR	Invitrogen	V1025-20
pcDNA4/T0	Invitrogen	V1020-20
pcDNA4/T0 mNeogreen-UL112-113	This study	N/A
pMD2.G	Addgene	12259
pMDLg/pRRE	Addgene	12251
pRSV-Rev	Addgene	12253
pSG5-p43	Park et al., 2006	N/A
pSG5-p84	Park et al., 2006	N/A

pmCherry-C1	Clontech	V011976
pcDNA3.1-UL44	68	N/A
pmCherry-UL112-113	This study	N/A
pcDNA 3.1 UL112-113-mNeonGreen	This study	N/A
pcDNA mCherry-UL44	This study	N/A
pmCherry-UL44 Δ C	This study	N/A
pmCherry-UL44 Δ N	This study	N/A
pmCherry-UL44 Δ C+p43IDR	This study	N/A
pCGN-pp71	T. Shenk Lab	N/A

7.6 Gibson cloning primers

Name	Sequence
	pcDNA mCherry-UL112-113
Fw Vector mCherry	CTTGGTACCGAGCTCGGATCATGGTGAGCAAGGGCGAGGA

Rv UL112 linker mCherry	ACGGTAGTAGGGAGATCCAT TGATCCACCGGATCCACCTGATCCACCGGATCCACCTGATCCACCGGATCCACC CTTGACAGCTCGTCCATGC
Fw UL112-113	ATGGATCTCCCTACTACCGT
Rv pcDNA-UL112-113	CGGCGACGGCGGCGACGGCGTTAATCGTCGAAAAACGCCG
	pcDNA mNeongreen-UL112-113
Fw vector mNeongreen	GGGAGACCCAAGCTTGGTACATGGTGAGCAAGGGCGAGGA
Rv UL112-113 linker mNeongreen	ACGGTAGTAGGGAGATCCATTGATCCACCGGATCCACCTGATC CACCGGATCCACCTGATCCACCGGATCCACCCTTGACAGCTCGTCCATGC
Rv vector UL112-113	TGATGGATATCTGCAGAATTGAGACAAGGTGGTGAAGTGT
	pcDNA UL112-113-mNeonGreen
Fw Vector UL112-113	GGGAGACCCAAGCTTGGTACATGGATCTCCCTACTACCGT
RV MNEONGREEN-LINKER-UL112-113	TCCTCGCCCTTGCTCACCATTGATCCACCGGATCCACCTGATCCA CCGGATCCACCTGATCCACCGGATCCACC ATCGTCGAAAAACGCCGCGA

Fw mNeonGreen	ATGGTGAGCAAGGGCGAGGA
Rv vector mNeonGreen	TGATGGATATCTGCAGAATTTTACTTGTACAGCTCGTCCA
	pcDNA mCherry-UL44
Fw Vector mCherry	GGGAGACCCAAGCTTGGTACCATGGTGAGCAAGGGCGAGGA
Rv UL44 Linker mCherry	AGACGCGTCTTGCGATCCAT CGACGGCGGGCGACGGCGGGCGACGGCGGGCGACGGCGGGCGACGGCG GCTTGTACAGCTCGTCCATGC
Fw UL44	ATGGATCGCAAGACGCGTCT
Rv Vector UL44	TGATGGATATCTGCAGAATTCTAGCCGCACTTTTGCTTCT
	pmCherry-UL44ΔC
Fw UL44 N-term (1-290) + NLS	TCAGATCTCGAGCTCAAGCTATGGATCGCAAGACGCGTCT
Rv UL44 (1-290) NLS Vector Gibson	GTACCGTCTGACTGCAGAATTCTAGCCGCACTTCTGCTTCT
	pmCherry-UL44ΔN
Fw mCherry-UL44 C-term	AGTCCGGACTCAGATCTCGAAATTACGTCGGGAACAGC

Rv UL44 C-term	CGACTGCAGAATTCGAAGCTCTAGCCGCACTTTTGCTT
	pmCherry-UL44ΔC+p43IDR
Fw UL44 (1-290)NLS vector Gibson	TCAGATCTCGAGCTCAAGCTATGGATCGCAAGACGCGTCT
Rv Gibson (18) Only for 44 + p43	GTACCGTCGACTGCAGAATTTTAAAACGCGGACTGCGAGG
	pHR-SFFVp-p43 IDR mCherry sspB
	AGGCAGGTGGACAGTGGATCATGAATCAGACTTTCGACGT
Fw Vector p43 Core	TCCTCGCCCTTGCTCACCATTCTCCACCAAACGCGGACTGC GAGGAGGCTGAGGCGC
Rv mCherry linker p43 Core	ATGGTGAGCAAGGGCGAGGA
Fw mCherry Core	TCCAGAGGTACCACCGGATCCCTTGACAGCTCGTCCATGC
Rv Vector mCherry Core	pHR-SFFVp-p84 IDR mCherry sspB
	AGGCAGGTGGACAGTGGATCATGAATCAGACTTTCGACGT
Fw Vector p43 Core	TCCTCGCCCTTGCTCACCATTCTCCACCATCGTCGAAAAACGCCGATCGAGGCGGC
Rv mCherry linker p84 Core	ATGGTGAGCAAGGGCGAGGA

Fw mCherry Core	TCCAGAGGTACCACCGGATCCCTTGTACAGCTCGTCCATGC
-----------------	---

7.7 BAC mutagenesis primers

Name	Sequence	
	pcDNA mNeongreen UL112-113 Kanamicin Shuttle	pcDNA mNeongreen UL112-113 KpnI digested
Fwd-InsKan-N	GCGGTACCGGAGCACTGCGCGGACCACCTACA CCTTTGCCAAGCCAATGGCCGCTAACTA	
Kan Rv KpnI	CCGGTACCGCCACTGTTACAACCAATTAAC	
	Primers for recombination	
Fwd-HR-N	GCTCCACGGCCTCCGACGAGCGTTGCGCTCGCG CTTTGCGCCGCCGCGTCATGGTGAGCA	
RV-HR-N	AGGATGCGGTTAGGATTCGC	

7.8 Antibiotics

Name	Application	Concentration	Reference
ampicillin	selection of bacteria	100 µg/ml	Roth
chloramphenicol	selection of bacteria	15 µg/ml	Roth
kanamycin	selection of bacteria	100 µg/ml	Roth

penicillin	cell culture supplement	100 U/ml	Sigma-Aldrich
streptomycin	cell culture supplement	100 µg/ml	Sigma-Aldrich
puromycin	selection of transduced cells	1 µg/ml	Sigma-Aldrich
Blasticidin	selection of transduced cells	8 µg/ml	Invitrogen
L-(+)-Arabinose	Selection of bacteria	1%(w/v)	Sigma-Aldrich

7.9 Kits

Name	Reference
innuPREP DNA mini kit	Analytik Jena
mi-Plasmid Miniprep Kit	Metabion
NucleoBond Gel and PCR Clean-up	Macherey-Nagel
NucleoBond Xtra Midi	Macherey-Nagel
Cell Titer-Glo Luminescent Cell Viability Assay kit	Promega
Gibson Assembly Ultra Master Mix A and Mix B	Synthetic Genomics Inc
Click-iT™ Plus EdU Cell Proliferation Kit for Imaging, Alexa Fluor™ 555 dye	Thermo Fischer
Vivaspin® 6, 10 kDa MWCO Polyethersulfone	Sartorius

7.10 Buffers

7.10.1 Buffers for DNA purification and agarose gel electrophoresis

Name	Components	pH
50 X TAE buffer	2M Tris-HCl 50 mM EDTA 8.0 5,7 % (v/v) acetic acid	8.0
10 X TBE buffer	990 mM Tris-HCl 40 mM EDTA 8.0 990 mM boric acid	8.0
S1 Buffer	50 mM Tris-HCl 100 µg/mL RNase A 10 mM EDTA	8.0
S2 Buffer	200 mM NaOH 1 % (v/v) SDS	
S3 Buffer	2.8 M calcium acetate	5.2

7.10.2 Buffers for SDS polyacrylamide gel electrophoresis (SDS-PAGE), Western Blot, and Immunofluorescence

Name	Components	pH
SDS-Resolving Gel	3M Tris-HCl 10 % or 15 % Acrylamide 50 % Glycerol 0.3 % SDS	8,45
SDS-Stacking Gel	3M Tris-HCl 4% Acrylamide 0.3 % SDS	8,45

10 x Laemmli running buffer	250 mM Tris 1.92 M glycine 1 % (w/v) SDS	
2 x SDS-Buffer	150 mM Tris 2 mM EDTA 20 % (v/v) glycerol 4 % (v/v) SDS 10 % β -mercaptoethanol bromophenol blue 10 % β -mercaptoethanol	6.8
10 X TBS-T Buffer	100 mM Tris-HCl 1.5 mM NaCl 1 % Tween 20	7.5
Western Blot Transfer Buffer	50 mM Tris 40 mM Glycin 0,04 % SDS 20 % Methanol	
Fixation Buffer for immunofluorescence	4% Paraformaldehyde in PBS	
Permeabilization buffer	0,3% Triton X-100 in PBS	
Blocking buffer	3% BSA in PBS	
Fibronectin coating buffer for slide	Fibronectin 1:100 in PBS	

7.10.3 Buffers for protein purification

Name	Components	pH
5X Native buffer	250 mM NaH_2PO_4 2,5M NaCl	7.4
High salt storage buffer	500 mM KCl, 50 mM Tris	7,4
Equilibration buffer	Native buffer + with 10mM imidazole	
Washing buffer	Native with 25 mM imidazole	
Elution buffer	Native with 250 mM imidazole	

7.11 Devices and equipment

Name	Reference
Nikon A1 confocal laser scanning microscope (CLSM)	Nikon
Spinning Disk Nikon (Yokogawa W2 and Andor iXON888 cameras) Nikon	Nikon
ECLIPSE Ts2	Nikon
Centrifuge 5414R	Eppendorf
Centrifuge 5810R	Eppendorf

Thermomixer comfort 5355	Eppendorf
Gene Pulser XCell	Bio-Rad
GelDoc XR	Bio-Rad
Automatic Cell Counter TC10	Bio-Rad
Trans-Blot Turbo Transfer System	Bio-Rad
Sterile Bench HeraSafe	Heraeus
Hera Cell CO2 incubator	Heraeus
Sorvall RC 6+ Centrifuge	Thermo Fischer Scientific
NanoDrop ND-2000 Spectrophotometer	Peqlab
Sterile Bench HeraSafe	Heraeus
Hera Cell CO2 incubator	Heraeus
BD FACSAria™ III Cell Sorter	BD Biosciences
Roller shaker SRT9D	Stuart
Sonic Sonifier B12	Branson
Nikon TI-based TIRF microscope	Nikon

7.12 Software

Name	Source	Identifier
ImageJ/Fiji	Laboratory for Optical and Computational Instrumentation, University of Wisconsin at Madison, Madison, Wisconsin, USA	http://imagej.net/software/fiji/
CLC Main Workbench 7.7	QIAGEN Bioinformatics	
Image Lab Software 5.2.1	Bio-Rad	
Oligo Analyzer Tool	IDT	https://eu.idtdna.com/calc/analyzer/
NIS-Elements	Nikon	http://www.microscope.healthcare.nikon.com/products/software/nis-elements
GraphPad Prism 5	GraphPad Software Inc	http://www.graphstats.net/graphpad-prism
Affinity Designer	Affinity Designer – Professional	http://affinity.serif.com

	Graphic Design Software	
IUpred	109	http://www.iupred2a.elte.hu

8 Methods

8.1 Molecular biology methods

8.1.1 Preparation of electrocompetent bacteria

E. coli strains DH10B and GS1783 have been used to produce electro-competent bacteria. For both, 2 to 5 ml of 10 ml overnight cultures were inoculated into 200 ml of warm LB medium and grown in a shaking incubator at 180 rpm and 30 °C or 37 °C for GS1783 or DH10B, respectively. The OD₆₀₀ was measured using a cell density meter Ultrospec 10 (Amersham Biosciences) for checking bacterial growth. After reaching an OD₆₀₀ between 0.5 and 0.6, the DH10B strain cultures were cooled on ice for 20 minutes. The GS1783 strain cultures were incubated at 42 °C for 15 minutes to induce recombinase expression and then cooled down, as well as the DH10B. The bacteria were centrifuged at 6000g x 10 minutes to remove the medium, washed in destained water twice, and finally once in glycerol 10%. Finally, bacteria were resuspended in glycerol 10%, and aliquots of 50 µl were made and stored at -80 °C.

8.1.2 Transformation of bacteria

Electrocompetent bacteria were transformed with DNA using an electroporation device, Gene Pulser XCell (BioRad). 50 µl of bacteria were mixed with different amounts of DNA depending on the type: 200 ng of PCR linear DNA, 2 µl of Gibson cloning reaction, 2 µl of ligation mixes, or 1 ng of the plasmid. DNA was incubated with bacteria for 15 minutes on ice and then transferred in a 2 mm electroporation cuvette. Bacteria were pulsed using the following settings: 2500 V, 25 µF, and 200 Ω. After the electroporation, bacteria were resuspended in a 950 µl warm medium without antibiotics and shaken on a Thermomixer at the appropriate temperature, depending on the strain (Eppendorf), for 1 hour. Bacteria were then plated on an LB agar plate and incubated overnight at 30 °C or 37 °C.

8.1.3 Isolation of DNA from bacteria: Plasmid mini Prep

Single clone Bacteria carrying the desired plasmid were inoculated in a 5 ml LB medium with antibiotics and incubated in a shaking incubator overnight. Plasmid DNA was extracted using a mini-prep kit (Metabion) according to the kit protocol. The plasmid was resuspended in 50 µl elution buffer.

8.1.4 Isolation of DNA from bacteria: BAC mini Prep

Single clone Bacteria were inoculated in 5 ml LB medium with antibiotics and incubated in a shaking incubator overnight. 2 ml of the overnight culture was transferred in a 2 ml tube and spun down at 5000 g for 10 minutes at 4 °C. BAC DNA was isolated by using alkaline lysis and isopropanol precipitation. The bacteria pellet was resuspended in 150 µl of S1 buffer and then lysed on ice for 5 minutes by adding 150 µl of S2 buffer. 150 µl of the S3 buffer was used to stop the lysis. After 7 minutes of incubation, the mixture for centrifuge at 10.000 g for 20 minutes at 4 °C to remove the lysis debris. The supernatant was mixed thoroughly with 400 µl isopropanol, and the DNA was pelleted in at 10.000 g for 30 minutes at 4°C. The pellet was washed in 700 µl Ethanol 70% and centrifuged again. The Ethanol was removed by pipetting, and the pellet was dried by incubation in a thermoblock at 50°C. The pellet was resuspended in 50 µl destained water.

8.1.5 Isolation of DNA from bacteria: BAC/plasmid midi Prep

Single clone bacteria were inoculated in 200 ml medium and cultured overnight in a shaking incubator at the appropriate condition. Plasmid DNA and BAC were extracted by using a “NucleoBond Xtra Midi” (Metabion) kit with the “high-copy” or “low-copy” protocols, respectively. The pellet resulting from BAC extraction was dried and resuspended in a laminar flow hood under sterile conditions.

8.1.6 Long-term storage of bacteria

1 ml of bacteria overnight culture was mixed with 1 ml of autoclaved 60% (v/v) glycerol and frozen at -80°C.

8.1.7 DNA sequencing

DNAs were sequenced by SEQLAB Sequence Laboratories or by Eurofins Genomics. DNA preparation for sequencing was made accordingly to the company guidelines.

8.1.8 Polymerase chain reaction (PCR)

PCR was carried out using high-fidelity Precisor Polymerase (BioCat) according to the manufacturer's protocol.

8.1.9 Restriction digestion of DNA

DNA was digested using 1 µl of FastDigest (FD) restriction enzymes in Fast Digest buffer. Digestion was carried out for 1h at 37 °C.

8.1.10 Agarose gel electrophoresis and purification of DNA fragments from gel

Plasmids and PCR products were mixed with loading dye and resolved on 1% (W/v) agarose TAE gels for 1 hour at 120 V. Digested BAC DNA was resolved on 0.6% (W/v) agarose TBE gels at 60 V overnight, imaged and then run at 120 V for 1 hour for better resolving the high molecular size bands. TAE and TBE gels contained 0.5 µg/ml ethidium bromide and were visualized by UV light using a GelDoc XR + (BioRad). O'GeneRuler (ThermoFisher) was loaded into gels as a reference size ladder.

8.1.11 Gibson assembly and restriction enzyme cloning

Plasmids encoding tagged proteins were generated by Gibson assembly. For this purpose, the target vectors were linearized using one or two restriction enzymes. The DNA fragments from the desired genes were generated by PCR, adding 20 bp of overlapping sequences with the adjacent DNA fragments. The fragments and the vectors were purified from the agarose gel and ligated following the Gibson Assembly Ultra protocol.

8.1.12 *En passant* mutagenesis

For fluorescent tagging of the UL112-113 proteins, the BAC clone of HCMV strain TB40/E, TB40-BAC4¹⁷² was modified by two-step mediated red recombination¹⁰⁸. First, a universal transfer construct containing mNeogreen-UL112-113 and the Kanamycin system was prepared. A flexible 6x GGS linker was inserted between mNeogreen and UL112-113 to avoid disrupting UL112-113 functionality. The I-SceI/kan cassette was PCR-amplified from pEPkan-S2 (Addgene #61601) and inserted into the KpnI site of pcDNA-mNeonGreen-UL112. The mNeogreen-UL112-113-kanamycin construct was amplified by PCR with primers containing homologous regions for the viral genome (Primers Fwd-HR-N and Rv-HR-N), and template DNA was removed by DpnI digestion. As explained previously, the electrocompetent GS1783 bacteria containing TB40/E BAC were transformed with the linear DNA and plated in an LB agar plate containing Chloramphenicol and Kanamycin at 30 °C

overnight. Eight clones were picked and inoculated in an LB medium for extracting DNA by mini prep.

Isolated BAC DNA was digested by digestion enzymes and compared to the wild type. 2 clones showing the correct pattern were selected for the second recombination. Single colonies of the two clones were inoculated into 2 ml LB medium containing only Chloramphenicol and incubated for 2-3 h at 30 °C. 2% l-arabinose was added to the media, and bacteria were incubated for another hour. The recombinase expression was induced by incubating the bacteria at 42°C in a shaking water bath for 30 minutes. Bacteria were then incubated for 3 hours at 30 °C. Bacteria culture was diluted at 1:1000 or 1:10000 with medium depending if the OD was lower or higher than 0.5, respectively. 100µl of the diluted culture was plated on an LB agar plate containing chloramphenicol and 1% L-arabinose and incubated overnight at 30°C. BAC from several clones was extracted and analyzed by restriction enzyme digestion. The gene was PCR amplified and sequenced to check the correct insertion of the mNeongreen tag and the integrity of the UL112-113 gene. Purified DNA from clones was used for virus reconstitution in human fibroblasts.

8.2 Cell biology and virology methods

8.2.1 Cell culture

All cells were incubated in a Hera Cell Co² incubator, and all the cell culture-related work was performed using the HeraSafe (Heraeus) laminar flow hood. All cells were grown in Dulbecco's modified Eagle medium (DMEM) supplemented with 10% FCS, 100 U/mL penicillin, and 100 µg/mL streptomycin. T-REx-293-mNeonGreen-UL112-113 cells were cultivated with Doxycycline-free serum and 5 µg/ml blasticidin. Cells were grown in 10 or 15 cm³ plates till they reached 80-90% confluency, after which they were split at 1:10 (293 cells) or 1:3 (Fibroblast) ratio, according to the specific cell line. The splitting was performed by removing the medium, washing the cells in PBS, and adding 0.5/3ml of trypsin, depending on the plate size. The trypsin-induced detachment was monitored using a cell culture microscope and inactivated by adding an excess of fresh medium. All cells used in this study were tested regularly for mycoplasma contamination by PCR. An automated cell counter (TC10, Bio-Rad) determined the number of cells.

8.2.1 Freezing and thawing of cells

For long-term storage, cells were centrifuged 8 minutes at 180g at 37 °C and resuspended in FCS containing 10% DMSO. Cells were kept at -80 °C for the short term and then transferred in liquid nitrogen for long-term storage. Cells were thawed fast in a water bath at 37 °C, mixed with medium, and centrifuged for 8 minutes. Cells were resuspended in a 10 ml medium and transferred to a 10 cm³ plate. The day after, the medium was changed to remove the dead cells.

8.2.3 Plasmid transfection

HEK-293A, HEK-293T, and HEK-293T-REx cells were transfected using PEI. For lentivirus production and T-REx-293-mNeonGreen-UL112-113 cell line, 0.5×10^6 cells/well were seeded in a 6 wells plate. For each well, 3 µg of total plasmid DNA were mixed with antibiotic-free medium and incubated with 9 µg/µl PEI for 5 minutes. The mixture was incubated overnight, and the medium was replenished the day after. T-REx-293-mNeonGreen-UL112 cells were generated by transfecting T-REx-293 with pcDNA4/T0 mNeonGreen-UL112, while transduced cells were selected with 200 µg/mL Zeocin for five days. For microscopic assays, 2×10^4 cells were seeded in 8 wells (Ibidi) and incubated with 1 0.3 µg DNA and 0.9 µg/µl PEI.

8.2.4 Transfection of BAC DNA

For the reconstitution of HCMV from BAC, the DNA was transfected in eukaryotic cells using an electroporation device, Gene Pulser XCell (BioRad). For each transfection, 4 plates of around 70% confluent MRC-5 cells were trypsinized and centrifuged at 180 g for 8 minutes. Cells were washed in 10 ml OptiMEM-1, pelleted again, and resuspended in 200 µl OptiMEM-I. One µg of pCGN-pp71 plasmid and 3 µg of the desired BAC DNA were carefully added to the medium and pipetted. Cells were transferred in a 4 mm electroporation cuvette and electroporated using the following settings: 220 V, Capacitance 950 µF. After the electroporation, 800 µl of OptiMEM-I was added to the cells, and floating debris was carefully removed by pipetting. Cells were then plated in 10 cm³ and supplemented with 9 ml of fresh DMEM + 10% FCS medium. Reconstitutions of infectious HCMV-NeonGreen-UL112 and HCMV-UL32-GFP were monitored by detecting GFP or mNeongreen positive cells using the ECLIPSE Ts2 (Nikon) inverted microscope equipped with LED illuminators. Infected cells were mixed with uninfected MRC-5 fibroblast to achieve a higher titer.

8.2.5 Lentivirus production

For lentivirus production, HEK-293T cells were transfected using 1,5 µg of lentiviral constructs (0.3 µg pMD2.G, 0.6 µg pMDLg/pRRE, 0.6 µg pRSV-Rev) and 1.25 µg of the desired constructs (either pHR-SFFVp-NLS-iLID::EGFP::FTH1, pHR-SFFVp-HNRNPA1C::mCherry::SspB, pHR-SFFVp-mCherry::SspB, pHR-SFFVp-p43ΔN::mCherry::SspB or pHR-SFFVp-p84ΔN::mCherry::SspB). Harvesting of the infectious supernatant was performed at 48 and 72 hours post-transfection by collecting the media and filtering it with a 0.45µm filter to remove cell debris. The supernatant was used immediately or stored at 4°C for a maximum of 1 week.

8.2.6 Lentivirus transduction for production of corelet-expressing cells

Around 1×10^6 293A cells were plated in 6 wells plate and transduced with 2 ml of pHR-SFFVp-NLS-iLID::EGFP::FTH1 infectious lentivirus in the presence of 3 µl Polybrene (Millipore). The medium was changed after overnight incubation, and cells were split in a 10 cm³ plate when confluency was reached. One week after, 1×10^6 transduced cells were plated in a 6-well plate and transduced either with 2 ml of pHR-SFFVp-HNRNPA1C::mCherry::SspB, pHR-SFFVp-mCherry::SspB, pHR-SFFVp-p43ΔN::mCherry::SspB or pHR-SFFVp-p84ΔN::mCherry::SspB lentiviruses. Following transductions, cells were expanded in 10 cm³ plates. On the week after transduction, double fluorescent cells were selected by using the BD FACSAria™ III Cell Sorter.

8.2.7 HCMV virus stock production and concentration

Several 15 cm³ semi-confluent plates of MRC-5 cells were infected with each virus with an MOI of 0.02. Virus infectivity was monitored by visualization with an ECLIPSE Ts2 (Nikon) inverted microscope. Infectious supernatant was collected every 2 days starting when almost all the cells were infected. The supernatant was stored at -80 °C. For the concentration of the virus stock, the infectious supernatant was first centrifuged 15 minutes at 6000 g 4 °C to remove the cellular debris. The supernatant was then pelleted through 3 hours of centrifugation at 26000 g 4 °C and resuspended in 1 ml of fresh DMEM medium overnight. The virus was centrifuged again at 26000 g for 1 hour for further debris removal on a 20% sucrose cushion. The resulting pellet was resuspended in DMEM medium overnight, aliquoted, and stored at -80 °C. Three aliquots of each purified virus were stored for the definition of virus concentration by TCID₅₀/ml.

8.2.8 Production of EdU-labeled stocks

For the production of EdU-labelled virus stocks, MRC-5 cells were infected with mNeongreen-UL112 or HCMV-UL32-GFP viruses at an MOI of 1. The day after, the medium was supplemented with 2 μ M EdU. The EdU-containing medium was replenished daily, and the virus supernatant was harvested starting at 4 dpi. The virus supernatant was collected every day until almost complete cell detachment. The virus supernatant was purified as previously described. The labeled viruses were titered as described before using the standard TCID₅₀/ml protocol.

8.2.9 HCMV titration using TCID₅₀ /ml

TCID₅₀/ml method was used to determine the virus concentration, and 2 x 96 wells plates were used for each virus titration. Around 1×10^3 MRC-5 cells were seeded in each well of a 96-well plate. The day after, serial dilution (from 10^{-3} to 10^{-10}) of the virus was prepared, and each dilution was added to one entire row of wells for two 96-well plates. The plates were subjected to centrifugal enhancement (1000g, 30 minutes, 37°C) or directly incubated for 14 days without centrifugal enhancement. The number of positive wells was determined by fluorescence detection of infected cells, while the viral titer was calculated using the Spearman-Kärber formula.

8.2.10 Viral infections

Cells were infected with HCMV using different MOI based on the TCID₅₀/ml of the desired virus stock. The following formula determined the determination of the volume of virus stock needed:

$$V(ml) = \frac{\text{number of cells} \times \text{MOI}}{\text{TCID}_{50} / \text{ml}}$$

Cells were infected by replacing the culture media with fresh media supplemented with the virus. The medium was replenished 2 hours after infection to remove the excess of the virus.

8.2.11 Hexanediol and propylene glycol treatments

1,6-Hexanediol (Sigma) powder was dissolved in complete DMEM and stored at 4°C. Propylene glycol (Sigma) was added directly to the medium and stored at 4°C. Cells were grown on a 35 mm dish (ibidi) coated with Fibronectin bovine plasma (Millipore) for pulse experiments. Cells were then treated with the desired compound concentrations, and the effect was assayed by direct

visualization in live-cell imaging or after fixation. In chase experiments in live-cell imaging, the medium was changed directly at the microscope using a pipette.

8.3 Biochemistry methods

8.3.1 SDS polyacrylamide gel electrophoresis (SDS-Page) and western-blot

The cells were washed in PBS and boiled at 95°C in 2x SDS buffer for 10 minutes. Proteins were separated in polyacrylamide gels composed of a stacking gel of 4% acrylamide percentage and a 10 % acrylamide percentage resolving gel. The proteins were first stacked in the gel at 40V until the proteins reached the resolving gel and then ran at 120V until they reached the gel's end. Proteins were transferred on nitrocellulose membrane at 25V for 60 minutes using a Transblot Semi-dry Transfer Cell (Biorad). The membrane was washed in TBS-T buffer and incubated for 1 hour in 5% milk powder to block nonspecific antibody sites. Membranes were stained with primary antibodies overnight at 4°C (anti-mNeongreen, 32F6, Chromotek, 1:1000) and the day after with secondary antibody conjugated to horseradish peroxidase (anti mouse HRP, 1:5000) for 1 hour at RT. After 3 washing in TBS-T, the membrane was incubated with the Pierce™ ECL Western Blotting Substrate (Thermo Fischer), and chemiluminescence was detected using X-ray films.

8.3.2 Blue coomassie staining

Gels were fixed in coomassie fixing buffer (50% methanol,10% acetic acid,40% water) for 30 minutes, stained in a solution containing the 0.1 % (v/v) of blue Coomassie for 30 min, and destained overnight in coomassie destaining buffer (40% methanol, 10% acetic acid, 50% water). Coomassie-stained Gels were imaged using a commercial office scanner (Epson).

8.3.3 UL112-113 proteins purification

To purify UL112-113 isoforms, twenty 15 cm³ plates of T-REx-293-mNeonGreen-UL112-113 cells were prepared, each with around 2 million cells. The day after, the expression of mNeongreen-UL112-113 proteins was induced by 2 mg/ml doxycycline addiction. Expression of fluorescent proteins was monitored by fluorescent microscopy, and cells were harvested 2-3 days post-induction, depending on the protein expression and confluency. The conditioned medium was removed, and cells were washed in PBS. Cells were then detached using a cell scraper (Sigma-

Aldrich), collected in 50 ml falcons, and centrifuged at 200 g x 8 minutes. The pellet was then mixed with 16 ml native buffer 1x with a cocktail of protease inhibitors and subjected to three freeze-thawing cycles for lysing the cells. The cells were frozen in an ethanol-dry ice bath and thawed at 50°C in a water bath. Subsequently, for shearing the cellular DNA, the lysate was passed through an 18-gauge needle four times and sonicated 15 seconds x4 times at 5-10 W using a cell sonicator (Branson). The lysate was centrifuged at 15000 g x 30 minutes to remove aggregate and cell debris, and the supernatant was incubated with 500 µl equilibrated HisPur Ni-NTA Resin (Thermo Fischer) overnight at 4°C using a rolling shaker (Stuart). The beads were centrifuged at low speed (200g x 5 minutes) and washed in Equilibration buffer 3 times. Proteins were eluted by incubating the beads with 1 ml of Elution buffer containing 250 mM Imidazole for 10 minutes. The elution step was monitored by microscope visualization and repeated 2-3 times to elute more proteins. Proteins were spun at 1000g to remove the beads and concentrated at 4°C on a Sartorius Vivaspinn column 6 10 kDa. After two washing steps to remove the excess imidazole, the proteins were resuspended in a high-salt buffer to prevent unwanted phase separation. Proteins were stored at -80 °C or used immediately for further applications.

8.4 Microscopy methods

8.4.1 Light microscopy modalities

Confocal laser scanning microscopy was done using a Nikon TI2-based A1R unit with PMT and GaAsP detectors, standard 404, 489, 561, and 637 laser lines, and the relevant filter sets. Nikon 1.4 NA 60x Plan Apo or a Nikon NA 0.9 40x objectives were employed for image acquisition; the pixel size was optimized to enable maximal resolution in NIS-Elements. Spinning disk microscopy was conducted on a Nikon TI2-based system with a Yokogawa W2, a Nikon 1.49 NA Plan Apo objective, and an Andor iXON888 EMCCD; the resulting pixel size was 130nm, and image acquisition was made with NIS-Elements. Furthermore, the setup was furnished with 405, 488, 561, and 640 laser lines and the corresponding filter sets. Lastly, wide-field fluorescence microscopy was conducted on a Nikon TI-based TIRF setup with a Nikon 60x 1.40 NA Plan-Apo objective and an Andor iXON897 EMCCD and was also equipped with 405, 488, 561, and 640 laser lines and corresponding filter sets.

8.4.2 Immunofluorescence

For immunofluorescence staining, 3×10^4 MRC-5 cells were seeded on μ -slide 8 wells (ibidi) one day before infection. Cells were then infected at an MOI of 1, and the medium was changed 2 hours later to remove the excess virus. Cells were fixed at different time points using 4% PFA and permeabilized per 20 minutes in PBS containing 0.2% Triton X-100. After washing with PBS, cells were blocked using 3% BSA in PBS for 30 minutes and incubated overnight at 4°C with primary antibodies. After 3 washing steps, samples were incubated with 1:1000 diluted Alexa-Fluor-coupled secondary antibodies for 45 min at room temperature. Nuclei were stained using a 1:2000 Hoechst 33342 solution (ThermoFisher) for 10 min. Following monoclonal antibodies/antisera were used for Immunofluorescence at the indicated concentrations: HCMV pUL44 (CA006, Virusys, 1:1000), mNeongreen (32F6, Chromotek, 1:1000), BrdU (ab6326, Abcam, 1:500), Goat anti-Mouse IgG Alexa 555 (Invitrogen, A32727, 1:2000), Goat anti-Mouse IgG Alexa 647 (Invitrogen, A32727, 1:2000), Goat anti-Rabbit IgG Alexa 647 (Invitrogen, A32733, 1:2000), Anti-RNA polymerase II CTD repeat YSPTSPS (phospho S5) (Abcam, ab5131, 1:1000).

8.4.3 EdU label of the incoming viral genome

To visualize the incoming viral genomes, around 2×10^4 MRC-5 cells were seeded in 8 wells (Ibidi) and incubated overnight. Cells were infected at an MOI of 1 with the EdU-labeled viruses, washed in PBS, and fixed in 4% PFA at 4°C overnight. Cells were fixed at different time points, depending on the experiments. After fixation, the cells were washed extensively in 3% BSA, permeabilized, and processed for immunofluorescence protocol, as described before. After washing steps in 3% BSA, cells were processed with the Click-iT® EdU Imaging Kits (Thermo Fischer). A Click-iT® solution was prepared according to the manufacture protocol, containing CuSO₄, Alexa fluor azide 555, and an additive for protecting the fluorescence from antibodies and proteins. The cells were dried using a vacuum pump and incubated with 300 μ l of the Click-iT® solution for 30 minutes, protected from light. Finally, cells were washed three times in 3% BSA and three times in PBS. Cells were imaged using a confocal microscope (Nikon A1) in maximum resolution mode.

8.4.4 Labeling of the replicating genome by EdU and BrdU

For the labeling of the replicating genome by EdU, infected cells were pulsed for 2 hours with 10 μ M of the nucleoside analog. Cells were then washed in PBS, fixed in 4% PFA at 4°C overnight, and

processed with the Click-iT® EdU Imaging Kits (Thermo Fischer) as described before. Infected cells were treated with 100 µM BrdU for 6 hours to label the replicating genome by BrdU. Cells were washed once in medium and three times in PBS before fixation and permeabilization, performed as described before. Detection of BrdU requires denaturation of the DNA, which was performed by incubation with a 2 N HCL solution for 30 minutes at RT. The acid was then neutralized by adding a 0.1 M sodium borate buffer solution (pH 8.5) for 30 minutes at room temperature. After extensive washing in PBS, BrdU was stained by immunofluorescence using the BrdU (ab6326, Abcam,1:500) antibody, as described before. For the visualization of the incoming and the replicating viral genomes, the Click-iT® EdU Imaging Kit was used after the BrdU staining and washing in 3% BSA.

8.4.5 In vitro phase separation assay

For assaying in vitro phase separation of UL112-113, the freshly prepared proteins were centrifuged at 16000g for 30 minutes using a benchtop centrifuge 5415R (Eppendorf) to remove aggregate. Protein concentration was then measured by detecting the 280 absorbances using a NanoDrop-1000 (Peylab) spectrophotometer. The proteins were mixed in a tube with buffers with increasing KCL concentration to obtain 500, 150, or 75 mM KCL concentration. Proteins were then spotted on 18 wells dish (Ibidi) previously coated with 1% gelatin. Proteins were then immediately visualized by a confocal microscope (Nikon A1) or a Nikon TI-based TIRF microscope (Nikon), used in widefield mode.

8.4.6 Live-cell imaging

Life cell experiments on the different systems were conducted with identical humidified incubation chambers, heated to 37°C, and 5% CO₂ controlled by a gas mixer. Cells were grown in Ibidi 35mm glass-bottom dishes or in Ibidi 8 wells, depending on the experiment. Plates were previously coated with bovine Fibronectin (Millipore Sigma) for fibroblast experiments or with 1% gelatin for experiments with 293 cells.

8.4.7 Fluorescence Recovery After Photobleaching (FRAP)

For FRAP, a 1 µm ROI was photobleached for 0.0625 seconds using the same laser wavelength as imaging on a Nikon A1R confocal scanning microscope. Fluorescence intensity was recorded for up to two minutes at two frames per second using NIS-element software. At least ten cells per

condition were analyzed, with three areas marked with regions of interest for each cell over time: the bleached sample area SA, the whole nucleus as reference REF, and an area outside representing the background BG. BG was then subtracted from SA and REF measurements over time to create SAcorr and REFcorr, respectively, correcting for fluctuations in the illumination. The ratio of these was then divided by the mean of the last 10 time points of SA before photobleaching ($S_{\text{Accorr}}/R_{\text{Efcorr}}/S_{\text{Ainit}}$) and plotted in Prism. To obtain the mobile fraction, the recovery was calculated by dividing the difference between the mean of SAcorr of the first 10 frames after fluorescence recovery had saturated and SAbleach (the first measured frame after bleaching SA) by the difference between SAinit and SAbleach ($(S_{\text{Afinal}} - S_{\text{Ableach}}) / (S_{\text{Ainit}} - S_{\text{Ableach}})$). We used GraphPad Prism version 5.0.0 for Windows to calculate the mobile fraction and the recovery half-time. To determine the mobile fraction, we estimated the recovery by subtracting SAbleach (the first measured frame after bleaching SA) from SAfinal (the mean of SAcorr of the first 10 frames after fluorescence recovery had saturated) and dividing the result by the difference between SAinit and SAbleach ($(S_{\text{Afinal}} - S_{\text{Ableach}}) / (S_{\text{Ainit}} - S_{\text{Ableach}})$). We fitted the recovery curves to a nonlinear regression curve and extracted the K_m to calculate the recovery half-time. Finally, we divided the resulting ratio by the mean of the last ten time points of SA before photobleaching SA ($S_{\text{Accorr}}/R_{\text{Efcorr}}/S_{\text{Ainit}}$) and plotted the results in Prism.

8.4.8 Corelet system local and global photoactivation

The Nikon A1R confocal scanning microscope was used to conduct photoactivation experiments. Cells that expressed the iLiD and sspB constructs were globally activated by exposing them to both 488 and 563 nm laser illumination for 10 minutes, then two minutes later, they were imaged with just 563 nm to demonstrate the reversibility of nucleation. The in vivo phase diagrams were plotted from the fluorescence intensities of 150 cells per condition. The fluorescence intensities of the nucleoplasm were assessed before photoactivation to measure the core-to-IDR ratio in the diluted phase. The dense phase ratio was calculated by calculating the fluorescence intensity of the droplets after photoactivation. Local photoactivation was done on cells that did not cluster after 10 minutes of global activation. This was done by alternating between 563 nm laser illumination for imaging and quick stimulation (0.125 seconds each) with 488 nm laser illumination at 0.01% laser power in a diffraction-limited spot.

8.4.9 Serial-block-face scanning electron microscopy (SBF-SEM)

Serial-block-face scanning electron microscopy was performed using a Jeol JSM-7100F scanning electron microscope (Jeol) equipped with a Gatan 3view stage (Gatan). Samples were imaged with a beam acceleration voltage of 3 kV, the current probe set to 1, and a 500 V positive charge applied to the sample holder. Regions of interest (ROIs) were defined manually to determine the portion of the image. A built-in diamond knife microtome was used to repeatedly cut 50 nm slices, which were imaged right after the cut to obtain the objects' tridimensional images.

8.4.10 CLEM and SBF-SEM staining

For the staining of the samples for CLEM, the cells were plated in a special gridded 35mm dish (Ibidi), infected at an MOI of 1, and imaged by confocal microscopy (Nikon A1) in live cell imaging. The position of the imaged cells was recorded thanks to the numbered grid of the dish. Cells were fixed right after the imaging process in a PBS solution containing 2% (m/v) PFA and 2,5 % (m/v) glutaraldehyde at 72 hpi (GA; Science Services) for 5 minutes at RT and 55 minutes on ice. For CLEM samples, fluorescence microscopy was performed after the initial fixation. The cells were washed 5 times with ice-cold D-PBS and post-fixed with a 1:1 mixture of ice-cold 4% (m/v) OsO₄/D-PBS and 5% (m/v) GA/D-PBS solutions directly on the dish by careful agitation. The following steps were used for staining, and after each step, the cells were washed 10 times with H₂O: 2% (m/v) OsO₄/1.5% (m/v) K₄Fe[CN]₆/2 mM CaCl₂ in H₂O for 1 hour, 0.5% (m/v) thiocarbohydrazide in H₂O for 30 minutes, 2% (m/v) OsO₄ in H₂O for 20 minutes, 1% (m/v) gallic acid in H₂O for 10 minutes, and 2% (m/v) uranyl acetate in H₂O at 4°C overnight. The sample was stained with Waltons lead aspartate solution for 30 minutes at 60°C. After staining, the sample was dehydrated using a progressive lowering of temperature dehydration process (PLT). The sample was incubated in a series of ethanol-water mixtures with increasing ethanol content while lowering the temperature at each step. The sample was then incubated in a mixture of 70% (v/v) freshly prepared Epon embedding medium in ethanol for 1 hour at room temperature, followed by incubation in 100% Epon overnight. The sample was then incubated for 6 hours in a conductive embedding medium consisting of 3% (m/m) Ketjen Black and 3% (m/m) silver flakes in Epon at room temperature before transferring the sample to 60°C for polymerization for 3 days. The region of interest (ROI) was cut out of the dish with cutting pliers and mounted coverslip facing upwards on a solid Epoxy block using 2 component glue (UHU Plus Endfest 300, UHU). The sample was then manually roughly trimmed to a 1.5 mm x

1.5 mm flattop pyramid using a razor blade. The polymer coverslip was then trimmed off using a diamond trimming knife and a Leica Ultracut microtome until approximately 175 of 180 μm were removed. The pyramid was then cut to its final block face size of 0.5 mm x 0.5 mm and removed from the mounting block with a total height of approximately 3 mm using a razor blade. Finally, the sample block was mounted on a Gatan 3view sample stub using a conductive silver epoxy glue and sputter coated with a 10 nm gold layer.

8.5 Microscopy Analysis

8.5.1 Fluorescence intensity profiles

Intensity profiles were measured in ImageJ by drawing a line across the relevant area and exporting the intensity measurements for each channel in excel files. The background measurement was performed by analyzing the mean fluorescence intensity of each channel in an area outside the cell in the same image, and its value was subtracted from all the intensity measurements. The intensities were then normalized to a 0-100% scale in GraphPad Prism version 8.0.0 for Windows and plotted against the position on the drawn line.

8.5.2 EdU surface area measurements for quantification of viral genome replication and colocalization

EdU surface areas were quantified using ImageJ software. Manual ROIs were drawn around nuclei identified by Hoechst staining. EdU-labeled areas were segmented by thresholding, creating a mask resembling the area. Resulting EdU-ROIs were then used to measure signal intensities in the UL112-113, UL44, Pol II, and BrdU channels where applicable. Co-localization was scored when the fluorescence intensity of the analyzed antigen was significantly higher than the background. BrdU and EdU labeled areas were segmented by thresholding to quantify the genome area, and the measure of their area was extracted. The total genome area was obtained when applicable by summing the incoming viral genomes (EdU) area with the adjacent replicating viral genome (BrdU) area.

9 References

1. McGeoch, D.J., and Gatherer, D. (2005). Integrating Reptilian Herpesviruses into the Family Herpesviridae. *J Virol* 79, 725–731. 10.1128/jvi.79.2.725-731.2005.
2. Gatherer, D., Depledge, D.P., Hartley, C.A., Szpara, M.L., Vaz, P.K., Benkő, M., Brandt, C.R., Bryant, N.A., Dastjerdi, A., Doszpoly, A., et al. (2021). ICTV Virus Taxonomy Profile: Herpesviridae 2021. *J Gen Virology* 102, 001673. 10.1099/jgv.0.001673.
3. Roizman, B., and Whitley, R.J. (2013). An Inquiry into the Molecular Basis of HSV Latency and Reactivation. *Annu Rev Microbiol* 67, 355–374. 10.1146/annurev-micro-092412-155654.
4. Cook, M.L., and Stevens, J.G. (1973). Pathogenesis of Herpetic Neuritis and Ganglionitis in Mice: Evidence for Intra-Axonal Transport of Infection. *Infect Immun* 7, 272–288. 10.1128/iai.7.2.272-288.1973.
5. Aimola, G., Beythien, G., Aswad, A., and Kaufer, B.B. (2020). Current understanding of human herpesvirus 6 (HHV-6) chromosomal integration. *Antivir Res* 176, 104720. 10.1016/j.antiviral.2020.104720.
6. Li, Y., Qu, T., Li, D., Jing, J., Deng, Q., and Wan, X. (2022). Human herpesvirus 7 encephalitis in an immunocompetent adult and a literature review. *Virol J* 19, 200. 10.1186/s12985-022-01925-9.
7. Bjornevik, K., Cortese, M., Healy, B.C., Kuhle, J., Mina, M.J., Leng, Y., Elledge, S.J., Niebuhr, D.W., Scher, A.I., Munger, K.L., et al. (2022). Longitudinal analysis reveals high prevalence of Epstein-Barr virus associated with multiple sclerosis. *Science* 375, 296–301. 10.1126/science.abj8222.
8. Cesarman, E., Chadburn, A., and Rubinstein, P.G. (2022). KSHV/HHV8-mediated hematologic diseases. *Blood* 139, 1013–1025. 10.1182/blood.2020005470.
9. Greene, W., Kuhne, K., Ye, F., Chen, J., Zhou, F., Lei, X., and Gao, S.-J. (2007). Aids-Associated Viral Oncogenesis. *Canc Treat* 133, 69–127. 10.1007/978-0-387-46816-7_3.
10. Zuhair, M., Smit, G.S.A., Wallis, G., Jabbar, F., Smith, C., Devleesschauwer, B., and Griffiths, P. (2019). Estimation of the worldwide seroprevalence of cytomegalovirus: A systematic review and meta-analysis. *Rev Med Virol* 29, 31.
11. Britt, W.J. (2018). Maternal Immunity and the Natural History of Congenital Human Cytomegalovirus Infection. *Viruses* 10, 405. 10.3390/v10080405.
12. Weisblum, Y., Panet, A., Haimov-Kochman, R., and Wolf, D.G. (2014). Models of vertical cytomegalovirus (CMV) transmission and pathogenesis. *Semin Immunopathol* 36, 615–625. 10.1007/s00281-014-0449-1.
13. Kenneson, A., and Cannon, M.J. (2007). Review and meta-analysis of the epidemiology of congenital cytomegalovirus (CMV) infection. *Rev Med Virol* 17, 253–276. 10.1002/rmv.535.
14. Cannon, M.J., and Davis, K.F. (2005). Washing our hands of the congenital cytomegalovirus disease epidemic. *Bmc Public Health* 5, 70. 10.1186/1471-2458-5-70.

15. Schleiss, M.R. (2008). Human Cytomegalovirus. *Curr Top Microbiol*, 361–382. 10.1007/978-3-540-77349-8_20.
16. Britt, W.J. (2017). Congenital Human Cytomegalovirus Infection and the Enigma of Maternal Immunity. *J Virol* 91. 10.1128/jvi.02392-16.
17. Dahle, A.J., Fowler, K.B., Wright, J.D., Boppana, S.B., Britt, W.J., and Pass, R.F. (2000). Longitudinal investigation of hearing disorders in children with congenital cytomegalovirus. *J Am Acad Audiol* 11, 283–290.
18. Scarpini, S., Morigi, F., Betti, L., Dondi, A., Biagi, C., and Lanari, M. (2021). Development of a Vaccine against Human Cytomegalovirus: Advances, Barriers, and Implications for the Clinical Practice. *Nato Adv Sci Inst Se* 9, 551. 10.3390/vaccines9060551.
19. Littler, E., Stuart, A.D., and Chee, M.S. (1992). Human cytomegalovirus UL97 open reading frame encodes a protein that phosphorylates the antiviral nucleoside analogue ganciclovir. *Nature* 358, 160–162. 10.1038/358160a0.
20. Paya, C., Humar, A., Dominguez, E., Washburn, K., Blumberg, E., Alexander, B., Freeman, R., Heaton, N., Pescovitz, M.D., and Group, V.S.O.T.S. (2004). Efficacy and Safety of Valganciclovir vs. Oral Ganciclovir for Prevention of Cytomegalovirus Disease in Solid Organ Transplant Recipients. *Am J Transplant* 4, 611–620. 10.1111/j.1600-6143.2004.00382.x.
21. Kimberlin, D.W., Lin, C.-Y., Sánchez, P.J., Demmler, G.J., Dankner, W., Shelton, M., Jacobs, R.F., Vaudry, W., Pass, R.F., Kiell, J.M., et al. (2003). Effect of ganciclovir therapy on hearing in symptomatic congenital cytomegalovirus disease involving the central nervous system: a randomized, controlled trial*. *J Pediatrics* 143, 16–25. 10.1016/s0022-3476(03)00192-6.
22. Boonsathorn, S., Pasomsub, E., Techasaensiri, C., and Apiwattanakul, N. (2019). Analysis of Ganciclovir-Resistant Cytomegalovirus Infection Caused by the UL97 Gene Mutation in Codons 460 and 520 in Pediatric Patients: A Case Series. *Open Forum Infect Dis* 6, ofz480. 10.1093/ofid/ofz480.
23. Lurain, N.S., and Chou, S. (2010). Antiviral Drug Resistance of Human Cytomegalovirus. *Clin Microbiol Rev* 23, 689–712. 10.1128/cmr.00009-10.
24. Goldner, T., Hewlett, G., Ettischer, N., Ruebsamen-Schaeff, H., Zimmermann, H., and Lischka, P. (2011). The Novel Anticytomegalovirus Compound AIC246 (Letermovir) Inhibits Human Cytomegalovirus Replication through a Specific Antiviral Mechanism That Involves the Viral Terminase. *J Virol* 85, 10884–10893. 10.1128/jvi.05265-11.
25. Perera, M.R., Wills, M.R., and Sinclair, J.H. (2021). HCMV Antivirals and Strategies to Target the Latent Reservoir. *Viruses* 13, 817. 10.3390/v13050817.
26. Kalejta, R.F. (2008). Tegument Proteins of Human Cytomegalovirus. *Microbiol Mol Biol R* 72, 249–265. 10.1128/mmbr.00040-07.
27. Chiu, W., and Rixon, F.J. (2001). High resolution structural studies of complex icosahedral viruses: a brief overview. *Virus Res* 82, 9–17. 10.1016/s0168-1702(01)00381-1.

28. Martí-Carreras, J., and Maes, P. (2019). Human cytomegalovirus genomics and transcriptomics through the lens of next-generation sequencing: revision and future challenges. *Virus Genes* 55, 138–164. 10.1007/s11262-018-1627-3.
29. Murphy, E., Rigoutsos, I., Shibuya, T., and Shenk, T.E. (2003). Reevaluation of human cytomegalovirus coding potential. *Proc National Acad Sci* 100, 13585–13590. 10.1073/pnas.1735466100.
30. Zhang, L., Yu, J., and Liu, Z. (2020). MicroRNAs expressed by human cytomegalovirus. *Virology* 17, 34. 10.1186/s12985-020-1296-4.
31. Weekes, M.P., Tomasec, P., Huttlin, E.L., Fielding, C.A., Nusinow, D., Stanton, R.J., Wang, E.C.Y., Aicheler, R., Murrell, I., Wilkinson, G.W.G., et al. (2014). Quantitative Temporal Viromics: An Approach to Investigate Host-Pathogen Interaction. *Cell* 157, 1460–1472. 10.1016/j.cell.2014.04.028.
32. Stern-Ginossar, N., Weisburd, B., Michalski, A., Le, V.T.K., Hein, M.Y., Huang, S.-X., Ma, M., Shen, B., Qian, S.-B., Hengel, H., et al. (2012). Decoding Human Cytomegalovirus. *Science* 338, 1088–1093. 10.1126/science.1227919.
33. Sijmons, S., Ranst, M.V., and Maes, P. (2014). Genomic and Functional Characteristics of Human Cytomegalovirus Revealed by Next-Generation Sequencing. *Viruses* 6, 1049–1072. 10.3390/v6031049.
34. Liu, J., Jardetzky, T.S., Chin, A.L., Johnson, D.C., and Vanarsdall, A.L. (2018). The Human Cytomegalovirus Trimer and Pentamer Promote Sequential Steps in Entry into Epithelial and Endothelial Cells at Cell Surfaces and Endosomes. *J Virol* 92. 10.1128/jvi.01336-18.
35. Wang, D., and Shenk, T. (2005). Human cytomegalovirus virion protein complex required for epithelial and endothelial cell tropism. *Proc National Acad Sci* 102, 18153–18158. 10.1073/pnas.0509201102.
36. Ogawa-Goto, K., Tanaka, K., Gibson, W., Moriishi, E., Miura, Y., Kurata, T., Irie, S., and Sata, T. (2003). Microtubule Network Facilitates Nuclear Targeting of Human Cytomegalovirus Capsid. *J Virol* 77, 8541–8547. 10.1128/jvi.77.15.8541-8547.2003.
37. Nitzsche, A., Paulus, C., and Nevels, M. (2008). Temporal Dynamics of Cytomegalovirus Chromatin Assembly in Productively Infected Human Cells. *J Virol* 82, 11167–11180. 10.1128/jvi.01218-08.
38. Strang, B.L., Boulant, S., Kirchhausen, T., and Coen, D.M. (2012). Host Cell Nucleolin Is Required To Maintain the Architecture of Human Cytomegalovirus Replication Compartments. *mBio* 3, e00301-11.
39. Fortunato, E.A., and Spector, D.H. (1998). p53 and RPA Are Sequestered in Viral Replication Centers in the Nuclei of Cells Infected with Human Cytomegalovirus. *J Virol* 72, 2033–2039. 10.1128/jvi.72.3.2033-2039.1998.
40. Penfold, M.E., and Mocarski, E.S. (1997). Formation of cytomegalovirus DNA replication compartments defined by localization of viral proteins and DNA synthesis. *Virology* 239, 46–61.
41. Wright, D., Staprans, S., and Spector, D. (1988). Four phosphoproteins with common amino termini are encoded by human cytomegalovirus AD169. *J Virol* 62, 331–340. 10.1128/jvi.62.1.331-340.1988.
42. Dremel, S.E., and Didychuk, A.L. (2022). Better late than never: A unique strategy for late gene transcription in the beta- and gammaherpesviruses. *Semin Cell Dev Biol*. 10.1016/j.semcdb.2022.12.001.

43. Mariamé, B., Kappler-Gratias, S., Kappler, M., Balor, S., Gallardo, F., and Bystricky, K. (2018). Real-Time Visualization and Quantification of Human Cytomegalovirus Replication in Living Cells Using the ANCHOR DNA Labeling Technology. *J Virol* 92, e00571-18. 10.1128/jvi.00571-18.
44. Dittmer, A., Drach, J.C., Townsend, L.B., Fischer, A., and Bogner, E. (2005). Interaction of the Putative Human Cytomegalovirus Portal Protein pUL104 with the Large Terminase Subunit pUL56 and Its Inhibition by Benzimidazole- d -Ribonucleosides. *J Virol* 79, 14660–14667. 10.1128/jvi.79.23.14660-14667.2005.
45. Hagen, C., Dent, K.C., Zeev-Ben-Mordehai, T., Grange, M., Bosse, J.B., Whittle, C., Klupp, B.G., Siebert, C.A., Vasishtan, D., Bäuerlein, F.J.B., et al. (2015). Structural Basis of Vesicle Formation at the Inner Nuclear Membrane. *Cell* 163, 1692–1701. 10.1016/j.cell.2015.11.029.
46. Procter, D.J., Banerjee, A., Nukui, M., Kruse, K., Gaponenko, V., Murphy, E.A., Komarova, Y., and Walsh, D. (2018). The HCMV Assembly Compartment Is a Dynamic Golgi-Derived MTOC that Controls Nuclear Rotation and Virus Spread. *Dev Cell* 45, 83-100.e7. 10.1016/j.devcel.2018.03.010.
47. Sanchez, V., Greis, K.D., Sztul, E., and Britt, W.J. (2000). Accumulation of Virion Tegument and Envelope Proteins in a Stable Cytoplasmic Compartment during Human Cytomegalovirus Replication: Characterization of a Potential Site of Virus Assembly. *J Virol* 74, 975–986. 10.1128/jvi.74.2.975-986.2000.
48. Sanchez, V., Sztul, E., and Britt, W.J. (2000). Human Cytomegalovirus pp28 (UL99) Localizes to a Cytoplasmic Compartment Which Overlaps the Endoplasmic Reticulum-Golgi-Intermediate Compartment. *J Virol* 74, 3842–3851. 10.1128/jvi.74.8.3842-3851.2000.
49. Severi, B., Landini, M.P., and Govoni, E. (1988). Human Cytomegalovirus morphogenesis: an ultrastructural study of the late cytoplasmic phases. *Arch Virol* 98, 51–64. 10.1007/bf01321005.
50. Irmiere, A., and Gibson, W. (1983). Isolation and characterization of a noninfectious virion-like particle released from cells infected with human strains of cytomegalovirus. *Virology* 130, 118–133. 10.1016/0042-6822(83)90122-8.
51. Ishov, A.M., Stenberg, R.M., and Maul, G.G. (1997). Human cytomegalovirus immediate early interaction with host nuclear structures: definition of an immediate transcript environment. *J Cell Biology* 138, 5–16. 10.1083/jcb.138.1.5.
52. Ahn, J.H., Jang, W.J., and Hayward, G.S. (1999). The human cytomegalovirus IE2 and UL112-113 proteins accumulate in viral DNA replication compartments that initiate from the periphery of promyelocytic leukemia protein-associated nuclear bodies (PODs or ND10). *J Virol* 73, 10458–10471.
53. Tavalai, N., Adler, M., Scherer, M., Riedl, Y., and Stamminger, T. (2011). Evidence for a dual antiviral role of the major nuclear domain 10 component Sp100 during the immediate-early and late phases of the human cytomegalovirus replication cycle. *J Virol* 85, 9447–9458.
54. Albright, E.R., and Kalejta, R.F. (2016). Canonical and Variant Forms of Histone H3 Are Deposited onto the Human Cytomegalovirus Genome during Lytic and Latent Infections. *J Virol* 90, 10309–10320. 10.1128/jvi.01220-16.
55. Koriath, F., Maul, G.G., Plachter, B., Stamminger, T., and Frey, J. (1996). The Nuclear Domain 10 (ND10) Is Disrupted by the Human Cytomegalovirus Gene Product IE1. *Exp Cell Res* 229, 155–158. 10.1006/excr.1996.0353.

56. Snaar, S.P., Vincent, M., and Dirks, R.W. (1998). RNA Polymerase II Localizes at Sites of Human Cytomegalovirus Immediate-early RNA Synthesis and Processing. *J Histochem Cytochem* 47, 245–254. 10.1177/002215549904700213.
57. Pari, G.S., and Anders, D.G. (1993). Eleven loci encoding trans-acting factors are required for transient complementation of human cytomegalovirus oriLyt-dependent DNA replication. *J Virol* 67, 6979–6988. 10.1128/jvi.67.12.6979-6988.1993.
58. Strang, B.L., Boulant, S., Chang, L., Knipe, D.M., Kirchhausen, T., and Coen, D.M. (2012). Human cytomegalovirus UL44 concentrates at the periphery of replication compartments, the site of viral DNA synthesis. *J Virol* 86, 2089–2095.
59. Pari, G.S., and Anders, D.G. (1993). Eleven loci encoding trans-acting factors are required for transient complementation of human cytomegalovirus oriLyt-dependent DNA replication. *J Virol* 67, 6979–6988.
60. Sarisky, R.T., and Hayward, G.S. (1996). Evidence that the UL84 gene product of human cytomegalovirus is essential for promoting oriLyt-dependent DNA replication and formation of replication compartments in cotransfection assays. *J Virol* 70, 7398–7413.
61. Li, M., Ball, C.B., Collins, G., Hu, Q., Luse, D.S., Price, D.H., and Meier, J.L. (2020). Human cytomegalovirus IE2 drives transcription initiation from a select subset of late infection viral promoters by host RNA polymerase II. *Plos Pathog* 16, 1–30. 10.1371/journal.ppat.1008402.
62. Spector, D.J. (2015). UL84-independent replication of human cytomegalovirus strains conferred by a single codon change in UL122. *Virology* 476, 345–354.
63. Manska, S., and Rossetto, C.C. (2021). Characteristics of Immediate-Early 2 (IE2) and UL84 Proteins in UL84-Independent Strains of Human Cytomegalovirus (HCMV). *Microbiol Spectr* 9, e00539-21. 10.1128/spectrum.00539-21.
64. Ahn, J.-H., and Hayward, G.S. (2000). Disruption of PML-Associated Nuclear Bodies by IE1 Correlates with Efficient Early Stages of Viral Gene Expression and DNA Replication in Human Cytomegalovirus Infection. *Virology* 274, 39–55. 10.1006/viro.2000.0448.
65. Yamamoto, T., Suzuki, S., Radsak, K., and Hirai, K. (1998). The UL112/113 gene products of human cytomegalovirus which colocalize with viral DNA in infected cell nuclei are related to efficient viral DNA replication. *Virus Res* 56, 107–114. 10.1016/s0168-1702(98)00032-x.
66. Iwayama, S., Yamamoto, T., Furuya, T., Kobayashi, R., Ikuta, K., and Hirai, K. (1994). Intracellular localization and DNA-binding activity of a class of viral early phosphoproteins in human fibroblasts infected with human cytomegalovirus (Towne strain). *J Gen Virol* 75, 3309–3318.
67. Park, M.-Y., Kim, Y.-E., Seo, M.-R., Lee, J.-R., Lee, C.H., and Ahn, J.-H. (2006). Interactions among four proteins encoded by the human cytomegalovirus UL112-113 region regulate their intranuclear targeting and the recruitment of UL44 to prereplication foci. *J Virol* 80, 2718–2727.
68. Schommartz, T., Tang, J., Brost, R., and Brune, W. (2017). Differential Requirement of Human Cytomegalovirus UL112-113 Protein Isoforms for Viral Replication. *J Virol* 91, e00254-17.

69. Wang, S.-K., Jiang, M.J., Lin, S.-R., Chen, M.-Y., Wang, H.-H., and Duh, C.-Y. (2015). Calpains mediate the proteolytic modification of human cytomegalovirus UL112-113 proteins. *J Gen Virol* 96, 1115–1126. 10.1099/vir.0.000040.
70. Li, J., Yamamoto, T., Ohtsubo, K., Shirakata, M., and Hirai, K. (1999). Major Product pp43 of Human Cytomegalovirus UL112-113 Gene Is a Transcriptional Coactivator with Two Functionally Distinct Domains. *Virology* 260, 89–97. 10.1006/viro.1999.9800.
71. Wells, R., Stensland, L., and Vieira, J. (2009). The human cytomegalovirus UL112-113 locus can activate the full Kaposi's sarcoma-associated herpesvirus lytic replication cycle. *J Virol* 83, 4695–4699. 10.1128/jvi.02241-08.
72. Hein, M.Y., and Weissman, J.S. (2022). Functional single-cell genomics of human cytomegalovirus infection. *Nat Biotechnol* 40, 391–401. 10.1038/s41587-021-01059-3.
73. Kim, Y.-E., and Ahn, J.-H. (2010). Role of the Specific Interaction of UL112-113 p84 with UL44 DNA Polymerase Processivity Factor in Promoting DNA Replication of Human Cytomegalovirus ν . *J Virol* 84, 8409–8421. 10.1128/jvi.00189-10.
74. Caragliano, E., Bonazza, S., Frascaroli, G., Tang, J., Soh, T.K., Grünewald, K., Bosse, J.B., and Brune, W. (2022). Human cytomegalovirus forms phase-separated compartments at viral genomes to facilitate viral replication. *Cell Reports* 38, 110469. 10.1016/j.celrep.2022.110469.
75. Wilson, E.B. (1899). The Structure of Protoplasm. *Science* 10, 33–45. 10.1126/science.10.237.33.
76. Walter, H., and Brooks, D.E. (1995). Phase separation in cytoplasm, due to macromolecular crowding, is the basis for microcompartmentation. *Febs Lett* 361, 135–139. 10.1016/0014-5793(95)00159-7.
77. Gunton, J.D. (2005). Fluctuations and Stochastic Phenomena in Condensed Matter, Proceedings of the Sitges Conference on Statistical Mechanics Sitges, Barcelona/Spain, May 26–30, 1986. *Lect Notes Phys*, 35–54. 10.1007/3-540-17206-8_2.
78. Brangwynne, C.P., Eckmann, C.R., Courson, D.S., Rybarska, A., Hoege, C., Gharakhani, J., Jülicher, F., and Hyman, A.A. (2009). Germline P Granules Are Liquid Droplets That Localize by Controlled Dissolution/Condensation. *Science* 324, 1729–1732.
79. Banani, S.F., Lee, H.O., Hyman, A.A., and Rosen, M.K. (2017). Biomolecular condensates: organizers of cellular biochemistry. *Nat Rev Mol Cell Bio* 18, 285–298. 10.1038/nrm.2017.7.
80. Berry, J., Brangwynne, C.P., and Haataja, M. (2018). Physical principles of intracellular organization via active and passive phase transitions. *Rep Prog Phys* 81, 046601. 10.1088/1361-6633/aaa61e.
81. Bracha, D., Walls, M.T., Wei, M.-T., Zhu, L., Kurian, M., Avalos, J.L., Toettcher, J.E., and Brangwynne, C.P. (2018). Mapping Local and Global Liquid Phase Behavior in Living Cells Using Photo-Oligomerizable Seeds. *Cell* 175, 1467-1480.e13.
82. Shimobayashi, S.F., Ronceray, P., Sanders, D.W., Haataja, M.P., and Brangwynne, C.P. (2021). Nucleation landscape of biomolecular condensates. *Nature* 599, 503–506. 10.1038/s41586-021-03905-5.
83. Ibach, H., and Lüth, H. (2009). *Solid-State Physics: An Introduction to Principles of Materials Science* | SpringerLink. <https://link.springer.com/book/10.1007/978-3-540-93804-0>.

84. Auer, S., and Frenkel, D. (2001). Prediction of absolute crystal-nucleation rate in hard-sphere colloids. *Nature* *409*, 1020–1023. 10.1038/35059035.
85. Ditlev, J.A., Case, L.B., and Rosen, M.K. (2018). Who's In and Who's Out—Compositional Control of Biomolecular Condensates. *J Mol Biol* *430*, 4666–4684. 10.1016/j.jmb.2018.08.003.
86. Banani, S.F., Rice, A.M., Peeples, W.B., Lin, Y., Jain, S., Parker, R., and Rosen, M.K. (2016). Compositional Control of Phase-Separated Cellular Bodies. *Cell* *166*, 651–663. 10.1016/j.cell.2016.06.010.
87. Ahmad, Y., Boisvert, F.-M., Gregor, P., Cobley, A., and Lamond, A.I. (2009). NOPdb: Nucleolar Proteome Database—2008 update. *Nucleic Acids Res* *37*, D181–D184. 10.1093/nar/gkn804.
88. Ishov, A.M., Sotnikov, A.G., Negorev, D., Vladimirova, O.V., Neff, N., Kamitani, T., Yeh, E.T., Strauss, 3rd J F, and Maul, G.G. (1999). PML is critical for ND10 formation and recruits the PML-interacting protein daxx to this nuclear structure when modified by SUMO-1. *J Cell Biology* *147*, 221–234. 10.1083/jcb.147.2.221.
89. Choi, J.-M., Holehouse, A.S., and Pappu, R.V. (2020). Physical Principles Underlying the Complex Biology of Intracellular Phase Transitions. *Annu Rev Biophys* *49*, 1–27. 10.1146/annurev-biophys-121219-081629.
90. Harmon, T.S., Holehouse, A.S., Rosen, M.K., and Pappu, R.V. (2017). Intrinsically disordered linkers determine the interplay between phase separation and gelation in multivalent proteins. *Elife* *6*, e30294. 10.7554/elife.30294.
91. Wang, J., Choi, J.-M., Holehouse, A.S., Lee, H.O., Zhang, X., Jahnel, M., Maharana, S., Lemaitre, R., Pozniakovsky, A., Drechsel, D., et al. (2018). A Molecular Grammar Governing the Driving Forces for Phase Separation of Prion-like RNA Binding Proteins. *Cell* *174*, 688-699.e16. 10.1016/j.cell.2018.06.006.
92. Söding, J., Zwicker, D., Sohrabi-Jahromi, S., Boehning, M., and Kirschbaum, J. (2019). Mechanisms for Active Regulation of Biomolecular Condensates. *Trends Cell Biol* *30*, 4–14. 10.1016/j.tcb.2019.10.006.
93. Jack, A., Kim, Y., Strom, A.R., Lee, D.S.W., Williams, B., Schaub, J.M., Kellogg, E.H., Finkelstein, I.J., Ferro, L.S., Yildiz, A., et al. (2022). Compartmentalization of telomeres through DNA-scaffolded phase separation. *Dev Cell* *57*, 277-290.e9. 10.1016/j.devcel.2021.12.017.
94. Shin, Y., Chang, Y.-C., Lee, D.S.W., Berry, J., Sanders, D.W., Ronceray, P., Wingreen, N.S., Haataja, M., and Brangwynne, C.P. (2018). Liquid Nuclear Condensates Mechanically Sense and Restructure the Genome. *Cell* *175*, 1481-1491.e13. 10.1016/j.cell.2018.10.057.
95. Chong, P.A., Vernon, R.M., and Forman-Kay, J.D. (2018). RGG/RG Motif Regions in RNA Binding and Phase Separation. *J Mol Biol* *430*, 4650–4665. 10.1016/j.jmb.2018.06.014.
96. Patel, A., Lee, H.O., Jawerth, L., Maharana, S., Jahnel, M., Hein, M.Y., Stoynov, S., Mahamid, J., Saha, S., Franzmann, T.M., et al. (2015). A Liquid-to-Solid Phase Transition of the ALS Protein FUS Accelerated by Disease Mutation. *Cell* *162*, 1066–1077.
97. Muzzopappa, F., Hertzog, M., and Erdel, F. (2021). DNA length tunes the fluidity of DNA-based condensates. *Biophys J* *120*, 1288–1300. 10.1016/j.bpj.2021.02.027.
98. Shin, Y., and Brangwynne, C.P. (2017). Liquid phase condensation in cell physiology and disease. *Science* *357*, eaaf4382. 10.1126/science.aaf4382.

99. Wegmann, S., Eftekharzadeh, B., Tepper, K., Zoltowska, K.M., Bennett, R.E., Dujardin, S., Laskowski, P.R., MacKenzie, D., Kamath, T., Commins, C., et al. (2018). Tau protein liquid–liquid phase separation can initiate tau aggregation. *Embo J* 37, e98049. 10.15252/embj.201798049.
100. Jawerth, L., Fischer-Friedrich, E., Saha, S., Wang, J., Franzmann, T., Zhang, X., Sachweh, J., Ruer, M., Ijavi, M., Saha, S., et al. (2020). Protein condensates as aging Maxwell fluids. *Science* 370, 1317–1323. 10.1126/science.aaw4951.
101. Lin, J. (2022). Modeling the aging of protein condensates. *Phys Rev Res* 4, L022012. 10.1103/physrevresearch.4.l022012.
102. Patel, A., Malinowska, L., Saha, S., Wang, J., Alberti, S., Krishnan, Y., and Hyman, A.A. (2017). ATP as a biological hydrotrope. *Science* 356, 753–756. 10.1126/science.aaf6846.
103. Owen, I., and Shewmaker, F. (2019). The Role of Post-Translational Modifications in the Phase Transitions of Intrinsically Disordered Proteins. *Int J Mol Sci* 20, 5501. 10.3390/ijms20215501.
104. Frey, S., Richter, R.P., and Görlich, D. (2006). FG-Rich Repeats of Nuclear Pore Proteins Form a Three-Dimensional Meshwork with Hydrogel-Like Properties. *Science* 314, 815–817. 10.1126/science.1132516.
105. Boke, E., Ruer, M., Wühr, M., Coughlin, M., Lemaitre, R., Gygi, S.P., Alberti, S., Drechsel, D., Hyman, A.A., and Mitchison, T.J. (2016). Amyloid-like Self-Assembly of a Cellular Compartment. *Cell* 166, 637–650. 10.1016/j.cell.2016.06.051.
106. Oliveira, G.A.P. de, Cordeiro, Y., Silva, J.L., and Vieira, T.C.R.G. (2019). Chapter Nine Liquid-liquid phase transitions and amyloid aggregation in proteins related to cancer and neurodegenerative diseases. *Adv Protein Chem Str* 118, 289–331. 10.1016/bs.apcsb.2019.08.002.
107. Mirdita, M., Schütze, K., Moriwaki, Y., Heo, L., Ovchinnikov, S., and Steinegger, M. (2022). ColabFold: making protein folding accessible to all. *Nat Methods* 19, 679–682. 10.1038/s41592-022-01488-1.
108. Tischer, B.K., Smith, G.A., and Osterrieder, N. (2010). In Vitro Mutagenesis Protocols, Third Edition. *Methods Mol Biology* 634, 421–430. 10.1007/978-1-60761-652-8_30.
109. Dosztányi, Z., Csizmok, V., Tompa, P., and Simon, I. (2005). IUPred: web server for the prediction of intrinsically unstructured regions of proteins based on estimated energy content. *Bioinformatics* 21, 3433–3434.
110. Caragliano, E., Brune, W., and Bosse, J.B. (2022). Herpesvirus Replication Compartments: Dynamic Biomolecular Condensates? *Viruses* 14, 960. 10.3390/v14050960.
111. Kroschwald, S., Maharana, S., and Simon, A. (2017). Hexanediol: a chemical probe to investigate the material properties of membrane-less compartments. *Matters*. 10.19185/matters.201702000010.
112. Geiger, F., Acker, J., Papa, G., Wang, X., Arter, W.E., Saar, K.L., Erkamp, N.A., Qi, R., Bravo, J.P., Strauss, S., et al. (2021). Liquid–liquid phase separation underpins the formation of replication factories in rotaviruses. *Embo J* 40, e107711. 10.15252/embj.2021107711.
113. Mochida, K., and Gomyoda, M. (1987). Toxicity of ethylene glycol, diethylene glycol, and propylene glycol to human cells in culture. *B Environ Contam Tox* 38, 151–153. 10.1007/bf01606573.

114. Park, M.-Y., Kim, Y.-E., Seo, M.-R., Lee, J.-R., Lee, C.H., and Ahn, J.-H. (2006). Interactions among Four Proteins Encoded by the Human Cytomegalovirus UL112-113 Region Regulate Their Intranuclear Targeting and the Recruitment of UL44 to Prereplication Foci. *J Virol* 80, 2718–2727. 10.1128/jvi.80.6.2718-2727.2006.
115. Muscolino, E., Schmitz, R., Lorocho, S., Caragliano, E., Schneider, C., Rizzato, M., Kim, Y.-H., Krause, E., Lisnić, V.J., Sickmann, A., et al. (2020). Herpesviruses induce aggregation and selective autophagy of host signalling proteins NEMO and RIPK1 as an immune-evasion mechanism. *Nat Microbiol* 5, 331–342. 10.1038/s41564-019-0624-1.
116. Feric, M., Vaidya, N., Harmon, T.S., Mitrea, D.M., Zhu, L., Richardson, T.M., Kriwacki, R.W., Pappu, R.V., and Brangwynne, C.P. (2016). Coexisting Liquid Phases Underlie Nucleolar Subcompartments. *Cell* 165, 1686–1697.
117. Chen, D., and Huang, S. (2001). Nucleolar components involved in ribosome biogenesis cycle between the nucleolus and nucleoplasm in interphase cells. *The Journal of cell biology* 153, 169–176.
118. McSwiggen, D.T., Mir, M., Darzacq, X., and Tjian, R. (2019). Evaluating phase separation in live cells: diagnosis, caveats, and functional consequences. *Genes Dev* 33, 1619–1634.
119. Preston, C.M., Mabbs, R., and Nicholl, M.J. (1997). Construction and Characterization of Herpes Simplex Virus Type 1 Mutants with Conditional Defects in Immediate Early Gene Expression. *Virology* 229, 228–239. 10.1006/viro.1996.8424.
120. Sampaio, K.L., Cavnac, Y., Stierhof, Y.-D., and Sinzger, C. (2005). Human Cytomegalovirus Labeled with Green Fluorescent Protein for Live Analysis of Intracellular Particle Movements. *J Virol* 79, 2754–2767. 10.1128/jvi.79.5.2754-2767.2005.
121. Li, J., Yamamoto, T., Ohtsubo, K., Shirakata, M., and Hirai, K. (1999). Major product pp43 of human cytomegalovirus U(L)112-113 gene is a transcriptional coactivator with two functionally distinct domains. *Virology* 260, 89–97.
122. Kim, Y.E., and Ahn, J.H. (2010). Role of the specific interaction of UL112-113 p84 with UL44 DNA polymerase processivity factor in promoting DNA replication of human cytomegalovirus. *J Virol* 84, 8409–8421.
123. Kim, Y.-E., Park, M.Y., Kang, K.J., Han, T.H., Lee, C.H., and Ahn, J.-H. (2015). Requirement of the N-terminal residues of human cytomegalovirus UL112-113 proteins for viral growth and oriLyt-dependent DNA replication. *J Microbiol* 53, 561–569. 10.1007/s12275-015-5301-3.
124. Fliss, P.M., and Brune, W. (2012). Prevention of Cellular Suicide by Cytomegaloviruses. *Viruses* 4, 1928–1949. 10.3390/v4101928.
125. Paintsil, E., and Cheng, Y.-C. (2009). Encyclopedia of Microbiology (Third Edition). Pathogenesis Article Titles, 223–257. 10.1016/b978-012373944-5.00178-4.
126. Appleton, B.A., Loregian, A., Filman, D.J., Coen, D.M., and Hogle, J.M. (2004). The Cytomegalovirus DNA Polymerase Subunit UL44 Forms a C Clamp-Shaped Dimer. *Mol Cell* 15, 233–244. 10.1016/j.molcel.2004.06.018.

127. Silva, L.A., Loregian, A., Pari, G.S., Strang, B.L., and Coen, D.M. (2010). The Carboxy-Terminal Segment of the Human Cytomegalovirus DNA Polymerase Accessory Subunit UL44 Is Crucial for Viral Replication ∇ . *J Virol* *84*, 11563–11568. 10.1128/jvi.01033-10.
128. Kamagata, K., Iwaki, N., Hazra, M.K., Kanbayashi, S., Banerjee, T., Chiba, R., Sakomoto, S., Gaudon, V., Castaing, B., Takahashi, H., et al. (2021). Molecular principles of recruitment and dynamics of guest proteins in liquid droplets. *Sci Rep-uk* *11*, 19323. 10.1038/s41598-021-98955-0.
129. Kamagata, K., Iwaki, N., Kanbayashi, S., Banerjee, T., Chiba, R., Gaudon, V., Castaing, B., and Sakomoto, S. (2022). Structure-dependent recruitment and diffusion of guest proteins in liquid droplets of FUS. *Sci Rep-uk* *12*, 7101. 10.1038/s41598-022-11177-w.
130. Riback, J.A., Zhu, L., Ferrolino, M.C., Tolbert, M., Mitrea, D.M., Sanders, D.W., Wei, M.-T., Kriwacki, R.W., and Brangwynne, C.P. (2020). Composition-dependent thermodynamics of intracellular phase separation. *Nature* *581*, 209–214. 10.1038/s41586-020-2256-2.
131. Cho, W.-K., Spille, J.-H., Hecht, M., Lee, C., Li, C., Grube, V., and Cisse, I.I. (2018). Mediator and RNA polymerase II clusters associate in transcription-dependent condensates. *Science* *361*, 412.
132. Du, M., and Chen, Z.J. (2018). DNA-induced liquid phase condensation of cGAS activates innate immune signaling. *Science* *361*, 704.
133. Patel, A., Lee, H.O., Jawerth, L., Maharana, S., Jahnel, M., Hein, M.Y., Stoyanov, S., Mahamid, J., Saha, S., Franzmann, T.M., et al. (2015). A Liquid-to-Solid Phase Transition of the ALS Protein FUS Accelerated by Disease Mutation. *Cell* *162*, 1066–1077. 10.1016/j.cell.2015.07.047.
134. Wang, S.-K., Hu, C.-H., Lu, M.-C., Duh, C.-Y., Liao, P.-C., and Tyan, Y.-C. (2009). Novel virus-associated proteins encoded by UL112–113 of human cytomegalovirus. *J Gen Virol* *90*, 2840–2848. 10.1099/vir.0.013037-0.
135. Schommartz, T., Loroche, S., Alawi, M., Grundhoff, A., Sickmann, A., and Brune, W. (2016). Functional Dissection of an Alternatively Spliced Herpesvirus Gene by Splice Site Mutagenesis. *J Virol* *90*, 4626–4636.
136. Ciocco-Schmitt, G.M., Karabekian, Z., Godfrey, E.W., Stenberg, R.M., Campbell, A.E., and Kerry, J.A. (2002). Identification and Characterization of Novel Murine Cytomegalovirus M112–113 (e1) Gene Products. *Virology* *294*, 199–208.
137. Taniguchi, T., Shimamoto, T., Isegawa, Y., Kondo, K., and Yamanishi, K. (2000). Structure of Transcripts and Proteins Encoded by U79-80 of Human Herpesvirus 6 and Its Subcellular Localization in Infected Cells. *Virology* *271*, 307–320.
138. Nott, T.J., Petsalaki, E., Farber, P., Jervis, D., Fussner, E., Plochowietz, A., Craggs, T.D., Bazett-Jones, D.P., Pawson, T., Forman-Kay, J.D., et al. (2015). Phase Transition of a Disordered Nuage Protein Generates Environmentally Responsive Membraneless Organelles. *Mol Cell* *57*, 936–947. 10.1016/j.molcel.2015.01.013.
139. Shevtsov, S.P., and Dundr, M. (2011). Nucleation of nuclear bodies by RNA. *Nat Cell Biol* *13*, 167–173. 10.1038/ncb2157.

140. Sourvinos, G., Tavalai, N., Berndt, A., Spandidos, D.A., and Stamminger, T. (2007). Recruitment of human cytomegalovirus immediate-early 2 protein onto parental viral genomes in association with ND10 in live-infected cells. *J Virol* *81*, 10123–10136. 10.1128/jvi.01009-07.
141. Gu, H., Liang, Y., Mandel, G., and Roizman, B. (2005). Components of the REST/CoREST/histone deacetylase repressor complex are disrupted, modified, and translocated in HSV-1-infected cells. *Proc National Acad Sci* *102*, 7571–7576. 10.1073/pnas.0502658102.
142. Park, J.-J., Kim, Y.-E., Pham, H.T., Kim, E.T., Chung, Y.-H., and Ahn, J.-H. (2007). Functional interaction of the human cytomegalovirus IE2 protein with histone deacetylase 2 in infected human fibroblasts. *J Gen Virol* *88*, 3214–3223. 10.1099/vir.0.83171-0.
143. Yeewa, R., Chaiya, P., Jantrapirom, S., Shotelersuk, V., and Piccolo, L.L. (2022). Multifaceted roles of YEATS domain-containing proteins and novel links to neurological diseases. *Cell Mol Life Sci* *79*, 183. 10.1007/s00018-022-04218-0.
144. Wagenknecht, N., Reuter, N., Scherer, M., Reichel, A., Müller, R., and Stamminger, T. (2015). Contribution of the Major ND10 Proteins PML, hDaxx and Sp100 to the Regulation of Human Cytomegalovirus Latency and Lytic Replication in the Monocytic Cell Line THP-1. *Viruses* *7*, 2884–2907. 10.3390/v7062751.
145. Suzich, J.B., Cuddy, S.R., Baidas, H., Dochnal, S., Ke, E., Schinlever, A.R., Babnis, A., Boutell, C., and Cliffe, A.R. (2021). PML-NB-dependent type I interferon memory results in a restricted form of HSV latency. *Embo Rep* *22*, e52547. 10.15252/embr.202152547.
146. Schilling, E.-M., Scherer, M., Reuter, N., Schweininger, J., Müller, Y.A., and Stamminger, T. (2017). The Human Cytomegalovirus IE1 Protein Antagonizes PML Nuclear Body-Mediated Intrinsic Immunity via the Inhibition of PML De Novo SUMOylation. *J Virol* *91*. 10.1128/jvi.02049-16.
147. Gawn, J.M., and Greaves, R.F. (2002). Absence of IE1 p72 Protein Function during Low-Multiplicity Infection by Human Cytomegalovirus Results in a Broad Block to Viral Delayed-Early Gene Expression. *J Virol* *76*, 4441–4455. 10.1128/jvi.76.9.4441-4455.2002.
148. Seitz, S., Heusel, A.T., Stamminger, T., and Scherer, M. (2022). Promyelocytic Leukemia Protein Potently Restricts Human Cytomegalovirus Infection in Endothelial Cells. *Int J Mol Sci* *23*, 11931. 10.3390/ijms231911931.
149. Xu, P., Mallon, S., and Roizman, B. (2016). PML plays both inimical and beneficial roles in HSV-1 replication. *Proc National Acad Sci* *113*, E3022–E3028. 10.1073/pnas.1605513113.
150. Paulus, C., Harwardt, T., Walter, B., Marxreiter, A., Zenger, M., Reuschel, E., and Nevels, M.M. (2020). Revisiting promyelocytic leukemia protein targeting by human cytomegalovirus immediate-early protein 1. *Plos Pathog* *16*, e1008537. 10.1371/journal.ppat.1008537.
151. Kobilier, O., Lipman, Y., Therkelsen, K., Daubechies, I., and Enquist, L.W. (2010). Herpesviruses carrying a Brainbow cassette reveal replication and expression of limited numbers of incoming genomes. *Nature Communications* *1*, 146.
152. Schwartz, M., Shnayder, M., Nachshon, A., Arazi, T., Kitsberg, Y., Samia, R.L., Lavi, M., Kuint, R., Tsabari, R., and Stern-Ginossar, N. (2023). Molecular characterization of human cytomegalovirus infection with single-cell transcriptomics. *Nat Microbiol*, 1–14. 10.1038/s41564-023-01325-x.

153. Wei, M.-T., Elbaum-Garfinkle, S., Holehouse, A.S., Chen, C.C.-H., Feric, M., Arnold, C.B., Priestley, R.D., Pappu, R.V., and Brangwynne, C.P. (2017). Phase behaviour of disordered proteins underlying low density and high permeability of liquid organelles. *Nat Chem* 9, 1118–1125. 10.1038/nchem.2803.
154. Ward, J.J., Sodhi, J.S., McGuffin, L.J., Buxton, B.F., and Jones, D.T. (2004). Prediction and Functional Analysis of Native Disorder in Proteins from the Three Kingdoms of Life. *J Mol Biol* 337, 635–645. 10.1016/j.jmb.2004.02.002.
155. Mozzi, A., Forni, D., Cagliani, R., Clerici, M., Pozzoli, U., and Sironi, M. (2020). Intrinsically disordered regions are abundant in simplexvirus proteomes and display signatures of positive selection. *Virus Evol* 6, veaa028. 10.1093/ve/veaa028.
156. Seyffert, M., Georgi, F., Tobler, K., Bourqui, L., Anfossi, M., Michaelsen, K., Vogt, B., Greber, U.F., and Fraefel, C. (2021). The HSV-1 Transcription Factor ICP4 Confers Liquid-Like Properties to Viral Replication Compartments. *Int J Mol Sci* 22. 10.3390/ijms22094447.
157. Everett, R.D. (1988). Analysis of the functional domains of herpes simplex virus type 1 immediate-early polypeptide Vmw110. *J Mol Biol* 202, 87. 10.1016/0022-2836(88)90521-9.
158. McSwiggen, D.T., Hansen, A.S., Teves, S.S., Marie-Nelly, H., Hao, Y., Heckert, A.B., Umemoto, K.K., Dugast-Darzacq, C., Tjian, R., and Darzacq, X. (2019). Evidence for DNA-mediated nuclear compartmentalization distinct from phase separation. *eLife* 8, e47098.
159. Boehning, M., Dugast-Darzacq, C., Rankovic, M., Hansen, A.S., Yu, T., Marie-Nelly, H., McSwiggen, D.T., Kokic, G., Dailey, G.M., Cramer, P., et al. (2018). RNA polymerase II clustering through carboxy-terminal domain phase separation. *Nat Struct Mol Biol* 25, 833–840. 10.1038/s41594-018-0112-y.
160. Uppal, T., Banerjee, S., Sun, Z., Verma, S.C., and Robertson, E.S. (2014). KSHV LANA—The Master Regulator of KSHV Latency. *Viruses* 6, 4961–4998. 10.3390/v6124961.
161. Broussard, G., and Damania, B. (2020). Regulation of KSHV Latency and Lytic Reactivation. *Viruses* 12, 1034. 10.3390/v12091034.
162. Vladimirova, O., Leo, A.D., Deng, Z., Wiedmer, A., Hayden, J., and Lieberman, P.M. (2021). Phase separation and DAXX redistribution contribute to LANA nuclear body and KSHV genome dynamics during latency and reactivation. *Plos Pathog* 17, e1009231. 10.1371/journal.ppat.1009231.
163. Ling, P.D., Rawlins, D.R., and Hayward, S.D. (1993). The Epstein-Barr virus immortalizing protein EBNA-2 is targeted to DNA by a cellular enhancer-binding protein. *Proc National Acad Sci* 90, 9237–9241. 10.1073/pnas.90.20.9237.
164. Peng, Q., Wang, L., Qin, Z., Wang, J., Zheng, X., Wei, L., Zhang, X., Zhang, X., Liu, C., Li, Z., et al. (2020). Phase Separation of Epstein-Barr Virus EBNA2 and Its Coactivator EBNA1 Controls Gene Expression. *J Virol* 94. 10.1128/jvi.01771-19.
165. Yang, Y., Ye, X., Dai, R., Li, Z., Zhang, Y., Xue, W., Zhu, Y., Feng, D., Qin, L., Wang, X., et al. (2021). Phase separation of Epstein-Barr virus EBNA2 protein reorganizes chromatin topology for epigenetic regulation. *Commun Biology* 4, 967. 10.1038/s42003-021-02501-7.

166. Metrick, C.M., Koenigsberg, A.L., and Heldwein, E.E. (2020). Conserved Outer Tegument Component UL11 from Herpes Simplex Virus 1 Is an Intrinsically Disordered, RNA-Binding Protein. *Mbio* 11, e00810-20. 10.1128/mbio.00810-20.
167. Hidalgo, P., Pimentel, A., Mojica-Santamaría, D., Stromberg, K. von, Hofmann-Sieber, H., Lona-Arrona, C., Dobner, T., and González, R.A. (2021). Evidence That the Adenovirus Single-Stranded DNA Binding Protein Mediates the Assembly of Biomolecular Condensates to Form Viral Replication Compartments. *Viruses* 13, 1778. 10.3390/v13091778.
168. Muscolino, E., Luoto, L.-M., and Brune, W. (2021). Viral Induced Protein Aggregation: A Mechanism of Immune Evasion. *Int J Mol Sci* 22, 9624. 10.3390/ijms22179624.
169. Risso-Ballester, J., Galloux, M., Cao, J., Goffic, R.L., Hontonnou, F., Jobart-Malfait, A., Desquesnes, A., Sake, S.M., Haid, S., Du, M., et al. (2021). A condensate-hardening drug blocks RSV replication in vivo. *Nature* 595, 596–599. 10.1038/s41586-021-03703-z.
170. Etibor, T.A., Vale-Costa, S., Sridharan, S., Brás, D., Becher, I., Mello, V.H., Ferreira, F., Alenquer, M., Savitski, M.M., and Amorim, M.J. (2022). Rules for hardening influenza A virus liquid condensates. *Biorxiv*, 2022.08.03.502602. 10.1101/2022.08.03.502602.
171. Bresnahan, W.A., Hultman, G.E., and Shenk, T. (2000). Replication of Wild-Type and Mutant Human Cytomegalovirus in Life-Extended Human Diploid Fibroblasts. *J Virol* 74, 10816–10818. 10.1128/jvi.74.22.10816-10818.2000.
172. Sinzger, C., Hahn, G., Digel, M., Katona, R., Sampaio, K.L., Messerle, M., Hengel, H., Koszinowski, U., Brune, W., and Adler, B. (2008). Cloning and sequencing of a highly productive, endotheliotropic virus strain derived from human cytomegalovirus TB40/E. *J Gen Virol* 89, 359–368. 10.1099/vir.0.83286-0.

10 Appendix

10.1 Curriculum Vitae

PERSONAL DETAILS

Enrico Caragliano, born the 29.12.1989 in Messina (ME), Italy (IT).

EDUCATION

PhD candidate since February 2018

PhD student at the Leibniz Institute for virology (LIV) and Centre for Structural System Biology (CSSB) in Hamburg, Germany.

Enrolled in the Department of Chemistry, University of Hamburg, Hamburg, Germany.

Supervisors: Prof. Dr. Wolfram Brune, Prof. Dr. Jens Bernhard Bosse.

PhD project: Liquid-liquid phase separation as a principle for viral replication compartment formation.

Master's Degree September 2014 – March 2016

Master of Science in Biology degree at the “Università degli Studi di Messina,” Messina, Italy, with a grade of 110/110 cum laude.

Supervisor: Prof. Dr. Maria Teresa Sciortino

Master thesis project: Characterization of the apoptotic process during HSV-1 replication: role of viral protein UL47.

Bachelor's Degree September 2008 – July 2014

Biology degree at the “Università degli Studi di Messina,” Messina, Italy (IT), with a grade of 100/110.

Supervisor: Prof. Dr. Maria Teresa Lo Gullo

Project: Role, zonation and importance of mangroves in the ecosystem

High school September 2003 – July 2008

High school diploma at the “Liceo classico Giuseppe La Farina”, Messina, Italy (IT), with a grade of 77/100.

10.2 Toxicity of chemicals

substance	GHS symbol	hazard statements	precautionary statements
2-mercaptoethanol		H301 + H331-H310- H315-H317-H318-H373- H410	P261-P280-P301 + P310 + P330- P302 + P352 + P310-P305 + P351 + P338 + P310-P403 + P233
acetone		H225-H319-H336	P210-P305+P351+P338-P337+313- P403
acetic acid		H226-H314	P280-P305 + P351 + P338-P310
acrylamide		H301-H312 + H332- H315-H317-H319-H340- H350-H361f-H372	P201-P280-P301 + P310-P305 + P351 + P338-P308 + P313
ammonium bicarbonate		H302	P301 + P312 + P330
ammonium chloride		H302	P264-P270-P301+312-P330-P501

ammonium persulfate		H272-H302-H315-H317-H319-H334-H335	P220-P261-P280-P305 + P351 + P338-P342 + P311
ampicillin		H315-H317-H319-H334-H335	P261-P280-P305 + P351 + P338-P342 + P311
bis-acrylamide		H302 + H332	
bromophenolblue		H332-H302-H319	P261-P264-P280-P304+340-P312-P301+312-P330-P305+351+338-P337+313
boric acid		H360FD	P201-P308 + P313
chloramphenicol		H350	P201-P308 + P313
crystal violet		H319-H351-H411	P273-P281-P305 + P351 + P338
dimethyl sulfoxide		H227	P210-P280-P370+P378-P403+P235-P501
EDTA		H319	P305 + P351 + P338
ethanol		H225-H319	P210-P280-P305 + P351 + P338-P337 + P313-P403 + P235

ethidium bromide		H302-H330-H341	P260-P281-P284-P310
glycerin		H315-H319-H335	P280-P302+P352-P304+P340-P305+P351+P338
hydrochloric acid		H290-H314-H335	P261-P280-P305 + P351 + P338-P310
isopropanol		H225-H319-H336	P210-P261-P305 + P351 + P338
kanamycin		H360	P201-P308 + P313
liquid nitrogen		H281	P202-P271 + P403-P282
methanol		H225-H301 + H311 + H331-H370	P210-P260-P280-P301 + P310-P311
paraformaldehyde		H228-H302+H332-H315-H317-H318-H335-H341-H350	P202-P210-P270-P280-P305+P351+P338-P308+P313
penicillin		H317-H334	P261-P280-P342 + P311
sodium dodecyl sulfate		H315-H318-H335	P280-P304 + P340 + P312-P305 + P351 + P338 + P310

sodium hydroxide		H290-H314	P280-P305 + P351 + P338-P310
streptomycin		H302-H361	P281
TEMED		H225-H302-H314-H332	P210-P280-P305 + P351 + P338-P310
Triton X-100		H302-H319-H411	P273-P280-P301 + P312 + P330-P337 + P313-P391-P501

10.3 Acknowledgments

I want to thank my supervisors, Prof. Jens B. Bosse and Prof. Wolfram Brune, for allowing me to work on such a challenging project. They always gave me valuable advice, helped with scientific discussions, and showed significant involvement in my project. Moreover, they always allowed me to pursue my ideas, teaching me to think critically about results and plan the next steps.

Thank you to Prof. Thomas Dobner for agreeing to be one of the evaluators of my thesis.

Thank you to Prof. Kay Grünewald, Prof. Jens B. Bosse, and Prof. Andrew Torda, who agreed to be the examiners of my oral defense.

Thank you to Prof. Jens B. Bosse and Dr. Timothy K. Soh for the critical manuscript reading. Their help was crucial for the improvement of the quality of the work.

Thank you to Dr. Felix Flomm for the help with Correlative light electron microscopy (CLEM) And Dr. Timothy K. Soh for the help with the CLEM overlay.

Thank you to all present and former lab members of the LIV research unit virus-host interaction. Giada, Olha, Kestin, Renke, Yingqi, Irke, Luis, Tianyu, Martina, Xuan, Michaela, Theo, Eleonore, Florian, Jiajia, Victoria, Umit, Ina, Michaela, Atousa, Laura L., Laura S., Tommaso, Alexander, Stefano B., Stefano L, and Jan. For giving helpful advice, providing help and for having fun together also outside of the lab.

Thank you to all present and former lab members of the CSSB research unit Quantitative Virology: Tim, Felix, Saskia, Linda, Doerte, Alice, Jonas, Sofia, and Yannick, for creating a unique and relaxed environment for doing research.

Thank you to my parents, Claudia and Luigi, for always believing in me and pushing me to reach new goals despite the distance that separates us.

Thank to my girlfriend, Victoria, for her daily support and love.

10.4 Statement of Authorship

I hereby declare on oath that I have written the present dissertation on my own and have not used other than the acknowledged resources and aids. The submitted written version corresponds to the version on the electronic storage medium. I hereby declare that I have not previously applied for or pursued a doctorate (Ph.D. studies).

A handwritten signature in blue ink, appearing to read 'C. Prof. Dr. C. C. C.', is positioned below the text. The signature is written in a cursive style with a prominent vertical stroke.

Hamburg, 22 March 2023